A THEORETICAL AND EXPERIMENTAL STUDYOF SURFACTANT TRANSPORT FROM A MICELLAR SOLUTION TO A CLEAN AIR/WATER INTERFACE

Qing Song

A dissertation submitted to the Graduate Faculty in Engineering in partial fulfillment of the requirement for the degree of Doctor of Philosophy,The City University of New York

2004

This manuscript has been read and accepted for the Graduate Faculty in Engineering in satisfaction of the dissertation requirement for the degree of Doctor of Philosophy.

7/29/04
Date

Charles Maldarelli
Professor Charles Maldarelli
Chair of Examining Committee

7/30/04
Date

Alexander Couzis
Professor Alexander Couzis
Co-Chair of Examining Committee

7/29/2004
Date

Mumtaz K. Kassir
Professor Mumtaz K. Kassir
Executive Officer

Professor Charles Maldarelli

Professor Alex Couzis

Professor Morton Denn

Professor Lane Gilchrist

Professor Ponisseril Somasundaran

Supervisory Committee

The City University of New York

ABSTRACT

A Theoretical and Experimental Study of Surfactant Transport from a Micellar Solution to a Clean Air/Water Interface

By Qing Song

Under the supervision of Professor Charles Maldarelli and Alexander Couzis at Levich Institute and Chemical Engineering Department of City College of New York of CUNY

This dissertation studies the transport dynamics of a water soluble nonionic surfactant $C_{14}E_6$ at the air/water interface at concentration below the critical micelle concentration (CMC) and above the CMC. A method which involves using the pendant bubble as a monolayer film balance is used to directly measure the surface tension as a function of surface concentration. The equilibrium parameters could be uniquely determined by fitting the directly measured equation of state and adsorption isotherm. Instead remarkably different equilibrium parameters for the same surfactant system fit experimental data equally well in the traditional treatment. The kinetic constants are obtained by numerically solving the transport equations for surfactant transport from aqueous solution at concentration below the critical micelles concentration. Theoretically, a model was developed to describe the surfactant transport from micellar solution for the case in which the kinetic rate of breakdown of micelles into monomers is much faster than the rates of bulk diffusion of monomers and micelles. In this limit, the analysis becomes a singular perturbation one, in which micelles diffuse from the bulk to a boundary near the surface, where they breakdown and monomers then diffuse from the boundary onto the surface through a micelle-free zone. Numerical solutions were obtained for the transport equations using a front trapping scheme to solve for the time

dependent movement of the boundary between the micelle and micelle-free zones. Experimentally, dynamic reductions in surface tension were measured for adsorption onto a clean bubble surface by using the pendant bubble technique, and these were compared to the transport solutions. For low micellar concentrations, the experimental results were in perfect agreement with theory with no adjustable constants; for larger micellar concentrations the dynamic tension reductions become much faster then the theoretical predictions. The more rapid experimental relaxation in tension suggests that micelles may be adsorbing directly on the surface, a process not taken into account in the modeling and a significant conclusion of this study. Experimentally, visual evidence of the micelle-free zone next to the surface is provided by using fluorescence microscopy.

ACKNOWLEDGEMENTS

Among those people I have to thank, my advisor Professor Charles Maldarelli and Alexander Couzis stand out. Charles has been a consistent source of intellectual wealth and inspiration to me. Alex has been the source of deep technique knowledge as well.

Among my other committee members, Professor Ponisseril Somasundaran at Columbia University has significantly contributed to the intellectual content of this thesis. I am also really appreciated the contribution of Professor Acrivos at Levich Institute of City College. Among the way, Andy has posed probing approach which led to a very elegant solution for the movement of the micelle-free zone for the short contact times when the interface was first created. His lectures of perturbation method and creeping flow was a very educative and yet joyful experience in City College. In setting up the numerical algorithm, Professor John C. Strikwerda of the Computer Science and Statistics Department at the University of Wisconsin-Madison, has been great helpful for developing the highly efficient front trapping technique to model the movement of the micelle free zone boundary. I also want to thank Professors Morton Denn and Lane Gilchrist for serving on my thesis research committee and for offering their valuable suggestions on my research.

I would like to thank my dear friend Xiaojing Lu, who gave me a lot of help whenever I needed her. I also like to thank many graduate students and post-doc in City College that I have had pleasure of working with over the past several years for making my time at City College of New York memorable and deeply rewarding. Those people are Dr.

Fengqiu Fan, Dr. Jose Lorenzo, Dr. Ravichandra Palaparthi, Dr. German Drazer, Dr. Igor Baryshev, Ashish Taneja, Makonnen Payne, Jon Halverson, Nikhil O Kalyankar, Fengfeng Huang, Jingqin Cui, Andy Eng and Zhenrong Xu.

Finally, my undying gratitude is to my parents, my husband and my son, who gave me various supports. Their encouragement and love has been a crucial driving force in the pursuit of goals during my academic life.

Contents

List of Tables

Tables

List of Figures

Figures

CHAPTER 1 INTRODUCTION AND RESEARCH SCOPE

1.1 Dynamic Surface Tension

A surfactant is an amphiphillic molecule consisting of a nonpolar or hydrophobic group and a polar or hydrophilic group which are spatially disjoint from one another in the molecule. The nonpolar group (denoted by **R**) is usually a string of hydrocarbon methylene groups (-(CH_2)-) which are arranged in one (or more) chains each of which may be branched or unbranched. The polar group can be uncharged as a hydroxyl (**R**-OH), or polyoxyethylene ((**R**-(-OCH_2CH_2-)$_n$-OH) group, anionic as a carboxylate (**R**-COO^-), sulphate (**R**-SO_3^-) or sulphonate group (**R**-OSO_3^-), cationic as a quartenary ammonium group (**R**-NR'_3^+), or amphoteric (or zwitterionic) in which the polar group contains a negative and positive group as sulfbetaines (**R**-$N^+(CH_3)_2CH_2CH_2SO_3^-$).

Surfactants dissolved in fluid systems consisting of two immiscible phases of significantly different polarity have a strong tendency to adsorb at the interfaces between the phases. Surfactants relocate at fluid interfaces because at these interfaces they can configure themselves so that the polar moiety remains immersed in the aqueous phase (thereby enabling the strong interaction between the polar group and water) and the nonpolar moiety is positioned in the air or the hydrophobic phase. The adsorption lowers the free energy of the system, and reduces the surface or interfacial tension γ of the fluid interface in proportion to the amount adsorbed (or surface concentration).

As the bulk concentration of surfactant is increased, the adsorption at the surface becomes saturated, and additional surfactant dissolved in the liquid phases can form a

variety of bulk aggregate structures or micelles. Micelles are arranged so as to shield the part of the surfactant incompatible with the liquid phase. Thus for surfactants adsorbed in water, the simplest and first structure that emerges as the concentration is increased is the spherical micelle in which the chains cohere together in a core surrounded by a corona of the polar groups. This concentration is termed the critical micelle concentration or CMC. A comprehensive introduction to the chemistry of surfactant molecules is given in the text by Rosen[1] and of surfactant phase behavior in Evans and Wennerstrom[2].

When a fresh interface is formed in a solution containing a soluble surfactant, the amphiphiles immediately adjacent to the interface kinetically adsorb onto the surface, decreasing its sublayer concentration. If the bulk concentration is below the CMC, then surfactant monomer diffuses from the bulk phase to the sublayer to resupply surfactant. So the dynamic adsorption behavior is controlled by two steps: the first step is an adsorption process, which is governed by the kinetic jump of surfactant from the sublayer onto the surface; the second step is a bulk mass transfer process which is governed by the diffusion of surfactant from the bulk phase to the sublayer. A schematic of these processes is shown in Figure 1.1.

With the surfactant adsorption, the surface tension will decay from γ_0, the surface tension of the solvent, to the equilibrium surface tension γ_{eq}. The non-equilibrium surface tension is called dynamic surface tension (DST). The rate of tension reduction increases with increasing bulk solution concentration, C_b because both the kinetic and diffusive processes are faster. Kinetic and diffusive transport of surfactant below the CMC is reviewed in the survey article of Chang and Franses[3].

1.2 Technological Importance of Dynamic Surface Tension

Surfactants find many applications in interfacial industrial technologies because of their surface tension lowering ability. In practical applications, both the equilibrium and the dynamical surface tension behavior of surfactant solutions can be important, and in high speed interfacial processes, the dynamic surface tension behavior is the more important one. Examples include:

1. The rapid water wetting of fabric for surface treatment, dyeing, or resin impregnation[4-6]: An aqueous solution placed on the surface of a fabric penetrates into the fabric by capillary suction. Rapid wetting of the fabric is usually desired for the delivery of a resin or dye into the fiber matrix. Surfactant is often used to accelerate the wetting process. Surfactant adsorbing at the interface reduces the contact angle, causing the capillary pressure in the advancing liquid meniscus to decrease and thereby increasing the driving force for the impregnation flow. Bifurcation of the meniscus in the fabric matrix continually increases the interfacial area at the advancing front; this reduces the surface concentration at the front, requiring fast adsorption to maintain the rapid spreading. The importance of rapidly lowering the tension to increasing the rate of wetting is clearly demonstrated by Hua and Rosen[5], who measured the wetting out time (WOT; the time necessary for a standard section of textile, placed on the surface of an aqueous solution, to drop by its own weight into the solution because of the water impregnation) as a function of the dynamic tension of various surfactants as measured at one second from the interface creation by the maximum bubble pressure method. This work by Hua and Rosen

showed that the WOT correlated with the dynamic surface tension data for one second and not the equilibrium surface tension.

2. Surfactant facilitated drop spreading (cf. the text by Tadros[7] and the articles by Furmidge and coworkers[8-13]): Herbicides are delivered to the leafy surfaces of plants by dissolution of the surface active ingredients in an aqueous solution that is sprayed onto the foliage. The efficacy of a formulation depends on the amount of the surface active ingredients retained on the leaf surface. Deposited aqueous drops of the formulation usually do not spread well because of the waxy coat on the leaf surface, and they therefore tend to slide off of or bounce from the leaf surface. Surfactant is used to facilitate drop spreading and enhance droplet retention by increasing the drop contact area. Surfactant adsorbing from solution reduces the contact angle that increases the spreading rate. Adsorption must be rapid because as the drop spreads, new interfacial area is created and the surface concentration is depleted.
3. Foamability: Foam is produced when a gas is injected into a solution containing a soluble surfactant. High quality foams are produced from finally textured foams in which surfactant adsorbs rapidly to the growing surface of the bubble to reduce the tension and cause the bubble to detach at a small size.[14-16]

Other examples are found in enhanced oil recovery. Aqueous foams are often used to increase the sweep efficiency in carbon dioxide flooding processes, and dynamic tension controls the elasticity of the interface and thereby the stability of foam. More examples can be found in food processing, particularly involving emulsions containing proteins,

where the dynamic adsorption of the protein again controls the elasticity of the interface and the stability of the food emulsion and in slide coating.[17]

1.3 Research Scope

The above examples illustrate clearly that the rapid reduction of the interfacial tension by surfactant adsorption is crucial to the performance of these technologies. To achieve rapid reduction of the tension, high bulk concentrations of surfactant are used that typically exceed the CMC. Thus understanding the mechanisms of surfactant transport to the interface for micellar solutions and the accompanying reduction of tension is critical in designing and/or optimizing such processes. Despite this fact, most of the research done to date as we review in the chapter 2 focuses on understanding surfactant transport and tension reduction at concentrations below CMC.

When surfactant adsorbs from solution with a concentration greater than the CMC, several additional processes occur that are not present at low concentrations. Upon the creation of a clean interface in a micellar solution the adsorption of the surfactant monomers from the region adjacent to the surface upsets locally the micelle-monomer equilibrium causing micelles to dissociate. This results in a diffusive flux of micelles to the surface to restore the equilibrium. The diffusive transport of micelles and monomers and kinetic adsorption as well as the kinetics of micellar break-up then determine the rate of dynamic tension reduction. A general picture of surfactant and micelle diffusive transport and kinetic exchange above the CMC is shown in Figure 1.2.

The scope of this research is to develop a theoretical framework to describe the surfactant transport and dynamic surface tension reduction for solution concentrations above the CMC and verify the framework by appropriately designed experiments

measuring dynamic tension and visualizing the transport. The work will specifically focus on aqueous surfactant solutions, and use primarily the nonionic polyethylene oxide mono ether (polyethoxylated) surfactants C_iE_j ($CH_3(CH_2)_{i-1}(OCH_2CH_2)_jOH$). The thesis is organized in the following way. Literature Review is detailed in Chapter 2. Chapter 3 covers the measurement of equilibrium and dynamic surface tension, and determination of kinetic constants. Chapter 4 presents the proposed model which describes the surfactant transport from micellar solution to a clean air/water interface and comparison with experiments. The fluorescence visualization of this transport model is presented in Chapter 5. Chapter 6 describes the future work. Chapter 7 summarizes this dissertation research and presents the conclusions.

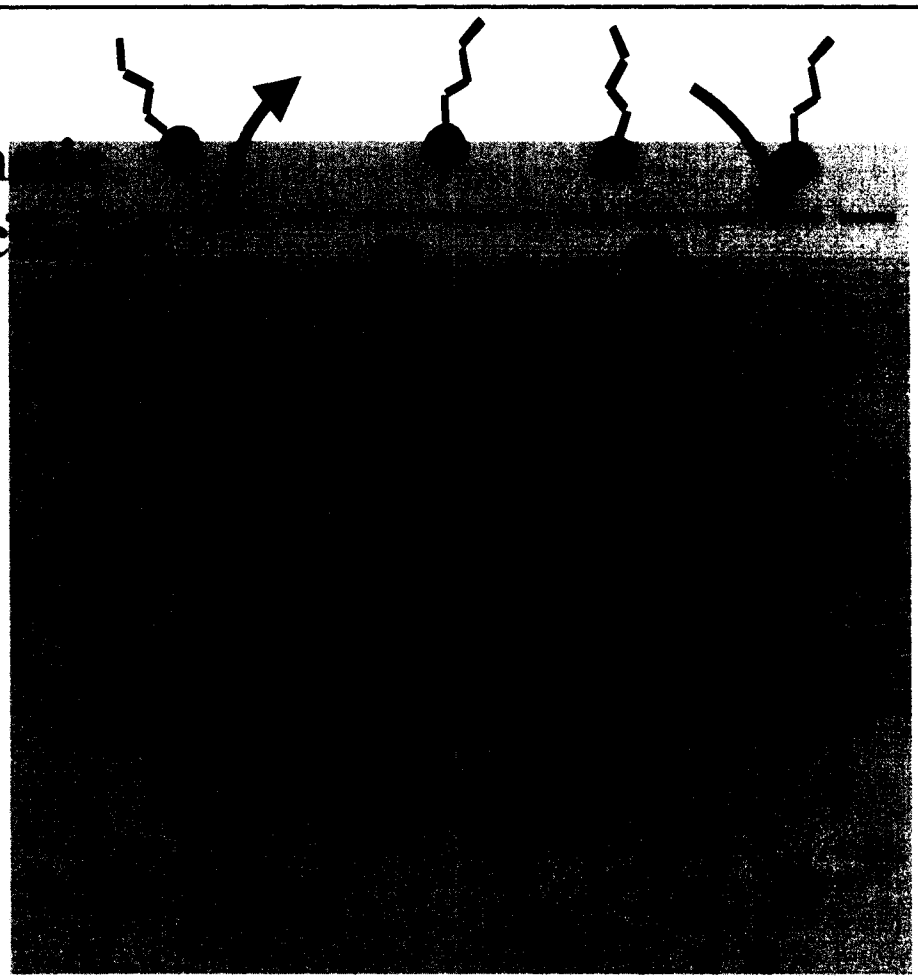

Figure 1.1: Schematic representation of surfactant adsorption onto the surface or desorption from the surface for bulk concentrations below the CMC

Kine
Exch

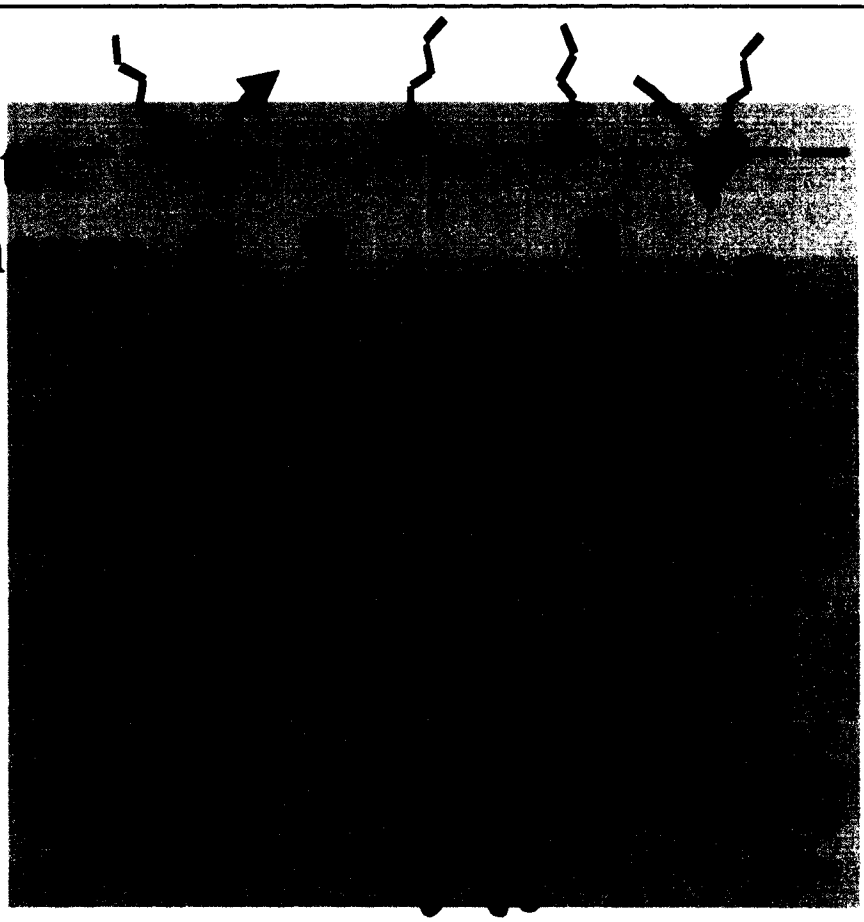

Figure 1.2: Schematic representation of surfactant adsorption/desorption from micelle solution

CHAPTER 2 LITERATURE REVIEW

2.1 Equilibrium Thermodynamics of Surfactant Adsorption: Adsorption Isotherms and Equations of State

The equilibrium adsorption isotherm $\Gamma(C_0)$ is the relationship between the surfactant concentration in the bulk C_0 and the adsorbed amount at the interface Γ. The *(equilibrium) equation of state* describes the dependence of the surface tension on the surface concentration ($\gamma(\Gamma)$). The Gibbs thermodynamic treatment[1] of an interface provides a relationship between the tension and the surface and bulk concentrations for solutions below the CMC where in addition it is assumed that the concentration of surfactant is dilute:

$$\Gamma = -\frac{1}{nRT}\frac{d\gamma}{d\ln(C_0)} \qquad (2.1)$$

Here Γ is the equilibrium surface concentration, C_0 is the bulk concentration, R is the gas constant, T the Kelvin temperature. n=1 for non-ionic surfactant, neutral molecules or ionic surfactants in the presence of excess electrolyte, and n=2 for 1:1 ionic surfactants, assuming the interface is of electrical neutrality, n=3 for bis (quaternary ammonium) surfactant. In the case of non-ideal solutions, the bulk concentration C_0 is replaced by the activity a.

Theoretical treatments of surfactant adsorption and the equation of state start by constructing an expression for the surface free energy of the monolayer, then obtaining the chemical potential and finally equating this potential to the bulk potential to obtain the isotherm. The companion expression for the equation of state is obtained by using the theoretical isotherm in the Gibbs equation and integrating. Two approaches for

constructing models for the equilibrium adsorption are the localized adsorption model where surfactant adsorbs onto specific sites (leading to the Langmuir and Frumkin isotherms), and non-local models which allow the surfactant to be mobile on the surface and lead to the Volmer and van der Waals models[2]. In what follows we describe these two different approaches, and finally an illustration of how, from equilibrium measurements of the tension as a function of the bulk concentration, the constants in these models are obtained.

2.1.1 Localized Models: Langmuir and Frumkin Isotherms

The Langmuir and Frumkin formulations for surfactant adsorption at an interface are a localized or site model in which surfactant adsorbs onto specific sites. The number of sites per unit area is given (in moles per unit area) by Γ_∞. This quantity is also known as the maximum packing concentration. In the site specific model the excess free energy of the surface containing N_∞ total sites and N filled sites in an area A is given by the standard chemical potential multiplied by N (i.e. $N\mu_s^\circ$), an entropy of mixing term and a term to account for the energy of interaction among neighboring molecules (with parameter α, positive for repulsion and negative for attraction):

$$A^s = N\mu_s^0 + RT\left[N\ln\left[\frac{N}{N_\infty}\right] + (N_\infty - N)\ln\left[\frac{N_\infty - N}{N_\infty}\right]\right] + N\alpha\frac{1}{2\Gamma_\infty}\frac{N}{A} \qquad (2.2)$$

From the above expression for the Helmholtz free energy, the chemical potential of the surfactant molecule follows from $\mu_s = \left(\frac{\partial A^s}{\partial N}\right)_{A,T}$ and the chemical potential is therefore given by:

$$\mu^s = \left[\frac{\partial A^s}{\partial N}\right]_{A,T} = \mu_s^0 + RT\ln\left[\frac{\theta}{1-\theta}\right] + \frac{N\alpha}{\Gamma_\infty A} = \mu_s^0 + RT\ln\frac{\theta}{1-\theta} + \alpha\theta \tag{2.3}$$

Where $\theta = \frac{\Gamma}{\Gamma_\infty} = \frac{N}{N_\infty}$ $\Gamma = \frac{N}{A}$

Equating this chemical potential to the potential of the surfactant molecule in the bulk $\mu_b = \mu_b^0 + RT\ln C_0$ yields the adsorption isotherm:

$$\frac{\theta}{1-\theta}\exp(K\theta) = \frac{C_0}{a} \tag{2.4}$$

Where $a = \exp(-\frac{\mu_b^0 - \mu_s^0}{RT})$ and $K = \alpha / RT$. Substituting the above adsorption isotherm (2.4) into the Gibbs adsorption equation (2.1) yields the equation of state:

$$\gamma = \gamma_c + RT\Gamma_\infty \ln(1-\frac{\Gamma}{\Gamma_\infty}) - \frac{K}{2}\left(\frac{\Gamma}{\Gamma_\infty}\right)^2 \tag{2.5}$$

Where γ_c is the tension of the clean interface. When K is equal to zero, the Langmuir adsorption isotherm and equation of state are obtained:

$$\frac{\theta}{1-\theta} = \frac{C_0}{a}$$
$$\gamma = \gamma_c + RT\Gamma_\infty \ln\left(1-\frac{\Gamma}{\Gamma_\infty}\right) \tag{2.6}$$

At the limit of low surface concentration, one recovers a Henry isotherm and a linear equation of state.

2.1.2 Non-localized Models: Van der Waals and Volmer Isotherms

For the nonlocalized models, surfactants move around on the surface. If the number of surfactants in an area A is N (Γ=N/A), the excess Helmholtz free energy is given by:

$$A^s = N\mu_s^0 + NRT(\ln\frac{N}{A} - 1) - NRT\ln(1 - \frac{N}{A}b) + \alpha N\frac{N}{A} \tag{2.7}$$

Where b is the excluded area per molecule and α is the interaction parameter

$$\mu_s = \left[\frac{\partial A^s}{\partial N}\right]_{A,T} = \mu_s^0 + RT\ln\Gamma - RT\ln(1-\Gamma b) + \Gamma RT\frac{b}{1-\Gamma b} + 2\alpha\Gamma \tag{2.8}$$

Using the same procedure as above we obtain the van der Waals adsorption isotherm and equation of state:

$$\begin{aligned} &\frac{\Gamma}{1-\Gamma b}\exp\left(\frac{\Gamma b}{1-\Gamma b}\right)\exp\left(\frac{2\Gamma\alpha}{RT}\right) = \exp\left(\frac{\mu_b^0 - \mu_s^0}{RT}\right)C_0 \\ &\gamma_c - \gamma = \frac{RT}{b}\left(\frac{\Gamma b}{1-\Gamma b}\right) + \alpha\Gamma^2 \end{aligned} \tag{2.9}$$

When there is no interaction between adsorbed molecules, we recover the Volmer isotherm and equation of state:

$$\begin{aligned} &C_0 = K_v\left(\frac{\Gamma}{\Gamma_\infty - \Gamma}\right)\exp\left(\frac{\Gamma}{\Gamma_\infty - \Gamma}\right) \\ &\gamma_c - \gamma = \frac{\Gamma RT}{1-\Gamma b} \end{aligned} \tag{2.10}$$

2.1.3 Equilibrium Measurements of the Surface Tension and Calculation of Adsorption Model Constants

There are many methods for measuring equilibrium surface tensions between liquid and air. These can be divided into the following: force methods, such as the Du Noüy ring, Wihelmy plate and drop weight techniques; shape methods such as the sessile, pendant and spinning drop or bubble techniques; pressure methods such as the maximum bubble pressure or growing drop method; and other methods such as the oscillating jet. These are reviewed in the text by Adamson and Gast[1]. In this study we will use the Wilhelmy plate and particularly the pendant bubble or drop technique as the latter is suitable for dynamic tensions as well, and so we review these below.

In the Wilhelmy plate method, a thin plate hangs from a force transducer (usually an electrobalance) which is attached to one of its edges; the opposite edge is allowed to touch the liquid/air surface creating a wetting perimeter around the plate. The plate is drawn into the liquid by the capillary force, and the action of this force on the plate is measured by the transducer. The tension is then calculated from the measured force which is equal to $\gamma\ell$ where ℓ is the wetted perimeter. If the liquid does not completely wet the surface but instead subtends a finite contact angle θ, then the action of the capillary force is $\gamma\ell\cos\theta$, where the contact angle must be measured separately;

In the pendant drop or bubble technique a hanging drop of the liquid is placed on the tip of a needle, or a bubble is formed at the rim of an inverted needle immersed in the liquid solution. The drop will tend to deform with the effect of gravitation; by measuring the shape of the drop or bubble, surface tension could be calculated. The most accurate procedure is to measure the bubble or drop profile from a digital image. Figure 2.1 is a schematic of the apparatus. The system consists of an image forming and recording system, a bubble forming system and a video-image profile digitizer. The image forming

and recording system has a light source (a halogen lamp with constant light intensity), a plano-convex lens system for collimating beam, a quartz cell enclosed in a thermostatically controlled chamber, an objective lens, and a video camera whose output is connected to a image digitizer installed in a computer. The bubble-forming system has a stainless-steel inverted needle, which is connected to the normally closed port of a three-way miniature solenoid valve via teflon tubing. The common port of the valve is connected by the same teflon tubing to an gas-tight Hamilton syringe placed in a syringe pump. The valve is controlled by the output signal of a computer. This setup allows for short times of bubble formation (less than few hundred milliseconds) . The experimental loci are determined by edge detection from the digital image. These loci are compared with theoretical interfacial shapes generated by the solution of the Young-Laplace equation; the surface tension, which governs the theoretical shape, is varied until the theoretical shape agrees well with the experimental loci. The Young-Laplace equation which defines the pressure drop across a curved interface can be transformed into three first-order differential equations for the spatial positions x and z and turning angle ϕ of the interface as a function of the arc length s. The first-order equations have the following form by nondimensionalizing variables by the radius of curvature at the apex (R_0), i.e. ($X = \frac{x}{R_0}, Z = \frac{z}{R_0}$, and $S = \frac{s}{R_0}$):

$$\begin{aligned} \frac{d\phi}{dS} &= 2 + BZ - \frac{\sin\phi}{X} \\ \frac{dX}{dS} &= \cos\phi \\ \frac{dZ}{dS} &= \sin\phi \end{aligned} \qquad (2.11)$$

Where B is the Bond number or capillary constant and is given by $\Delta\rho g R_0^2 / \gamma$, $\Delta\rho$ is the density difference between the fluids and g is the gravitational acceleration constant. The boundary condition of above equation is X(0)=Z(0)=ϕ(0)=0. Above equations are integrated and the surface tension is calculated by finding values of the Bond number and radii of curvature which minimizes the difference between the experimental and theoretical curves.

In Figure 2.2 we present some sample data for the equilibrium surface tension of the nonionic polyethoxylated surfactant $C_{12}E_6$ as a function of bulk concentration at the air/water interface using both the pendant bubble and the Wilhelmy plate techniques[3]. We note that both techniques are in reasonable agreement. Also shown in the figure is the fitting of the data to the Langmuir and Frumkin equations of state. From the Langmuir relation we find Γ_∞=2.42x10^{-6}mol/m^2 and a=1.137x10^{-4}mol/m^3 and for the Frumkin, Γ_∞=3.48x10^{-6}mol/m^2 a=3.49x10^{-5}mol/m^3 and K= 6.652 (indicating repulsion dominance). We note finally from the figure that at a high enough concentration the tension does not change with an increase in concentration. This indicates the formation of surfactant aggregates in the bulk (micelles), and the concentration at which this occurs is the critical micelle concentration or CMC.

2.2 Theory and Experiment on Dynamic Surface Tensions for Bulk Concentrations Below the Critical Micelle Concentration

2.2.1 Theoretical Formulation

The mass transfer picture for surfactant adsorption to a clean interface and the accompanying dynamic tension reduction from a uniform bulk phase with concentration

C_0 below the critical micelle concentration was sketched in the chapter 1 (for general reviews see Franses[4] and Miller[5-7]. The theoretical framework of this mass transfer begins with the formulation of the diffusion of surfactant in the bulk. We illustrate the formulation for a planar interface, with the surface at x=0 and with no convective effects:

$$\frac{\partial C}{\partial t} = D\frac{\partial^2 C}{\partial x^2} \tag{2.12}$$

$$D\frac{\partial C(0,t)}{\partial x} = \frac{d\Gamma(t)}{dt} \text{ at x=0} \tag{2.13}$$

With the initial and boundary conditions

$$C(x,t=0) = C_0 \tag{2.14}$$

$$\Gamma(t=0) = 0 \tag{2.15}$$

$$C(x=\infty,t) = C_0 \tag{2.16}$$

Here C(x,t) is the surfactant concentration, Γ is the surface concentration, t is the time, D is the monomer diffusivity coefficient in the bulk solution, x is the distance from the subsurface, C_0 is the initial bulk concentration. By the Laplace transform, the solution to above equations could be expressed in terms of unknown subsurface concentration $C_s(t)=C(x=0,t)$

$$\Gamma(t) = 2C_0(Dt/\pi)^{1/2} - (D/\pi)^{1/2}\int_0^t \frac{C(0,\tau)}{(t-\tau)^{1/2}}d\tau \tag{2.17}$$

This is the classical solution of Ward and Tordai for the unsteady diffusion toward an initially clean planar surface[8].

The above formulation is incomplete because the kinetics at x=0 has not been specified. In most cases, the adsorption/desorption step is formulated by means of an Arhenius rate equation of a localized adsorption model in which the adsorption rate is

proportional to the sublayer concentration C_s and the fraction of unoccupied surface area, while the desorption rate is proportional to the amount adsorbed[9-11]. Thus

$$\frac{d\Gamma}{dt} = \beta' \exp(-E_a / RT) C_s(\Gamma_\infty - \Gamma) - \alpha' \exp(-E_d / RT)\Gamma \qquad (2.18)$$

Where β' and α' are the kinetic rate constants for adsorption and desorption, E_a and E_d are the energies of activation for adsorption and desorption, respectively and are in principle functions of the surface concentration, Γ_∞ is the maximum surface concentration, T is the temperature, and R the gas constant. In the usual approach, the activation energy for adsorption is taken independent of the surface coverage, and that for desorption linear in the adsorbed amount. Thus

$$\frac{d\Gamma}{dt} = \beta\Gamma_\infty C_s(1 - \frac{\Gamma}{\Gamma_\infty}) - \alpha\Gamma \exp(K\Gamma / \Gamma_\infty) \qquad (2.19)$$

Here K is a nondimensional parameter describing a linear variation of the activation energy for desorption on coverage and accounting for the cohesive van der Waals forces between the hydrocarbon chains of surfactant molecules, and repulsive forces between the surfactant headgroups. At equilibrium, the above expression leads to the Frumkin isotherm derived early from equilibrium considerations (2.1.1):

$$\Gamma_{eq} = \Gamma_\infty \frac{C_0}{C_0 + a \bullet \exp\left(K\Gamma / \Gamma_\infty\right)} \qquad (2.20)$$

Where a= α/β. As we described earlier (2.1.3), the equilibrium constants a and K and maximum surface coverage Γ_∞ can obtained by fitting equilibrium data of surface tension as a function of the bulk concentration.

Solutions for the above set of equations in which the mass transfer in the bulk is coupled to kinetic exchange have been carried out for the case in which the kinetics is infinitely fast and the sublayer and surface are in equilibrium (diffusion limited), and the case in which the kinetics is finite. We discuss these two cases separately below.

2.2.1.1 Diffusion Limited

In this model the diffusion process from the bulk to subsurface is the rate-controlling step, and the timescale of adsorption from the subsurface to the interface is very fast. So this is a local equilibrium model; i.e. the surface concentration $\Gamma(t)$ is always at equilibrium with the sublayer concentration C(0,t), which changes as diffusion occurs. In this case, the thermodynamic equilibrium isotherm is applied to describe the relationship between $\Gamma(t)$ and C(0,t), and this is solved in conjunction with the Ward and Tordai expression. If the bulk concentration is small ($C_0/a \ll 1$) the quasi-equilibrium condition is linear, $\Gamma = K_H C$ where $K_H = \Gamma_\infty / a$ and we can obtain an analytical solution. For the sublayer concentration we find:

$$C(0,t)/C_0 = \Gamma/\Gamma_e = 1 - \exp(Dt/K_H^2)erf[(Dt)^{1/2}K_H] \qquad (2.21)$$

By considering the limiting behavior of the exponential and complementary error functions, we could obtain the short and long-time approximations for Eq.(2.21).

Short-time approximation

$$\frac{\Gamma}{\Gamma_e} = \frac{2}{K_H}\left(\frac{Dt}{\pi}\right)^{1/2}\left[1 - \frac{(\pi D)^{1/2}}{2K_H}t^{1/2} + \cdots\right] \qquad (2.22)$$

Long-time approximation

$$\frac{\Gamma}{\Gamma_e} = 1 - \frac{K_H}{(\pi D)^{1/2}}t^{-1/2}\left(1 - \frac{K_H}{2Dt} + \cdots\right) \qquad (2.23)$$

So we can see that Γ is only proportional to $t^{1/2}$at the initial state of adsorption, a result which can be shown to be true even for the case of a nonlinear isotherm.

For higher bulk concentrations the equations have to be solved numerically because of the nonlinearity of the Langmuir or Frumkin adsorption isotherms. These diffusion limited solutions have been undertaken by several authors, using a variety of techniques as reviewed by Franses and also Miller.[4-7]. Although the unsteady diffusion equation can be numerically solved directly, the usual approach is to solve the isotherm along with the Ward and Tordai equation by numerically integrating the convolution integral. Diffusion limited solutions will be illustrated below in comparison to the mixed simulations.

2.2.1.2 Mixed diffusion/kinetic adsorption

In contrast to the diffusion-controlled adsorption, in mixed diffusion/kinetic adsorption, the sorption kinetics are not infinitely fast, i.e. there is an activation energy barrier to transfer of the solute molecules between the subsurface and the surface. In this mechanism, the surfactant monomers undergo diffusion from the bulk phase to the sublayer, obeying the same diffusion equations as for the diffusion-controlled mechanism. When surfactant monomers arrive at the sublayer, monomers are not instantaneously adsorbed at the interface. In order to adsorb, a monomer has to overcome the energy barrier described by the kinetic exchange equation. This adsorption barrier will decrease the adsorption rate, and the transfer of monomers from the subsurface to the interface along with the diffusion are the rate-controlling steps. In this case, the Ward and Tordai equation has to be solved along with the first order kinetic equation to obtain $\Gamma(t)$.

Sutherland first solved the mixed kinetic adsorption with linear kinetics for $C_0/a<<1$ [12]. The time-dependent surface concentration $\Gamma(t)$ is given by:

$$\Gamma(t)/\Gamma_e = 1 - \frac{\beta}{\beta-\alpha}\exp(Dt\alpha^2)erfc[\alpha(Dt)^{1/2}] + \frac{\alpha}{\beta-\alpha}\exp(Dt\beta^2)erfc[\beta(Dt)^{1/2}] \qquad (2.24)$$

Here

$$\alpha = \frac{k_H^a}{2D} - (\frac{k_H^{a\,2}}{4D^2} - \frac{k_H^d}{D})^{1/2} \qquad (2.25)$$

and

$$\beta = \frac{k_H^a}{2D} + (\frac{k_H^{a\,2}}{4D^2} - \frac{k_H^d}{D})^{1/2} \qquad (2.26)$$

By considering the limiting behavior of the exponential and complementary error functions, Hansen gave certain limiting cases for this problem[13].

For short times,

$$\frac{\Gamma(t)}{\Gamma_e} = \frac{k_H^a t}{K_H}[1 - \frac{4k_H^a}{3(\pi D)^{1/2}}t^{1/2} + \cdots] \qquad (2.27)$$

For long times,

$$\frac{\Gamma(t)}{\Gamma_e} = 1 - \frac{K_H}{(\pi Dt)^{1/2}}[1 - \frac{K_H^2}{2Dt} + \frac{K_H}{k_H^a t} + \cdots] \qquad (2.28)$$

Thus significantly while the long time behavior is not affected, the additional kinetic step slows down the initial adsorption from an order $t^{1/2}$ to an order t.

For higher concentrations the mixed kinetic and diffusive transport has been solved by several authors as reviewed by Franses and Miller. [4-7] . An illustration[3] of the diffusion limited and mixed solutions for Frumkin kinetics for different values of C_b/a is given in Figure 2.3 (a) and (b). In these figures the nondimensional dynamic tension

$\gamma^* = \frac{\gamma_c - \gamma(\tau)}{\gamma_c - \gamma_e}$ is plotted as a function of the nondimensional time (τ=tD(a/Γ_∞)^2 for increasing values of the kinetic exchange $k_a=\alpha(\Gamma_\infty/a)^2/D)=\beta\Gamma_\infty^2/(Da)$. The parameters used in the simulation are those for $C_{12}E_6$ whose equilibrium adsorption was illustrated in Sec. (2.1.2): K = 6.652, a=3.49x10^{-5} mol/m^3, and Γ_∞=3.48x10^{-6} mol/m^2. Finally the value of the diffusion coefficient used D=6.0x10^{-10} m^2/s which was obtained by fitting kinetic data for this surfactant (see below).

Note from the above figures the faster relaxation for the diffusion control at the higher bulk concentrations, and the slower rate of relaxation for the mixed kinetic/diffusive transport relative to the diffusion control.

2.2.2 Measurements of Dynamic Tension Reduction and the Determination of the Kinetic Constants

The methods we have mentioned previously (Chapter 1.3) for measuring equilibrium tensions at the air/liquid surface – Wilhelmy plate, drop weight, the shape analysis of pendant drops and bubbles and the spinning drop, the maximum bubble pressure and oscillating jet methods - can all, in principle, be used to measure dynamic tension reductions as surfactant adsorbs onto an initially clean surface.[4-7] For clean interface adsorption and re-equilibration, by modeling the kinetic exchange, and the bulk diffusive and convective transport (for measurements that involve flow), the surface adsorption as a function of time can be predicted as a function of the surfactant transport parameters. From the equation of state the model prediction of the tension relaxation can be computed, and from a comparison of the model with the experimental results, ideally, the kinetic constants and the diffusion coefficient can be inferred.

The interpretation of the surface tension relaxations begins by assuming that kinetic exchange is very fast, and that the transport is diffusion controlled over the time scales (or frequencies) of the experiment. With this assumption, an apparent diffusion coefficient is calculated. It is difficult to measure separately the diffusion coefficient of surfactant monomers by independent methods such as light scattering because the monomer concentration is usually very low. The apparent value is therefore usually compared to a value obtained from the Stokes-Einstein equation (assuming some value for the hydrodynamic radius based on molecular considerations); if the apparent value is in reasonable agreement with the Stokes-Einstein value then no further interpretation of the experiment is done, the apparent value is considered as the diffusion coefficient, and the kinetic constants remain unresolved. If the calculated apparent diffusion coefficient differs greatly from the Stokes-Einstein expectation, then the transport process is either modeled as kinetically controlled, and comparison with data yields the kinetic parameters, or as mixed, and kinetic constants and diffusion coefficients are derived from a fit of the data. Recent research has shown in particular that by using high bulk concentrations of surfactant, the kinetic scale becomes progressively slower relative to diffusion, and kinetic effects can be ascertained and their kinetics measured.

An illustration of the measurement of the kinetic rate constants and the diffusion coefficient by this method is given in Figure 2.4 for the adsorption of $C_{12}E_6$ to a clean interface pendant bubble interface, with the dynamic tension measured by the shape analysis of the bubble[3]. In this measurement, the bubble is created impulsively in less than a tenth of a second; the hydrodynamic disturbance clears after one second and the modelling of the mass transfer follows the equations detailed in the previous section

without convection only in a spherical geometry to approximate the pendant form. The figure shows the relaxation at different bulk concentrations; as the concentration increases, the relaxations are faster and the tensions reduce to lower equilibrium values from the clean interface value of 72.6 dyne/cm (mN/m). Each of these concentrations are below the critical micelle concentration for $C_{12}E_6$.

2.3 Thermodynamics of Micellization

2.3.1 Chemical Potential

Once the concentration of surfactant solutions exceeds the critical micelle concentration (CMC), surfactant monomers will spontaneously self assemble to create a variety of structures. The hydrophobic groups such as hydrocarbon chains will present themselves inside the aggregates, which serve as favorable microenvironment for the location of hydrophobic groups. The hydrophilic head groups orient themselves toward the aqueous phase. In this process, the transfer of the hydrophobic groups out of water and into the oil-like interior of the aggregates drives micellization, and hydrophilic group's repulsion as they come close oppose it. Under such circumstances there exits specific limits for the growth of this process, and aggregates will cease to grow when they reach a certain size. Above the CMC, adding more surfactants simply produces more micelles over a considerable concentration range rather than further growth of existing micelles.

The thermodynamic principles of self-assembly could be treated by a variety of models. Here we chose the most general description, i.e. the multi-component solution model. In this model[14], the surfactant solution is visualized as a multi-component

system consisting of the solvent, surfactant monomers, and aggregates of all possible sizes and shapes. Each of these aggregates is regarded as a distinct chemical species with a characteristic chemical potential μ_i. The total Gibbs free energy of the solution consisting of N_s solvent molecules, N_1 surfactant monomer and N_n aggregates of aggregation number n is

$$G = N_s\mu_s + N_1\mu_1 + \sum N_n\mu_n \tag{2.29}$$

Here the subscript s refers to the solvent and n to the aggregate containing n surfactant molecules. At the equilibrium, the total Gibbs free energy is the minimum. This equilibrium condition, combined with the Gibbs-Duhem relation gives:

$$\delta G = (\delta N_s)\mu_s + (\delta N_1)\mu_1 + \sum(\delta N_n)\mu_n = 0 \tag{2.30}$$

With following constraints for a given total surfactant solution concentration:

$$N_1 + \sum gN_n = cons\tan t \quad \text{or} \quad \delta N_1 = -\sum g\delta N_n \quad \text{and} \quad \delta N_s = 0 \tag{2.31}$$

The equilibrium condition is reduced to $\frac{\mu_n}{n} = \mu_1$ (2.32)

This equation indicates that at the equilibrium the chemical potential of the surfactant monomer is equal to the chemical potential per molecule in an aggregate of possible sizes and shapes.

The chemical potential could be expressed as follows under the assumption of a dilute surfactant solution: $\mu_n = \mu_n^0 + kT\ln X_n$ (2.33)

Here the superscript 0 indicates the standard state of the species. It is defined as the pure solvent while the standard states of all the other species are taken as those corresponding to infinitely dilute solution conditions. It also expresses the mean interaction free energy

per molecule. X_n is the concentration of molecules in aggregates of number n (n=1, μ_1^0 and X_1 correspond to isolated molecules, or monomers in the solution)

Applying these relationships in the equilibrium equation of (2.33), we obtain:

$$\mu_n^0 + kT\ln X_n = n\left[\mu_1^0 + kT\ln X_1\right] \tag{2.34}$$

The aggregate size distribution could be derived from above

$$X_n = X_1^n e^{-\left(\frac{\mu_n^0 - n\mu_1^0}{kT}\right)} = X_1^n e^{-\left(\frac{n\Delta\mu_n^0}{kT}\right)} \tag{2.35}$$

$$\Delta\mu_n^0 = \frac{\left(\mu_n^0 - n\mu_1^0\right)}{n} = \frac{\mu_n^0}{n} - \mu_1^0 \tag{2.36}$$

Here $\Delta\mu_n^0$ is the difference in the standard chemical potentials between a surfactant monomer in solutions and a surfactant molecule in an aggregate of size n.

Equation 2.35 will become $X_n = X_1^n$ for $\Delta\mu_n^0 = 0$ n=2,3,4..., which means the molecules in different sized aggregates (including monomers) all experience the same interaction with their surroundings. Because of $X_1 < 1$, $X_n << X_1$ most of the molecules are in the monomer state (n=1). If $\Delta\mu_n^0$ increases as n increases, Equation 2.35 shows that the occurrence of large aggregates becomes less possible. To form large aggregates, the necessary condition is $\Delta\mu_n^0 < 0$ for some value of n, for example, if $\Delta\mu_n^0$ could progressively decrease with increasing n, or if $\Delta\mu_n^0$ could have a minimum value at some finite value of n. The exact functional variation of $\Delta\mu_n^0$ with n will determine many of physical properties of aggregates, such as their mean size and polydispersity.

From the kinetic point of view to consider the self-assembly of surfactant molecules, the association and dissociation of surfactant molecules could be represented as step-wise mechanism as following:

$$A_1 + A_{n-1} \underset{k_n^-}{\overset{k_n^+}{\rightleftharpoons}} A_n \tag{2.37}$$

In the step-wise association and dissociation mechanism, the aggregate of size n is assumed to form through the addition of a monomer to an aggregate of size n-1.

At equilibrium

$$k_n^+ X_1 X_{n-1} = k_n^- X_n \qquad K_n = \frac{k_n^+}{k_n^-} = \frac{X_n}{X_1 X_{n-1}} \tag{2.38}$$

So the equilibrium constant K_n could be linked to the chemical potential difference $\Delta\mu_n^0$ as following:

$$\ln K_n = \ln\left[\frac{X_n}{X_{n-1} X_1}\right] = -\left[\frac{n\Delta\mu_n^0 - (n-1)\Delta\mu_{n-1}^0}{kT}\right] = -\frac{d}{dn}\left[\frac{n\Delta\mu_n^0}{kT}\right] \tag{2.39}$$

Where the latter follows if n is considered to vary continuously.

2.3.2 Structures of aggregates

The forces between the amphiphilic molecules are also very important in determination of structures of amphiphilic molecules associated in the solutions. The hydrophobic attractions of the hydrophobic groups induce the molecules to associate, and the hydrophilic group's repulsions restrain the growth of aggregate. Among these two interactions, one tends to decrease and the other tends to increase the interfacial area per molecule, a. The hydrophobic or interfacial tensions acting at the hydrocarbon-water interface gives rise to the attractive interactions. Steric, a hydration and electrostatic

double-layer interactions between hydrophilic head groups contribute to repulsive interactions. So the repulsive head group forces and attractive hydrophobic interfacial forces will determine the optimum head group area a, at which $\Delta\mu_n^0$ is a minimum.

Israelachivili[15] examined the shapes of aggregates based on the molecular packing consideration. He assumed the hydrocarbon chains are to be fluid and incompressible. The geometry or 'packing' properties of these molecules depend on their optimal area a, the volume v of their hydrocarbon chain or chains, and the maximum effective length that chains can extend. This length is called critical chain length l_c, which sets a limit on chain extension. As expected, the critical chain length l_c is the same order as, though somewhat less than, the fully extended molecular length of the chains l_{max}, which is given by Tanford[16] for a saturated hydrocarbon chain with n carbon atoms:

$$l_c \le l_{max} \approx (0.154 + 0.1265n) \text{ and } v \approx (27.4 + 26.9n) \times 10^{-3} \qquad (2.40)$$

Nanometer for l_{max} and nm^3 for v; n is the number of methylene groups for a straight chain.

Once the optimal surface area a, hydrocarbon chain volume v and critical length l_c are specified for a given molecule -all these could be measured or estimated, and the structure which molecules could pack into consistent with these geometric constraints will be determined. It has been shown by Israelachivili[17] that for surfactants structures of optimal area a, hydrocarbon volume v and critical chain length l_c, the value of the dimensionless packing parameter or shape factor, $\frac{v}{al_c}$ will determine whether they will form spherical micelles ($\frac{v}{al_c} < \frac{1}{3}$), non-spherical micelles($\frac{1}{3} < \frac{v}{al_c} < \frac{1}{2}$), vesicles or

bilayers ($\frac{1}{2} < \frac{v}{al_c} < 1$), or the inverted structures $\frac{v}{al_c} > 1$. Although a great variety of different structures could satisfy above constraints, the entropically favored structure is the structure with the smallest aggregation number will result in the unique structure.

Micellar aggregation numbers are generally determined by light-scattering [18-20], diffusion, sedimentation velocity, sedimentation equilibrium[21], ultrasonic absorption[22], and time-resolved fluorescence[23]. Generally, if the 'dissimilarity' between the surfactant molecules and solvent is greater, the aggregation number is greater. Thus for polyoxyethylenated nonionic surfactants, the aggregation number tends to increase with increasing the length of the hydrophobic groups, and decrease in the number of oxyethylene units surfactants. The temperature has a big influence in aggregation number for polyoxyethlenated nonionic surfactants especially near 'cloud point'. An increase in the temperature could cause a large increase in the aggregation number for this kind of surfactants. For the ionic surfactants, the binding of the counterions to the micelles will contribute to the aggregation number, and the addition of neutral electrolytes also increases the aggregation number. The temperature has a small influence in the aggregation number for this kind of surfactants.

2.4 Experiment and Theory on Micellization Kinetics

Surfactant monomers tend to aggregate and form spherical micelles when the surfactant concentration reaches a critical micelle concentration (CMC). The micelle population density is polydisperse in the number of monomers per micelle, with a rather sharp distribution which can be approximated by a Gaussian function. Micelle aggregation numbers at equilibrium can be determined by fluorescence and light

scattering techniques[24] and usually range from approximately 10 to 100 monomers per micelle.

While micelles are often drawn as static structures of spherical aggregates of oriented molecules, micelles are in dynamic equilibrium with surfactant monomers in the bulk solution, and molecules in micelles are constantly being exchanged with surfactant monomers in the bulk solution. Micelle kinetic processes occur reasonably fast so that fast experimental relaxation procedures, such as temperature jump, pressure jump, stopped flow or ultrasonic absorption are used to study the rates of micelle formation. The main idea is to take a system that is initially at equilibrium, subject it to a small but rapid change in an intensive parameter (e.g. temperature or pressure), and then follow the relaxation to the new equilibrium state.

Measurements of this kind have shown that there are in general two relaxations, a fast relaxation τ_F in the range of $10^{-6} - 10^{-3}$ sec, and a slow relaxation τ_{SL} in the range of milliseconds to seconds. In the fast relaxation process, the number of micelles does not change. Instead, due to the imposed disturbance single monomers exchange with the micelles (Figure 2.5). The longer time constant reflects the micellar breakdown or formation process in which the number of micelles changes (Figure 2.6).

Table 2.1[24] shows as an illustration the measurements of two relaxation times of

Table 2.1: Relaxation times τ_F and τ_{SL} for some sodium alkyl sulfates

Surfactant	Temperature(°C)	Concentration(M)	τ_F(μs)	τ_{SL}(ms)
$NaC_{16}SO_4$	30	1×10^{-3}	760	350
$NaC_{14}SO_4$	25	2.1×10^{-3}	320	41
	30	2.1×10^{-3}	245	19
	35	2.1×10^{-3}	155	7
	25	3×10^{-3}	125	34
$NaC_{12}SO_4$	20	1×10^{-2}	15	1.8
	20	5×10^{-2}		50

a variety of surfactant solutions. We can see that τ_F usually falls in the range of 10^{-6} to 10^{-3} s, and τ_{SL}, in the range of 10^{-3} to 1s.

The kinetics of micelle association and dissociation was elaborately studied both experimentally and theoretically [25-29].The first attempt on the theoretical implementation of the step wise formation and disintegration of micelles was published by Kresheck et al in [29]. In Kresheck's model, the micelles are treated as monodisperse, i.e. containing the same number of monomers m. They further assume that the dissociation reaction of the micelles to be rate determining. Under these assumptions, only one relaxation process, arising from the formation of the micelles could be observed.

In 1974 Aniansson and Wall[25-27] published an analysis of the time constants of the relaxation processes. In their model for the kinetic process of micelle formation and disintegration, the relaxation in a micellar solution can be thought of as stepwise reaction scheme (see also Equation 2.36):

$$\begin{aligned} &A_1 + A_1 \underset{k_2^-}{\overset{k_2^+}{\rightleftharpoons}} A_2 \\ &A_1 + A_2 \underset{k_3^-}{\overset{k_3^+}{\rightleftharpoons}} A_3 \\ &\vdots \\ &A_1 + A_{s-1} \underset{k_s^-}{\overset{k_s^+}{\rightleftharpoons}} A_s \end{aligned} \qquad (2.41)$$

Where A_1 expresses the surfactant monomer, A_2 is the dimer, A_s is the s-mer, k_s^+ and k_s^- are the rate constants of association and dissociation respectively. Denoting by $C_s(t)$ the concentration of species C_s, s is the aggregation number. The size space could be divided into three important regions: oligomers, including the free monomers (s=1,2,3,...,

s_1); rare aggregates ($s=s_1+1,s_1+2,\ldots,s_2$); and abundant micelles ($s=s_2+1,s_2+2,\ldots s_3$). The concentration of the species C_s as a function of their aggregation number is plotted in figure 2.7. The kinetic equations for the bulk concentration of the species $C_s(t)$ are:

$$\frac{dC_1}{dt} = -2J_2 - \sum_{s=3}^{s_3} J_s \tag{2.42}$$

$$\frac{dC_s}{dt} = J_s - J_{s+1} \quad s=2,3,\ldots s_3 \tag{2.43}$$

Here $J_s(t)$ is the total rate of s-th reaction:

$$J_s = k_s^+ C_1 C_{s-1} - k_s^- C_s \qquad s=2,3,4\ldots s3 \tag{2.44}$$

At equilibrium $J_s=0$ and above equation gives following relation:

$$k_s^+ / k_s^- = \overline{C_s} / \left(\overline{C_1}\,\overline{C_{s-1}}\right). \tag{2.45}$$

The mass balance of free and aggregated monomers is

$$\sum_{s=1}^{s=s_3} sC_s = \overline{C} \tag{2.46}$$

Introducing the relative deviation from the equilibrium concentrations:

$$\xi_s(t) = \frac{C_s - \overline{C_s}}{C_s} \quad s=1,2,3,\ldots s_3 \tag{2.47}$$

So the flux could be represented as:

$$J_s = k_s^- \overline{C_s}\left[\xi_1(1+\xi_{s-1}) + \xi_{s-1} - \xi_s\right] \tag{2.48}$$

Aniansson and Wall analyzed the re-equilibration process from small deviations from equilibrium. Using the above formulation, the relaxation time for the slow process was obtained as:

$$\frac{1}{\tau_{SL}} = \frac{1}{R\overline{C_1}\beta_m} \frac{n_2\beta_n + m_2\beta_m}{n_2\beta_n + \sigma_m^2\beta_m} \tag{2.49}$$

$$\text{Here } m_2 = m^2 + \sigma_m^2 = \sum_{s_2+1}^{s_3} s^2 \bar{C}_s / \bar{C}_m \tag{2.50}$$

$$n = \sum_{1}^{s_1} s\bar{C}_s / \bar{C}_n \tag{2.51}$$

$$n_2 = n^2 + \sigma_n^2 = \sum_{1}^{s_1} s^2 \bar{C}_s / \bar{C}_n \tag{2.52}$$

$$\bar{C}_n = \sum_{1}^{s_1} \bar{C}_s \tag{2.53}$$

$$R = \sum_{s_1+1}^{s_2} (k_s^- \bar{C}_s)^{-1} \tag{2.54}$$

Where m_2 and n_2 are the second moments of the micellar and oligomer size distributions; σ_n and n are the dispersion and the mean aggregation number of the oligomers; $\bar{C}_n$ is the total oligomer concentration; $\beta_n = \bar{C}_n / \bar{C}_1$; R is termed the resistance of the transition region.

To derive an expression for the relaxation time for the fast process, Aniansson and Wall assume that the size distribution of the abundant micelles is broad enough to be considered as continuous. They assume a gaussian size distribution as following:

$$C_s = C_{\max} \exp\left(-\frac{(s-m)^2}{2\sigma_m^2}\right) \tag{2.55}$$

Where m is the mean aggregation number and σ_m is the dispersion. Using this distribution, Aniansson and Wall show:

$$\frac{1}{\tau_F} = \frac{k_m^-}{\sigma_m^2}(1 + \sigma_m^2 \beta_m) \tag{2.56}$$

$$\text{Here } k_m^- = \sum_{s_2+1}^{s_3} k_s^- \bar{C}_s / \bar{C}_m \tag{2.57}$$

$$\bar{C}_m = \sum_{s_2+1}^{s_1} \bar{C}_s \tag{2.58}$$

$$m = \sum_{s_2+1}^{s_1} s\bar{C}_s / \bar{C}_m \tag{2.59}$$

k_m^- is the mean dissociation rate constant of the micelles; $\beta_m = \bar{C}_m / \bar{C}_1$; $\bar{C}_1$ is the concentration of the free monomers (for non-ionic surfactants $\bar{C}_1 \approx CMC$; $\bar{C}_m$ is the total concentration of the micelles. ($\bar{C}_m \approx (\bar{C} - \bar{C}_1)/m\bar{C}_1$); $\bar{C}_s$ is the s-mer concentration; $\bar{C}$ is the total surfactant concentration; m is the mean aggregation number of the abundant micelles. (The bars indicate equilibrium values.)

From the above equation we can see that there is a linear relationship between $1/\tau_F$ and the total surfactant concentration, which is in agreement with experiment[28]. In practice, as the total surfactant concentration increases, the number of micelles increases which results in a decrease in intermicellar distance. So, the time period for a monomer to collide with a micelle is shorter at higher surfactant concentration. The magnitude of τ_F depends on the length of the hydrocarbon chain of the surfactant: the shorter the chain length, the faster is the relaxation time, since micelles are move loosely packed structures for shorter chain surfactants.

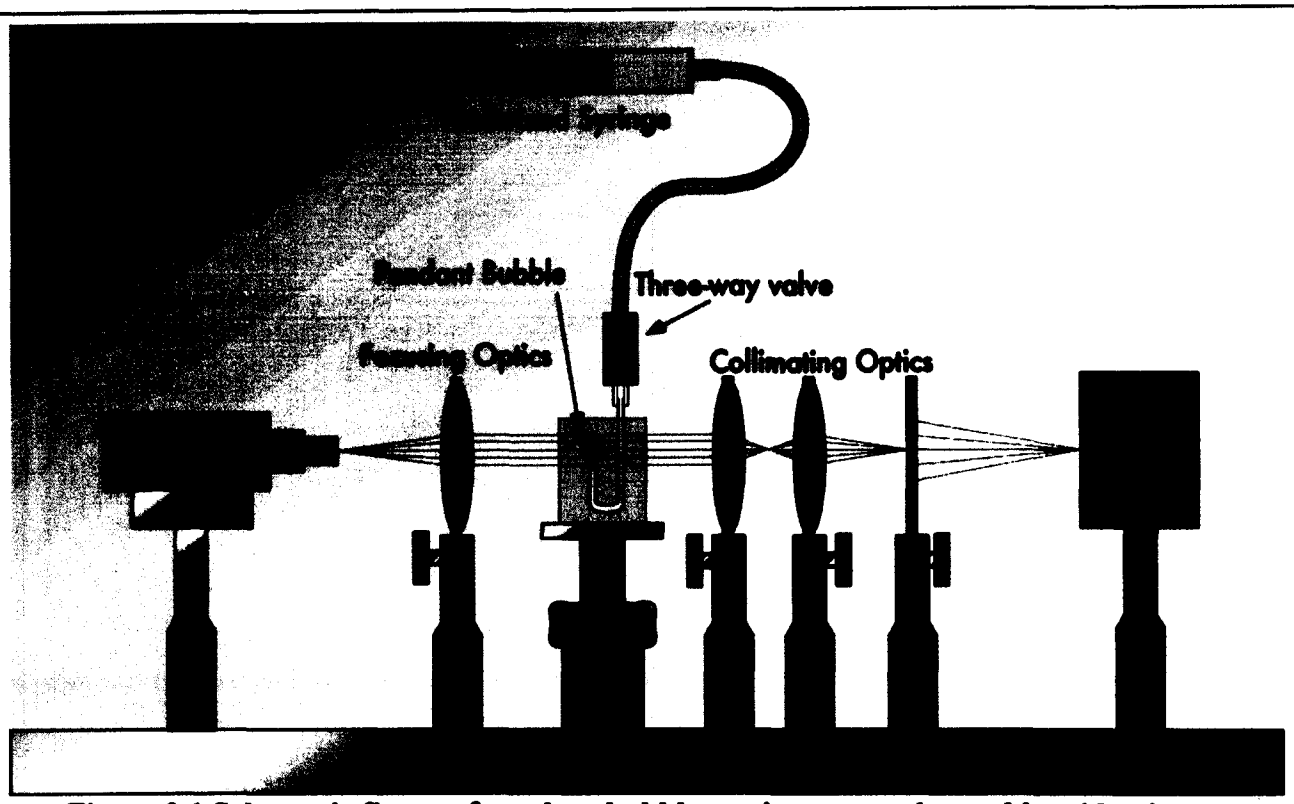

Figure 2.1 Schematic figure of pendant bubble tensiometry, enhanced by video-image digitization

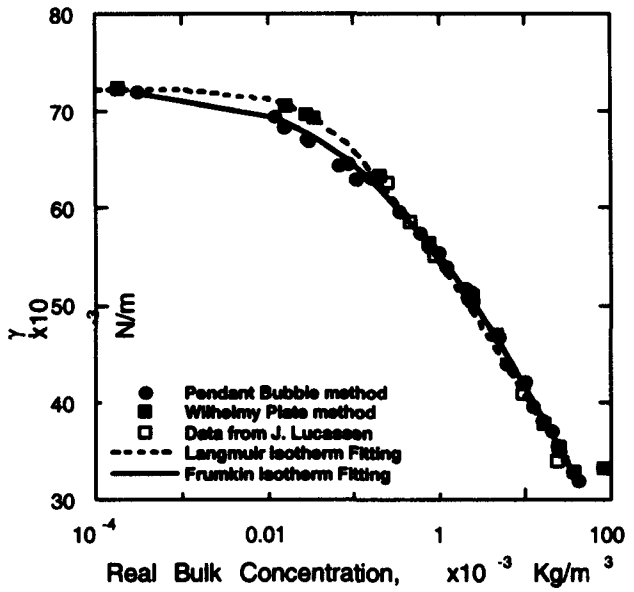

Figure 2.2 Equilibrium surface tensions for air/$C_{12}E_6$ aqueous solutions and the Langmuir and Frumkin isotherm fitting (Reprinted from Ref. 3)

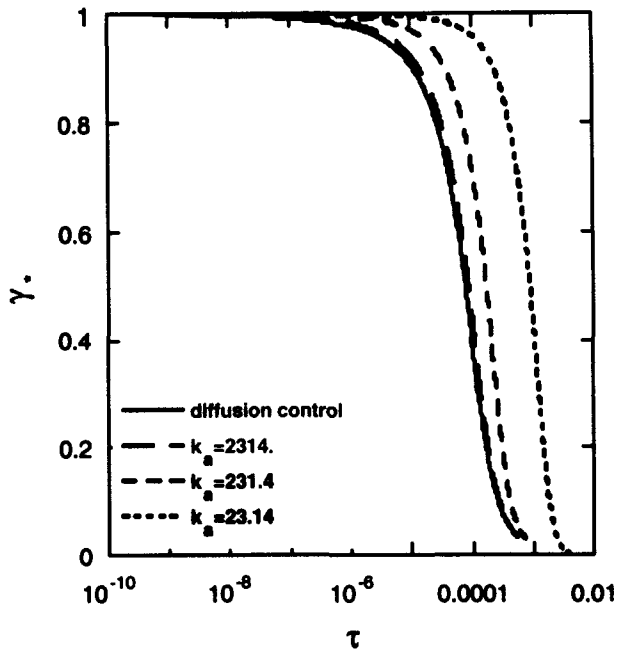

Figure 2.3: (a) Relaxations as a function of time for C_b/a=23.14 (Reprinted from Ref. 3)

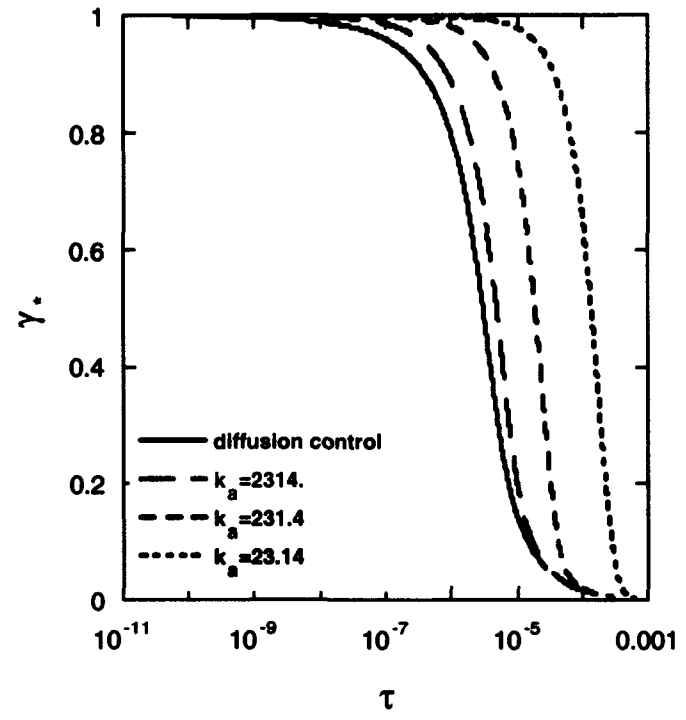

Figure 2.3 (b) Relaxations as a function of time for C_b/a=231.4 (Reprinted from Ref. 3)

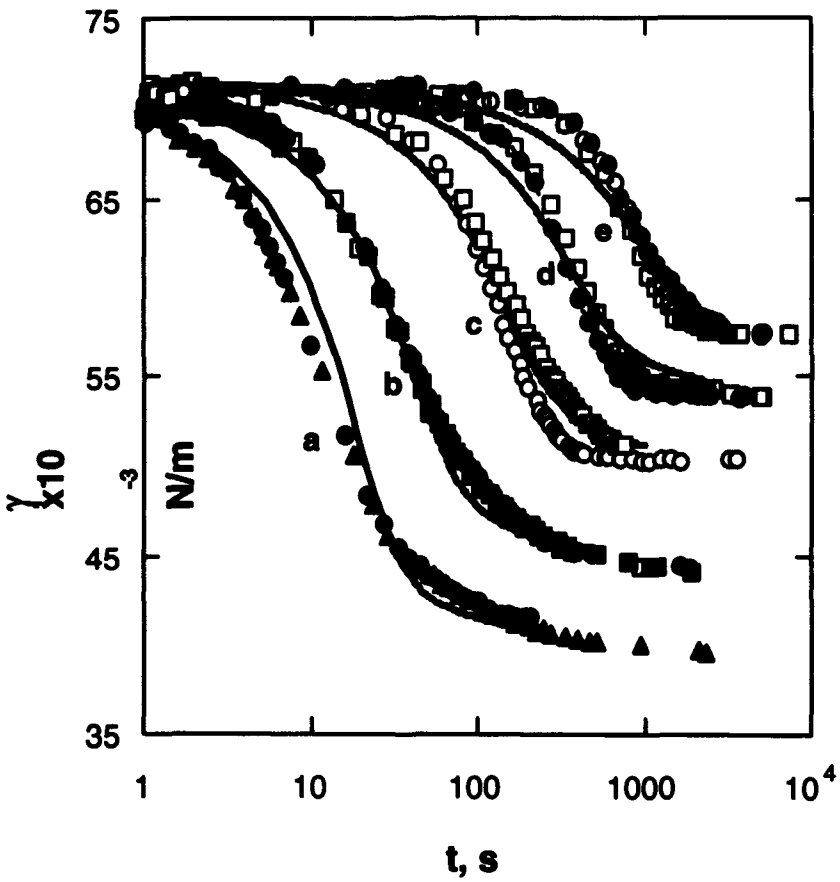

Figure 2.4 Dynamic surface tensions of clean surface adsorption in $C_{12}E_6$ aqueous solutions and mixed diffusive-kinetic control theoretical fit with $D=6.0x10^{-10}$ m^2/s and $\beta=4.0$ $m^3/(mol\ s)$: a) $C_b=12.28\ x10^{-3}$ kg/m^3; b) $C_b = 6.14\ x10^{-3}$ kg/m^3; c) $C_b = 2.456\ x10^{-3}$ kg/m^3; d) $C_b = 1.228\ x10^{-3}$ kg/m^3; e) $C_b = 0.614\ x10^{-3}$ kg/m^3 (Reprint from Ref 3.)

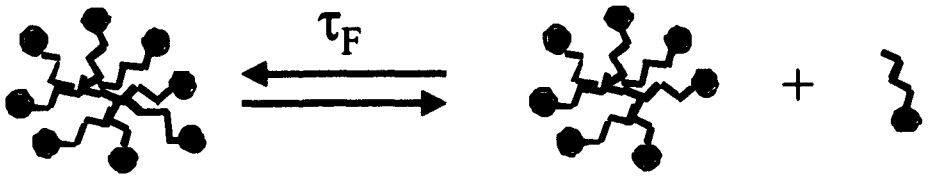

Figure 2.5 The fast relaxation process of single monomer exchange

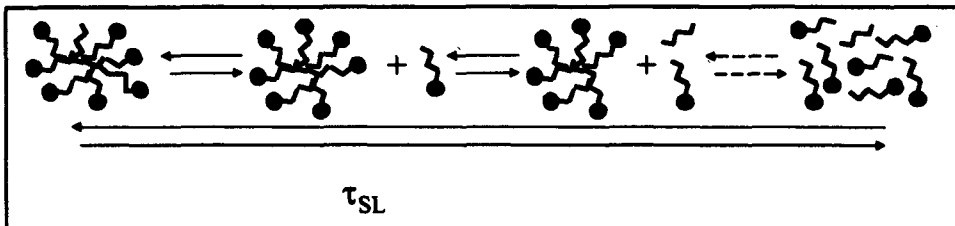

Figure 2.6 The slow relaxation process of micelle breakdown

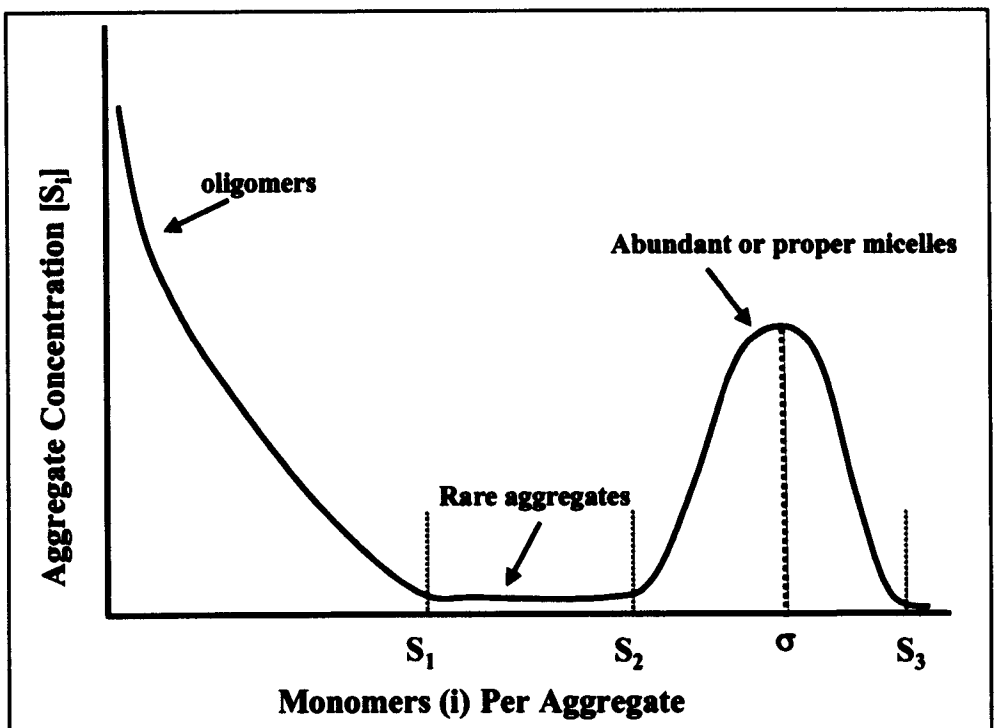

Figure 2.7 Size distribution of micelles in the stepwise model indicating oligomers, rare aggregates and abundant micelles.

CHAPTER 3 MEASUREMENT OF EQUILIBRIUM AND DYNAMIC SURFACE TENSIONS BELOW THE CRITICAL MICELLE CONCENTRATION, AND DETERMINATION OF KINETIC CONSTANTS

3.1 EXPERIMENTAL

3.1.1 Materials

The poly(ethylene glycol) alkyl ether surfactant $C_{14}E_6(CH_3(CH_2)_{13}(OCH_2CH_2)_6OH)$ obtained from Nikko Chemical Company, Ltd.(Japan), is stored in the dark under nitrogen, and is used without further purification. Fresh aqueous solutions are prepared for each experiment using deionized water from a Milli-Q water purification system fitted with an Organex-Q column to remove trace contaminants (Millipore, MA). The resistivity of the deionized water was at least 15MΩ cm.

3.1.2 Methods of Measurements of Equilibrium and Dynamic Surface Tension

The pendant bubble method is now a well-established and extremely accurate technique to measure and model dynamic surfactant transport to interfaces. The details of this method are given elsewhere[1,2] and reviewed on Chapter 2. Briefly, in this technique, a pendant bubble (V ~ 15μl) is formed rapidly (in a few tenths of second) at the tip of an inverted needle which is immersed in surfactant solutions of known concentration. As surfactant absorbs onto the interface, the tension is lowered, and the shape of the bubble, which is a balance between surface tension and gravitational forces,

elongates. The shape of the bubble at any time is governed by the Young-Laplace equation, which relates the pressure drop across the interface to the two radii of curvature. A digital image of the silhouette of the pendant bubble is used to obtain the loci of the pendant shape. The experimental loci are compared with the theoretical interface shape that is generated by the solution of the Young-Laplace equation. The surface tension, which determines the theoretical constructs, is then varied until an optimum is achieved between the theoretical shape and the experimental loci. A schematic of the pendant bubble apparatus is shown in Fig. 2.1 All experiments were undertaken at room temperature, 22-24°C. In each run, the initial tension (taken at the time when the bubble growth is completed) is close to that of pure water (72.3mN/m at 23±0.5 °C); measurements are usually taken until equilibrium is reached.

The pendant bubble apparatus was also used as a film balance to obtain an accurate equation of state. In this method, a bubble is formed in a surfactant solution, and surfactant is allowed to adsorb onto the surface until equilibrium is reached. The bubble is then rapidly expanded or contracted, and the tension is simultaneously measured during the area change as described above, obtaining plots of the tension as a function of the area, which can be normalized to the initial area. For insoluble surfactants directly deposited on a pendant drop, the initial amount of surfactant is known, and the tension as a function of the surface concentration can be obtained (see the studies of Neuman and coworkers[3] at the air-liquid interface and for DPPC at the liquid-liquid interface[4]). For soluble surfactants adsorbed from solution, the rapid expansions and contractions provide relative dilation rates much greater than those on a conventional planar trough, and thereby minimize exchange with the bulk. Consequently, plots of the tension as a

function of the relative area can be reinterpreted as tension as a function of relative surface concentration[2].

3.2 Equilibrium and Dynamic Surface Tension Measurements Below CMC and Determination of Adsorption Isotherm, Equation of State and Monomer Kinetic Constants and Diffusion Coefficient

3.2.1 Equilibrium adsorption and equation of state measurements

In this study, we use the Frumkin scheme (as reviewed in Chapter 2) to model the kinetic exchange of surfactant between the surface and the liquid sublayer immediately adjacent to the surface. In this model, adsorption is proportional to the the surface area unoccupied by surfactant multiplied by an Arhenius factor describing the activation energy for adsorption which is assumed independent of surface coverage. The desorption is proportional to the surface concentration and Arhenius activation energy factor which is assumed linear in the surface concentration. This linear dependence describes the effect of interactions between the adsorbed molecules on the desorption process. Thus

$$\frac{d\Gamma}{dt} = \beta\Gamma_\infty C_s(1-\Gamma/\Gamma_\infty) - \alpha\,\Gamma e^{K\Gamma/\Gamma_\infty} \tag{3.1}$$

Where Γ is the surface concentration, C_s is the sublayer concentration, α and β are kinetic rate constants for desorption and adsorption, respectively, Γ_∞ is the maximum packing concentration, K is a (non-dimensional) parameter accounting for the intermolecular interactions of adsorbed species (positive for repulsion, negative for attraction). For Langmuir adsorption K=0 and intermolecular interactions are not included. As we detail below, the Frumkin adsorption model including the intermolecular interaction can describe the $C_{14}E_6$ adsorption very well.

At equilibrium the net exchange is equal to zero and we obtain the equilibrium adsorption isotherm:

$$\frac{\Gamma}{\Gamma_\infty} = \frac{1}{1 + \frac{\alpha e^{kT/\Gamma_\infty}}{\beta C_0}} \tag{3.2}$$

From the equilibrium adsorption equation ($\Gamma(C_0)$) and the Gibbs-Duhem equation for the surface or interfacial tension ($d\gamma = -RT\Gamma d\ln C_0$), an equation of state relating the surface tension γ to the surface concentration can be obtained ($\gamma(\Gamma)$). For example for Frumkin kinetics, the equation of state is:

$$\gamma_c - \gamma = -RT\Gamma_\infty \left\{ \ln\left(1 - \frac{\Gamma}{\Gamma_\infty}\right) - \frac{1}{2} K \left[\frac{\Gamma}{\Gamma_\infty}\right]^2 \right\} \tag{3.3}$$

(here γ_C is the tension of the clean surface).

Usually the model parameters (cf Chapter 2) are obtained by matching (3.2) and (3.3) to equilibrium measurement of the tension as function of bulk concentration. Because of the large number of parameters, the fitting is not unique and different sets of parameters can fit the experimental data equally well. In this paper we use the alternate procedure in which the pendant bubble is used as a Langmuir trough to directly measure the equation of state. Γ_∞ and K are first obtained by fitting the pendant bubble Langmuir trough data to the equation of state, and then the equilibrium parameter α / β is evaluated by fitting the absorption isotherm to the equilibrium surface tension versus log bulk concentration curve. This approaches is detailed in Pan et al[2] and is summarized here. At a given bulk concentration C_0, a pendant bubble is formed, and allowed to come to equilibrium with an equilibrium surface concentration Γ_e and a surface tension γ_e. The bubble is then

rapidly expanded and subsequently compressed (or compressed and then expanded), the tension $\gamma(t)$ is recorded as a function of the relative surface concentration $\Gamma(t)/\Gamma(\gamma=65\text{dyne/cm})$. Where $\Gamma(\gamma=65\text{dyne/cm})$ is the surface concentration corresponding to a surface tension at 65 dyne/cm. Experiments were undertaken at different concentrations and repeated several times at the same concentration C_0. The assemblage of all experimental data is shown in figure 3.1. The correlation of all experimental data into one line verifies the conservation of mass and the fact that the equation of state is an instantaneous function of surface concentration.

The fitting of the data to the Langmuir and Frumkin equations of state are plotted in figure 3.2 alongside the data. For the Langmuir model we find $\Gamma_\infty=2.40\text{x}10^{-6}$ mol/m^2 and for the Frumkin, $\Gamma_\infty=3.32\text{x}10^{-6}$ mol/m^2 and K= 7.12 (indicating repulsion dominance). We note that the Frumkin model prediction agrees with the experimental data much better than that of Langmuir model. The Frumkin model takes into account the parameter K the effect of cohesive interactions between hydrocarbon chains, and the repulsive interactions of the ethoxylate headgroups. A negative K indicates that repulsion between the ethoxylated groups predominates over cohesion in the monolayer. The Langmuir equation of state does not take into account these intermolecular interactions.

The equilibrium surface tension as a function of bulk concentration is given in figure 3.2. We emphasize that the abscissa in this plot is the correct (or "real") concentration, i.e. the concentration in the bulk after the adsorption process onto the air/water interface of the pendant bubble quartz cell is complete. The corrected concentration is computed from the apparent concentration (C_{app}, the concentration in the solution which is poured into the dish or cell) by using the adsorption isotherm to account

for the adsorbed amount on the surface, i.e. we use C_{app} -Γ_e(A/V) to replace C_0 in the data fitting route, where A and V are the air/water area and solution volume respectively in the cell in which the bubble is formed. Also shown in the figure is the fitting of the data to the Langmuir and Frumkin equations of state. From the Langmuir relation we find α/β=8.3605×10^{-6} mol/m^3 and for the Frumkin, α/β=2.068×10^{-6} mol/m^3. We note finally from the figure that at a high enough concentration the tension plateaus indicating the formation of surfactant aggregates in the bulk (the critical micelle concentration or C_{CMC}). We note that the C_{CMC} is equal to approximately 4.36 x10^3 kg/m^3 (9.12 x10^{-6}M) and this is in good agreement with literature reports[5].

3.2.2 Dynamic surface tension measurements and determination of the kinetic constants

To determine the individual kinetic constants, we measure the dynamic relaxation in tension as surfactant adsorbs onto the initially clean surface of an impulsively created pendant bubble. We measure these relaxations at four different concentrations below the C_{CMC}, and the results are given in Figure 3.3.

For these dynamic tension experiments, by modeling the kinetic exchange, and the bulk diffusive transport to the interface, the surface adsorption as a function of time can be predicted as a function of the surfactant transport parameters. From the equation of state the model predictions of the tension relaxation can be computed, and from a comparison of the model tension relaxation predictions with the experimental results, ideally, the kinetic constants and the diffusion coefficient can be inferred. To model the relaxations we note first that in this measurement technique, the bubble is created

impulsively in less than a tenth of a second; the hydrodynamic disturbance clears after one second. We model the mass transfer after this one second; the diffusion of surfactant to the interface is then governed by the diffusion mass conservation equation without convection with the geometry approximated as spherical:

$$\frac{\partial C}{\partial t} = D\frac{1}{r^2}\frac{\partial}{\partial r}\left\{r^2\frac{\partial C}{\partial r}\right\} \tag{3.4}$$

and the boundary condition at the pendant bubble surface ($r=R_0$) given by :

$$D\frac{\partial C}{\partial r}\bigg|_{r=R0} = \frac{\partial \Gamma}{\partial t} \tag{3.5}$$

and at $r=\infty$

$$C(r \to \infty, t) = C_0 \tag{3.6}$$

Where C(r,t) is the bulk concentration of surfactant monomers, Γ is the surface concentration and D is the diffusion coefficients of surfactant monomers. The initial condition is:

$$C(r, t = 0) = C_0 \tag{3.7}$$

The adsorption kinetics are described by the Frumkin equation, as we have used these kinetics to describe the equilibrium adsorption:

$$\frac{d\Gamma}{dt} = \beta C(r = R_0, t)(\Gamma_\infty - \Gamma) - \alpha e^{K\frac{\Gamma}{\Gamma_\infty}\Gamma} \tag{3.8}$$

The above equations are first integrated to obtain the adsorption as a function of time. This integration is facilitated by using Laplace transforms to formulate the surface concentration in terms of the sublayer concentration $C_s(t) = C(r = R_o, t)$:

$$\Gamma(t) = 2\sqrt{\frac{D}{\pi}}\left[C_0\sqrt{t} - \int_0^{\sqrt{t}} C_s(t-\tau)d\sqrt{\tau}\right] + \frac{D}{R_0}\left[C_0 t - \int_0^{t} C_s(\tau)d\tau\right] \qquad (3.9)$$

Equations (3.8) and (3.9) are then solved numerically to obtain the adsorption $\Gamma(t)$ and the sublayer concentration $C_s(t)$ as a function of time. The equation of state $(\gamma_c - \gamma = -RT\Gamma_\infty\left\{\ln\left(1-\frac{\Gamma}{\Gamma_\infty}\right) - \frac{1}{2}K\left[\frac{\Gamma}{\Gamma_\infty}\right]^2\right\})$ obtained from the equilibrium measurements is then used to obtain the dynamic tension relaxation. In predicting the relaxation, the unknowns are the diffusion coefficient and the adsorption rate constant β. (The equilibrium measurements provide the adsorption /desorption ratio α/β and therefore α once β is known; the maximum packing concentration Γ_∞ and the intermolecular constant K are known from the fit of the pendnt bubble Langmuir trough data and equilibrium tension as a function of bulk concentration.) Simulations are run varying D and β until the predicted relaxations fit the experimental data at all the bulk concentrations. The results are shown in Figure 3.3; the theoretical simulations which best fit the dynamic relaxations are indicated by the bold lines, with $D=6.0\times10^{-10}$ m^2/s and $\beta=4.0$ $m^3/(mol\cdot s)$.

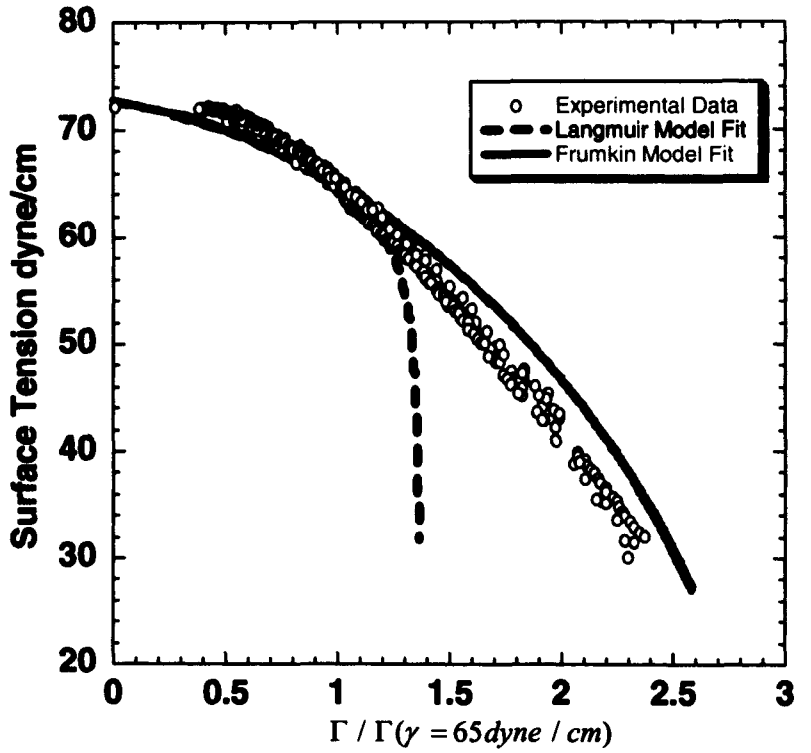

Figure 3.1 The tension as a function of surface concentration divided by surface concentration at the reference tension at 65dyne/cm, and the Langmuir and Frumkin equations of state of $C_{14}E_6$

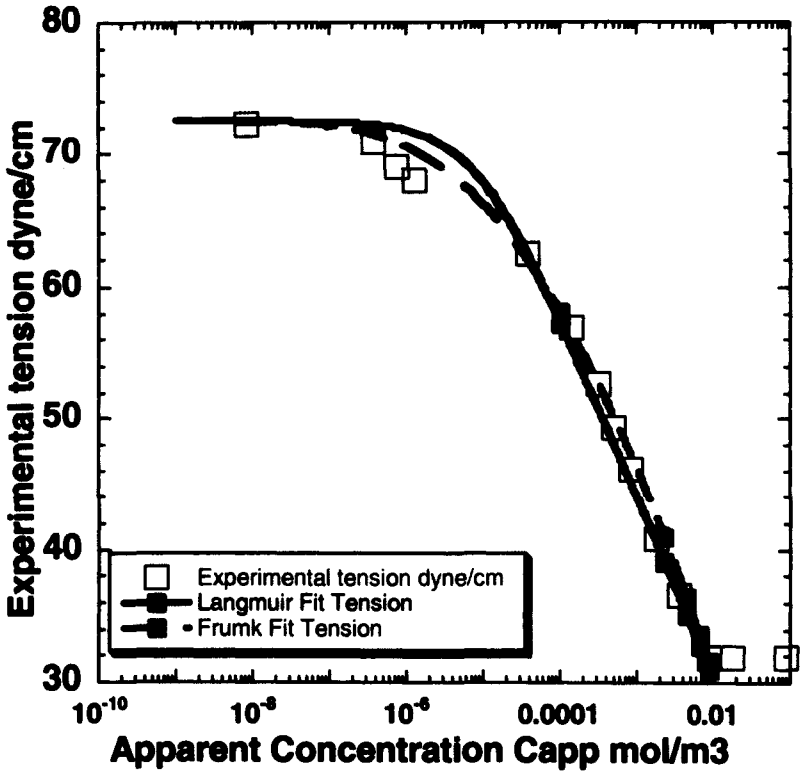

Figure 3.2 Equilibrium Surface Tension versus Apparent Bulk Concentration mol/m^3

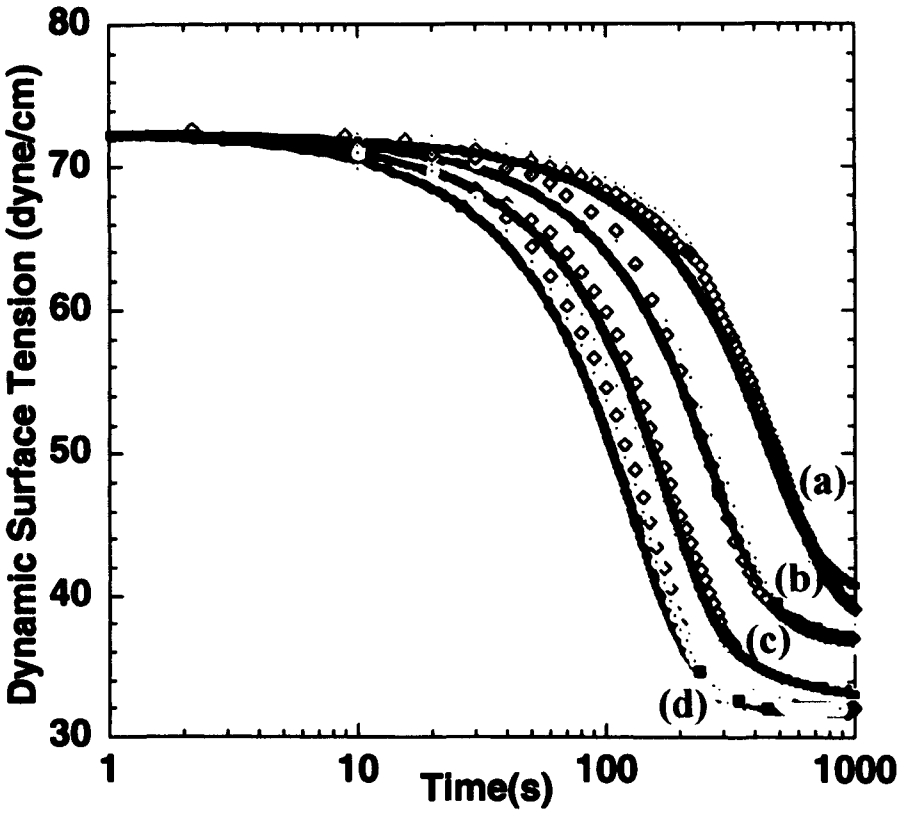

Figure 3.3 Dynamic surface tension of clean surface adsorption in $C_{14}E_6$ aqueous solution and mixed diffusive-kinetic control theoretical fit with $D=6.0\times10^{-10}m^2/s$ and $\beta=4.0m^3/(mol.s)$: (a) $C_0=3.68\times10^{-3}$ mol/m^3; (b) $C_0=4.39\times10^{-3}$mol/m^3; (c) $C_0=6.97\times10^{-3}$mol/m^3; (d) $C_0=9.18\times10^{-3}$ mol/m^3.

CHAPTER 4 THEORETICAL MODEL FOR SURFACTANT TRANSPORT TO A CLEAN INTERFACE FROM A MICELLAR SOLUTION AND COMPARISON WITH EXPERIMENTS

4.1 Introduction

Surfactants in solution tend to undergo micellization once the concentration of surfactant solution is higher than the critical micelle concentration (C_{CMC}) (cf Chapter 2). Although micelles are commonly assumed not to be surface active, their presence affects the transport and kinetic adsorption process. When surfactant adsorbs from solution at a concentration greater than the C_{CMC}, several additional processes occur that are not present at low concentrations. Upon the creation of a clean interface in a micellar solution the adsorption of the surfactant monomers from the region adjacent to the surface upsets locally the micelle-monomer equilibrium causing micelles to dissociate. This results in a diffusive flux of micelles to the surface to restore the equilibrium. The diffusive transport of micelles and monomers, kinetic adsorption of monomers as well as the kinetics of micellar break-up then determine the rate of dynamic tension reduction. A general picture of surfactant monomer and micellar diffusive transport and kinetic exchange above the C_{CMC} is shown in Figure 4.1.

The concentration of species is uniform in a homogeneous surfactant micellar solution. In this case, the diffusion and adsorption are not present and the kinetics of micellization is simple. Micellar kinetic processes occur very fast. So fast experimental relaxation procedures, such as temperature jump, pressure jump, stopped flow or ultrasonic absorption are used to study the rates of micelle formation. The main idea of these experiments is to take a system that is initially at equilibrium, subject it to a small

but rapid change in an intensive parameter (e.g. temperature or pressure), and then follow the relaxation to the new equilibrium state. Above experiments have shown that there are in general two relaxation processes in kinetics of micellization. In the fast relaxation process, the number of micelles does not change. Instead, due to the imposed disturbance single monomers exchange with the micelles characterized with a fast relaxation timescale τ_F in the range of $10^{-6} - 10^{-3}$ sec. The slow relaxation process corresponds the micellar breakdown or formation process in which the number of micelles changes. The timescale of slow relaxation τ_{SL} is in the range of milliseconds to seconds. The primary breakthrough theory was developed by Aniansson and co-workers[1-3]. In their model, they considered the micelle population density to be polydisperse in the number of monomers per micelle, with a rather sharp distribution which can be approximated by a Gaussian function. The micelle formation and disintegration follow a stepwise reaction scheme.

In non-homogeneous systems, both the diffusion and adsorption occur simultaneously, so the kinetics of micellization is very complicated. The concentrations of species are functions both of time and space. Creation of a fresh interface leads to instantaneous adsorption of surfactant monomers from the regions adjacent to the surface. As a result, the monomer sublayer concentration turns out to be lower than the equilibrium value, and hence the surfactant monomers diffuse from the far away bulk phase to the surface. At the same time, the local equilibrium between the micelles and monomers in the sublayer is perturbed causing micelles to dissociate. The depletion of monomers in the sublayer could be compensated partly at the expense of micellar dissociation if the monomer diffusion and kinetic adsorption is comparable with or less

than the rate of micellization process. Simultaneously, the micelle concentration is not uniform and leads to micellar diffusive transport. The diffusive transport of micelles and monomers, kinetic adsorption of monomers as well as the kinetics of micellar break-up then determine the rate of dynamic tension reduction. Depending on the relative rates of micelle breakup (τ_{SL}), the micelle diffusion rate, and the kinetic rate of monomer adsorption it may be possible to form a micelle free zone. In this case the vicinity of the interface is completely depleted of micelles, and the concentration of the monomer is lower that the C_{CMC}. When the micelle break-up rate is slower, the micelle free zone is not present; rather the concentration gradients for both micelles and monomers develop.

There has been limited work on the kinetics of adsorption from micellar solutions both theoretically and experimentally. The work of Lucassen [4] was the first attempt to describe quantitatively the dynamic interfacial properties of micellar solutions. Lucassen used the model of Kresheck et al [5] in which the micelles were assumed to be monodisperse with aggregation number N and the micellization process was treated by Nth order reaction scheme: $NS \underset{k_{-N}}{\overset{k_N}{\rightleftharpoons}} S_N$. Later Miller[6] numerically solved the respective diffusion equations for the monomers and the monodisperse micelles using the same model. Both Henry's adsorption isotherm and Lamgmuir's adsorption isotherm are used in computation, and the numerical results demonstrated that the adsorption relaxation in the presence of micelles is faster than that of below the C_{CMC}.

Joos and J. Van Hunsel applied the same model for the interpretation of the experimental data for the dynamic surface tension of micellar solutions [7], in which the effect of the micelles is accounted for by an effective diffusivity of the monomers. Joos and coworkers [8] attended to account for the micellization kinetics by adding an

additional term proportional to the deviation of the monomer concentration from the equilibrium value in the diffusion equation of monomer. This approach is equivalent to the pseudo-first-order reaction (PFOR) model, which is widely used in the chemical kinetics. Under the assumption that the diffusion of micelles could be neglected, they solved the respective boundary value problem using the concept of a diffusion penetration depth. In their model, the demicellization rate constants could be obtained from experimental data from oscillating-jet and flowing-film methods. Analogous theoretical framework was applied for Brij 85 micellar solutions[9,10], micellar Triton X-100 solutions[11,12] and sodium dodecyl sulfate (SDS) -dodecanol mixture systems[13,14].

Fainerman[15] first attempted to use the mathematical framework of the Annianson and Wall theory to develop in a consistent way conservation equations for monomers and micelles that accounts for bulk diffusion as well as the kinetics of micelle breakdown, assuming small deviations from equilibrium and an infinitely fast exchange of surfactant between the sublayer and surface. He examined two regimes, one in which the time scales for monomer and micelle diffusion are of the order of the slow kinetic time constant ($\frac{\tau_D^{monomer}}{\tau_{SL}} = O(1); \frac{\tau_D^{micelle}}{\tau_{SL}} = O(1)$) and one in which these scales are of the order of the fast kinetic scale ($\frac{\tau_D^{monomer}}{\tau_F} = O(1); \frac{\tau_D^{micelle}}{\tau_F} = O(1)$). For the case in which $\frac{\tau_D^{monomer}}{\tau_{SL}} = O(1); \frac{\tau_D^{micelle}}{\tau_{SL}} = O(1)$ Fainerman (see also Dushkin and Ivanov[16,17] and Noskov[18]) showed that the conservation equation for a small deviation of the monomer concentration from equilibrium ($\xi_1 = \frac{C_1 - C^*}{C^*}$) can be written for one dimensional (x)

diffusion in the form of a pseudo first order reaction (PFOR) as: $\frac{d\xi_1}{dt} = D\frac{\partial^2 \xi_1}{\partial x^2} - \frac{1}{\tau_{SL}}\xi_1$

where τ_{SL} is Aniansson and Wall's analytical expression for the timescale for the slow kinetic process. The slow time scale equations were used to describe surfactant transport from micellar solutions to an expanding bubble in the maximum bubble pressure method. Comparison of the simulations with measurements of the tension reduction provided a measurement of τ_{SL}, and were shown to compare favorably with direct measurements of τ_{SL}[19]. A similar approach has been used by Danov et al to describe transport to an interface whose equilibrium monolayer has been perturbed [20]. Diffusion equations for micelles and monomers derived by C. D. Dushkin et al[16], as we mentioned in the introduction, allows us to formulate mathematical problems for dynamic absorption from micellar solution.

4.2 Proposed Model

The above equations were derived only for small deviations from equilibrium. This restriction also relates to the PFOR model where the formation and depletion of monomers is described by a term proportional to the deviation of monomer concentration from its equilibrium value[8,15,21-24]. Most of the research on dynamic adsorption from micellar solutions have been based on experiment measuring dynamic surface tension, where the creation of a clean interface from surfactant micellar solution definitely leads to significant deviations from equilibrium, and consequently to non-linear processes in the system. These processes could not be taken into consideration entirely in above mathematical approaches, and consequently the comparison of results obtained from

linearized theory with the experimental data could not lead to accurate physical conclusion.

As we mentioned earlier, the time scale of micellar breakdown could be of the order of milliseconds to a few second [25]. The time scale of slow relaxation process for nonionic surfactant C_iE_j measured by stopped-flow techniques is about 10s or less[26]. The whole dynamic surface tension relaxation process for nonionic surfactant $C_{14}E_6$ at concentrations between C_{CMC} and $4C_{CMC}$ is about 100s or more. Compared to the time scale of slow relaxation process for the nonionic surfactants C_iE_j measured by the stopped-flow technique, the total dynamic surface tension relaxation process is at least an order of magnitude large. Based on this, we assume that the micellar breakup is infinitely fast compared to monomer and micelle diffusion and that the micellar breakup is not the limiting step. On the other hand, above assumption could be supported by the scaling arguments. Consider clean interface adsorption to a planar surface from a micellar solution in which the monomer concentration is maintained at C_{CMC} and micelle concentration is $C^0_{Micelle}$ in the bulk solution, the surface concentration at equilibrium is given by Γ_e. The maximum rate, at which bulk monomer diffusion proceeds, is obtained when the sublayer concentration remains at zero; the adsorption under these condition is given by $\Gamma(t) = 2C_{CMC}\sqrt{\frac{Dt}{\pi}}$ and the time for an equilibrium monolayer to form is therefore $\tau^{Monomer}_{Diffusion} = \pi\frac{\Gamma_e^2}{4DC^2_{CMC}}$. Similarly, the diffusion time scale for the micelle is $\tau^{Micelle}_{Diffusion} = \pi\frac{\Gamma_e^2}{4(\sigma C^0_{Micelle})^2 D_{Micelle}}$. The rate at which kinetics alone delivers material to the surface can be obtained by integrating the kinetic equation for the sublayer concentration

equal to C_{CMC} (i.e. no bulk diffusion); for the Langmuir equation the kinetic adsorption is given by $\Gamma(t) = \Gamma_e(1 - e^{-(\alpha+\beta C_{CMC})t})$ and the characteristic time to achieve equilibrium is given by $\tau_{Kinetic}^{Monomer} = \frac{1}{(\alpha + \beta C_{CMC})}$. By applying the parameters for $C_{14}E_6$, we obtain above characteristic time scale shown in table 4.1.

Table 4.1 Characteristic Time Scale of Nonionic Surfactants at Different Surfactant Concentrations

Surfactant Concentration mol/m^3	$1.27C_{CMC}$	$2.0C_{CMC}$	$3.0C_{CMC}$	$4.0C_{CMC}$
$\tau_{Diffusion}^{Monomer}$(s)	136.8	136.8	136.8	136.8
$\tau_{Diffusion}^{Micelle}$(s)	7507.92	547.3	136.83	60.814
$\tau_{Kinetic}^{Monomer}$(s)	27.4	27.4	27.4	27.4
$\tau_{Micelle}^{Breakup}$(s)	4~10	4~10	4~10	4~10
Whole dynamic surface tension relaxation time scale(s)	400	150	100	80

From table 4.1, it can be clearly seen that compared to the diffusion of the monomers and the micelles as well as kinetics, the time scale for micelle breakup is the smallest. Based on the above, we could assume that the micellar breakup is infinitely fast compared to monomer and micelle diffusion as well as kinetics.

With the assumption of infinitely fast micellar kinetics, micelles act as reservoirs to maintain the monomer concentration at the C_{CMC}; thus if micelles are present in a region of a solution domain, the monomer concentration is maintained at the C_{CMC} value. If micelles are not present, the monomer concentration is less than the C_{CMC}. Within this context of the condition of infinitely fast micellar break-up, we can now consider two cases: In the first, the rate of kinetic adsorption is slow relative to the bulk diffusion of micelles. The micelle bulk diffusion "keeps up" with the kinetic adsorption of monomers

from the sublayer to the surface, so that the monomer concentration never drops below the C_{CMC} and micelles are always present in the vicinity of the surface. Micellar breakup in the sublayer immediately adjacent to the surface matches the kinetic flux of monomers to the surface. Eventually as the surface becomes saturated and the kinetic flux of monomers decreases to zero, the matching micellar flux decreases and the solution returns to a uniform micellar phase.

In the second case at lower bulk micellar concentrations, the micelle diffusive flux is slower than the kinetic exchange so that after an induction period all micelles are consumed near the surface and a micelle free zone appears at the surface, and gradually moves into the bulk phase. At the front of the micelle free zone the micelles break up to supply surfactant monomers and keep the monomer concentration at C_{CMC}. Within the micelle free zone, monomer diffuses from the front to the surface where the concentration of monomer is decided by the kinetic equation and is below C_{CMC}. Within the region between the micelle free zone front and the bulk phase, the monomer concentration is equal to the C_{CMC}, and micelles diffuse from the bulk phase to the front of the micelle free zone to supply micelles breaking down at the front. As adsorption onto the surface proceeds and the surface becomes saturated, the kinetic flux to the surface decreases. The concentration gradient of monomers across the micelle-free zone is reduced and the front begins to move back towards the interface. The micelle diffusion gradient also relaxes as the monomer flux in the micelle free zone decreases. At equilibrium the front arrives back at the interface and the bulk solution eventually becomes a uniform micellar solution.

First we develop a criteria for the concentration below which the micelle free zone forms. We undertake these calculations for a planar surface and Langmuir adsorption to examine the competing roles of monomer and micelle diffusion without the complicating effects of curvature or intermolecular interactions on the surface. When theory is compared to experiments (Sec.4.3), the calculations are redone for the spherical geometry of the pendant bubble and the intermolecular interactions of the Frumkin isotherm are included. At t=0, a fresh planar interface is formed and surfactant monomers begin to adsorb onto the interface. Consider a semi-infinite surfactant solution with farfield concentration nC_{CMC} occupying the space with z>0 (the solution/air interface is placed at z=0). At t=0, the surface concentration ($\Gamma(t)$) is equal to zero, and the bulk monomer concentration is C_{CMC}, and micelle bulk concentration is C_M^0. C(z,t) and $C_M(z,t)$ are the concentration of monomers and micelles respectively at the distance z from the interface. We assume that the micelle diffusive flux is always fast enough to match the adsorption kinetics so that the micelle concentration is never zero and the monomer concentration is everywhere always equal to the C_{CMC}. We solve for the micellar diffusion necessary to match the kinetic flux. The diffusion equation for micelles is given as following:

$$\frac{\partial(\sigma C_M)}{\partial t} = D_M \frac{\partial^2(\sigma C_M)}{\partial z^2} \tag{4.1}$$

The boundary conditions at z=0 is:

$$D_M \left.\frac{\partial(\sigma C_M(z,t))}{\partial z}\right|_{z=0} = \frac{\partial \Gamma}{\partial t} \tag{4.2}$$

and at z=∞

$$\sigma C_M(\infty,t) = \sigma C_M^0 = (n-1)C_{CMC} \tag{4.3}$$

Where D_M is the diffusion coefficients of micelle and σ is the number of monomers per micelle. The initial condition is:

$$\sigma C_M(z \to \infty, 0) = \sigma C_M^0 = (n-1)C_{CMC} \tag{4.4}$$

The adsorption can be found directly and analytically (for Langmuir kinetics) under the circumstance that the monomer concentration in the sublayer remains uniform at C_{CMC}:

$$\frac{d\Gamma}{dt} = \beta C_{CMC}(\Gamma_\infty - \Gamma) - \alpha\Gamma = \beta C_{CMC}\Gamma_\infty - (\beta C_{CMC} + \alpha)\Gamma \tag{4.5}$$

The surface concentration as function of time $\Gamma(t)$ is obtained by integrating equation (4.5). By using the equation of state, the surface tension as function of dimensional time is calculated.

By scaling Equations (4.1-4.5) time with the kinetic scale and distance with the adsorption depth h (the distance underneath the surface which contains the same of surfactant as that adsorbed onto the surface at equilibrium):

$$t^* = (\beta C_{CMC} + \alpha)t \tag{4.6}$$

$$z^* = \frac{z}{h} \tag{4.7}$$

$$h = \frac{\Gamma_e}{C_T} = \frac{\Gamma_e}{nC_{CMC}} \tag{4.8}$$

$$\Gamma_e = \frac{\beta C_{CMC}\Gamma_\infty}{(\beta C_{CMC} + \alpha)} \tag{4.9}$$

The only non-dimensional groups are the ratio of the kinetic to the micelle diffusive time scale:

$$\left(\Omega_M^0\right)^2 = \frac{\tau_{Kinetic}^{Monomer}}{\tau_{Diffusion}^{Micelle}} \tag{4.10a}$$

or

$$\Omega_M^0 = \frac{C_M^0 \sigma \sqrt{D_M(\beta C_{CMC} + \alpha)}}{\beta C_{CMC} \Gamma_\infty} = \frac{(n-1) C_{CMC} \sqrt{D_M(\beta C_{CMC} + \alpha)}}{\beta C_{CMC} \Gamma_\infty} \tag{4.10b}$$

and n. In the above, Γ_e is the equilibrium surface concentration, and h is the adsorption depth. The bulk concentration of monomers in the micelles we express as $(n-1)C_{CMC}$ where $n-1 = \frac{\sigma C_M^0}{C_{CMC}}$ and the total bulk concentration of surfactant monomers is $C_T = nC_{CMC}$. Defined C_T as such, the adsorption length h could be expressed as $h = \frac{\Gamma_e}{C_T} = \frac{\Gamma_e}{nC_{CMC}}$. The non-dimensional formula of surface concentration as function of non-dimensional time $\Gamma(t^*)$ is from (4.11):

$$\Gamma(t^*) = \Gamma_e(1.0 - e^{-t^*}) \tag{4.11}$$

Applying the Laplace transform to (4.1) – (4.4), we can solve for the diffusion of micelles from the bulk to the surface, and in particular, the non-dimensional micelle concentration at the surface $C_M(z^* = 0, t^*)/C_M^0$ and micelle concentration at a non-dimensional distance z^* from the surface $C_M(z^*, t^*)/C_M^0$ as a function of non-dimensional time t^*.

$$\frac{C_M(z^* = 0, t^*)}{C_M^0} = 1.0 - \frac{1}{\sqrt{\pi}\Omega_M^0} \int_0^{t^*} e^{-t^*} \frac{e^{\omega^*}}{\sqrt{\omega^*}} d\omega^* \tag{4.12}$$

$$\frac{C_M(z^*, t^*)}{C_M^0} = 1.0 - \frac{1}{\sqrt{\pi}\Omega_M^0} \int_0^{t^*} e^{-\omega^*} \frac{1}{\sqrt{t^* - \omega^*}} \exp\left(-\frac{z^{*2}}{4B_M(t^* - \omega^*)}\right) d\omega^* \tag{4.13}$$

B_M is defined as $(n/n-1)^2 \Omega_M^{0\,2}$. The above equations clearly show that the micelle sublayer concentration is independent of σ, the number of monomers per micelle. Figure 4.2 shows the non-dimensional sublayer concentration of micelles $\frac{C_M(z^*=0,t^*)}{C_M^0}$ as a function of non-dimensional time t^* for four non-dimensional bulk concentrations Ω_M^0. We find that when the non-dimensional bulk concentration equals the critical value $\Omega_M^0 = 0.609$, the sublayer concentration becomes zero at a time $t^* = 0.855$. For all higher concentrations, micelle diffusion is fast enough so that the sublayer micelle concentration is never equal to zero. For all lower concentrations, the sublayer concentration of micelles becomes equal to zero at times less than 0.855, and for these lower concentrations at longer times the micelle free zone forms. We denote the (non-dimensional) critical time at which the sublayer concentration of micelles becomes equal to zero as $t^* = a^*$. Thus the parameter $\Omega_M{}^0$ $(\Omega_M^0 = \frac{(n-1)C_{CMC}\sqrt{D_M(\beta C_{CMC}+\alpha)}}{\beta C_{CMC}\Gamma_\infty})$ demarcates the appearance of the micelle free zone, and because it is a function of the properties of the monomers and micelles that are measurable (α, β, C_{CMC}, Γ_∞, σ and D_M) as well as the bulk concentration of micelles, it can be easily applied to real systems.

Ω_M^0 is the non-dimensional bulk micelle concentration, the value of the Ω_M^0 could be used to judge the emergence of the micelle free zone. When the non-dimensional bulk micelle concentration is larger than the critical value, i.e. $\Omega_M^0 > 0.609$, micelle diffusion is faster enough to keep up the kinetic adsorption, the micelle sublayer concentration never drops to zero, and the micelle free zone never occurs. In this case, the micelles at the sublayer break up to supply the monomers and maintain the monomer concentration

at the sublayer at the C_{CMC}. Since the monomer concentration is constant, the rate-limiting step to adsorption is the kinetic one, and the dynamic relaxation in concentration is given by Equation (4.11), with the relaxation in tension obtained from the equation of state. This is a limiting relaxation determined only by kinetics, and valid in principle for all bulk concentrations higher than the critical value.

In the case $\Omega_M^0 < 0.609$, micelle diffusion cannot keep up with the kinetic adsorption and the micelle sublayer concentration will drop to zero at a value $t^* = a^*$, and a micelle free zone will move outward from the surface (Figure 4.3). To describe this model, we first note that starting at time $t^* = 0$ and extending to a time $t^* = a^*$, micelle diffusion can keep up with kinetic adsorption and the sublayer concentration of monomer is equal to the C_{CMC} value. Equations (4.1)-(4.4) describe the micelle diffusion and adsorption. Inverting Laplace transforms for the bulk concentration of micelles provides analytical equations for the concentration distribution of micelles. Evaluating these distributions at a^* provides the micelle concentration distribution just before the micelle free zone begins to form. These distributions are shown in Figure 4.4 for three different bulk concentrations of micelles below the critical value.

For $t^* > a^*$ a micelle free zone develops (Fig. 4.3) and migrates into the bulk phase adjoining the interface. To solve for the transport of surfactant to the interface for this case, we break up the domain into two zones: (i) the micelle free zone ($0 < z < \delta(\tau)$) where only monomers are present and extending from the surface z=0 to the boundary between the micelle-free zone and the micelle zone (whose distance from the surface we mark as $\delta(\tau)$) and (ii) the micelle zone ($\delta(\tau) < z < \infty$) where micelles are present and diffuse towards the interface, and the monomer concentration is uniform

and equal to the C_{CMC} value. By scaling variables as following, we obtain the non-dimensional form for above model:

$$\tau = t - a \qquad B = \frac{D}{D_M}\left(\frac{n}{n-1}\right)^2 \Omega_M^{0\,2} \qquad B_M = \left(\frac{n}{n-1}\right)^2 \Omega_M^{0\,2} \qquad k = \frac{\beta C_{CMC}}{\alpha}$$

$$\delta^*(\tau^*) = \frac{\delta(\tau)}{h} \qquad C^* = \frac{C}{C_{CMC}} \qquad C_M^* = \frac{\sigma C_M}{\sigma C_M^0} \qquad \Gamma^* = \frac{\Gamma}{\Gamma_e} \qquad C_s^* = \frac{C_s}{C_{CMC}}$$

In the micelle free zone $0 < z^* < \delta^*(\tau^*)$, the diffusion of monomer $C^*(z^*, \tau^*)$ is given by:

$$\frac{\partial C^*}{\partial \tau^*} = B\frac{\partial^2 C^*}{\partial z^{*2}} \qquad 0 < z^* < \delta^*(\tau) \tag{4.14}$$

and in the micelle zone, the diffusion of micelles $C_M^*(z^*, \tau^*)$ is given by:

$$\frac{\partial C_M^*}{\partial \tau^*} = B_M\frac{\partial^2 C_M^*}{\partial z^{*2}} \qquad \delta^*(\tau^*) < z^* < \infty \tag{4.15}$$

At $z^* = 0$:

$$nB\frac{\partial C^*(0,\tau^*)}{\partial z^*} = \frac{\partial \Gamma^*}{\partial \tau^*} \tag{4.16}$$

$$\frac{\partial \Gamma^*}{\partial \tau^*} = C_s^*\left(1.0 - \Gamma^*\left(\frac{k}{1+k}\right)\right) - \frac{1}{(1+k)}\Gamma^* \tag{4.17}$$

And at the micelle free zone interface at $z^* = \delta^*(\tau^*)$

$$B\frac{\partial C^*(\delta^*(\tau^*),\tau^*)}{\partial z^*} = (n-1)B_M\frac{\partial C_M^*(\delta^*(\tau^*),\tau^*)}{\partial z^*} \tag{4.18}$$

$$C_M^*(\delta^*(\tau^*),\tau^*) = 0 \tag{4.19}$$

$$C^*(\delta^*(\tau^*),\tau^*) = 1.0 \tag{4.20}$$

Finally at $z^* = \infty$,

$$C_M^*(\infty,\tau) = 1.0 \tag{4.21}$$

With the given initial conditions are:

$$C^*(z^*,0)=1.0 \text{ and } C_M^*(z^*,0)=1.0 \qquad (4.22)$$

These equations are mostly easily solved by using a front trapping method as we describe in the appendix.

We plot in figure 4.5 the non-dimensional moving boundary $\delta^*(\tau^*)$ as function of square root of non-dimensional time $\sqrt{\tau^*}$. As the micelle free zone just begins, the micelle free zone $\delta^*(\tau^*)$ moves as a linear relationship of square root of non-dimensional time $\sqrt{\tau^*}$.

Figure 4.6a shows the non-dimensional moving boundary $\delta^*(\tau^*)$ as function of non-dimensional time τ^* at $\Omega_M^0 = 0.0477$ for later time. We note from this figure that the micelle free zone first develops with increasing time. With the adsorption onto the surface, the surface becomes saturated, and the kinetic adsorption rate to the surface decreases. This results in the decrease of concentration gradient of monomers across the micelle-free zone, which is indicated by figure 4.6b and 4.6d. At the front of the micelle free zone, the micelle flux should match the monomer flux, and the decrease of monomer flux across the micelle free zone causes the relaxation of micelle concentration gradient there, which is seen in figure 4.6c and 4.6e. This causes moving boundary $\delta(\tau)$ to move back towards the interface. When the equilibrium is approached, the kinetic adsorption exponentially decays, the front of micelle free zone come back to the interface till the micelle free zone finally disappear, .ie. $\delta^*(\tau^*)=0$, which occurs at about $\tau^* = 70$. Since then the micelle diffusion alone balance the exponentially decay of the kinetic adsorption, and the micelle concentration gradient gradually disappears and uniform bulk solution is approached. We break up $\delta^*(\tau^*)$ at different time. We plot in Figs 4.6b-4.6e the non-

dimensional monomer $C^*(z^*,\tau^*)$ and micelle concentration distribution $C_M^*(z^*,\tau^*)$ as a function of non-dimensional distance z^* corresponding to these times. Figures 4.6b and 4.6d show that once the micelle free zone occurs, the sublayer monomer concentration starts to decrease, and the monomer concentration gradient is developed in the micelle free zone with the migration of the micelle free zone into the bulk solution. The monomer concentration distribution in the micelle free zone becomes linear, a result which can be shown asymptotically. When the surface becomes saturated, the kinetic adsorption rate decreases. This causes the decrease of the monomer concentration gradient, the sublayer monomer concentration will increase because at the surface the monomer flux matches the kinetic adsorption. Eventually the monomer sublayer concentration comes back to C_{CMC}. Micelle concentration distribution starts with the initial distribution, which is shown in figure 4.4. The micelle concentration distribution is not linear. Figures 4.6c and 4.6e show the development of micelle concentration distribution since the micelle free zone starts. We could note from above figures that the micelle concentration gradient at the front of the micelle free zone decreases with increasing the time. This is because the kinetic adsorption rate decreases with the adsorption to the surface, and the monomer flux at the surface matches the kinetic adsorption. So the monomer concentration gradient decreases with the decrease of the rate of the kinetic adsorption. The linear behavior of monomer concentration in the micelle free zone will lead to decrease of the monomer concentration gradient at the front end of the micelle free zone. The monomer flux at the front of the micelle free zone matches the micelle concentration gradient there. This also causes the micelle concentration gradient to relax with the decrease of monomer

concentration at the front of micelle free zone. The return of the micelle concentration distribution will determine the return of the moving boundary $\delta^*(\tau^*)$.

We plot in figure 4.7 the non-dimensional moving boundary $\delta^*(\tau^*)$ as function of non-dimensional time τ^* at different non-dimensional surfactant concentration Ω_M^0. From figure 4.7 we could note that the maximum moving boundary length is larger at lower micelle bulk concentrations. This is because the initial micelle concentration gradient at the sublayer is larger at lower micelle bulk concentration, which is shown by figure 4.4. Before the micelle free zone starts, micelles break up to match kinetic adsorption, then micelle diffusive transport matches the micelle concentration gradient caused by the depletion of micelles. At lower micelle bulk concentration, the time period for such process is smaller, and the time period for micelle diffusion to reduce the micelle concentration difference is shorter. This results in the larger micelle concentration gradient at the lower micelle bulk concentration, so the driving force for the micelle free zone migration into the bulk phase is higher at the lower micelle bulk concentration. Theoretically we predict that the micelle free zone tends to infinity as the surfactant concentration approaches the C_{CMC}. Figure 4.8 shows the surface tension relaxation as function of non-dimensional time t^* for the Ω_M^0 below the critical value, and the limiting relaxation for the critical value.

4.3 Comparison of Micelle Transport Theory to Experimental Data

In order to compare the experimental data measured by the pendant bubble technique with the theoretical calculation, all above surfactant mass transfer equations are solved in the approximated pendant bubble spherical geometry for $C_{14}E_6$ assuming the

transport to be spherically symmetric and using Frumkin kinetics to describe the kinetic exchange, with the parameters Γ_∞, K, α and β as given from the equilibrium and dynamic tension relaxations below the C_{CMC}. For $C_{14}E_6$, the value of the critical micelle concentration below which the micelle free zone emerges is found from the definition of Ω_M^0 and the values of the kinetic constants and maximum packing concentration as measured previously. For the diffusion coefficient of the micelles, we use a value of $1.5x10^{-10}m^2/sec$, which was measured from previous studies of dynamic adsorption of $C_{14}E_6$ from micellar solutions onto a solid surface[43,44] and for R_o we use 1 mm, the characteristic size of the pendant bubble. Based on the value of these parameters, the non-dimensional sublayer micelle concentration $\frac{C_M(R_0,t)}{C_M^0}$ as function of time is plotted in figure 4.9. From figure 4.9, we find that the dimensional critical concentration is n=4.25 for $C_{14}E_6$. Thus for surfactant concentrations from just above the C_{CMC} to the $4.25C_{CMC}$, micelle free zones should exist. While for concentrations above $4.25C_{CMC}$ micelles exist everywhere in solution and no micelle free zone exists. In the case of $C_T < 4.25C_{CMC}$ micelle diffusion cannot keep up with the kinetic adsorption and the micelle sublayer concentration will drop to zero at a value $t = a$, and a micelle free zone will move outward from the surface as we described in detail before. Equations (4.1)-(4.4), which describe the micelle diffusion and adsorption, are written in spherical coordinate. Inverting Laplace transforms for the bulk concentration of micelles provides analytical equations for sublayer micelle concentration and the concentration distribution of micelle, which are described by Equation (4.23) and (4.24) in the non-dimensional form. Evaluating these distributions at $t = a$ provides the micelle concentration distribution just

before the micelle free zone begins to form. These distributions are shown in Figure 4.10 for three different bulk concentrations of micelles below the critical value.

$$\frac{C_M(R_0^*,t^*)}{C_M^0}=1.0-\frac{1}{\sqrt{\pi}\Omega_M^0}\int_0^{t^*}\frac{\partial\Gamma^*}{\partial\omega^*}\frac{1}{\sqrt{(t^*-\omega^*)}}d\omega^* + \frac{n}{n-1}\frac{1}{R_0^*}\int_0^{t^*}\frac{\partial\Gamma^*}{\partial\omega^*}\exp\left((t^*-\omega^*)\frac{B_M}{R_0^{*2}}\right)erfc\left(\frac{1}{2}\frac{\sqrt{(t^*-\omega^*)B_M}}{R_0^*}\right)d\omega^* \tag{4.23}$$

$$\frac{C_M(r^*,t^*)}{C_M^0}=1.0-\frac{1}{\sqrt{\pi}\Omega_M^0}\frac{R_0^*}{r^*}\int_0^{t^*}\frac{\partial\Gamma^*}{\partial\omega^*}\frac{1}{\sqrt{(t^*-\omega^*)}}\times \exp\left(-\frac{1}{4(t^*-\omega^*)}\left(\frac{(R_0^*-r^*)^2}{B_M}\right)\right)d\omega^* + \left(\frac{n}{n-1}\right)\frac{1}{r^*}\int_0^{t^*}\frac{\partial\Gamma^*}{\partial\omega^*}\exp\left(\frac{R_0^*-r^*}{R_0^*}+(t^*-\omega^*)\left(\frac{B_M}{R_0^{*2}}\right)\right)\times erfc\left(\frac{1}{2}\frac{(R_0^*-r^*)}{\sqrt{(t^*-\omega^*)B_M}}+\frac{\sqrt{(t^*-\omega^*)B_M}}{R_0^*}\right)d\omega^* \tag{4.24}$$

with the scaling the variable $r^*=\frac{r}{h}$ $\qquad$ $R_0^*=\frac{R_0}{h}$

The non-dimensional Fumkin kinetic equation is expressed as

$$\frac{\partial\Gamma^*}{\partial t^*}=C_s^*\left(1.0-\Gamma^*\left(\frac{k}{1+k}\right)\right)-\frac{1}{(1+k)}\Gamma^*\exp\left(K\Gamma^*\left(\frac{k}{1+k}\right)\right) \tag{4.25}$$

For $t>a$ a micelle free zone develops, equations (4.14)-(4.22) which describe the physical model, are written in spherical coordinate and using the Frumkin kinetics to describe the kinetic exchange. These equations are also solved by the front -trapping method.

The simulation of moving boundary $\delta(\tau)$ at different surfactant concentration are plotted in figure 4.11. Based on above theoretical principle, we did experiments of measuring dynamic surface tension of $C_{14}E_6$ surfactant solution at concentration $1.27C_{CMC}$, $2C_{CMC}$, $3C_{CMC}$ and $4C_{CMC}$. Figure 4.12 shows a comparison between measurements of the dynamic surface tension for bulk concentrations of $C_{14}E_6$ from 1-4 times the C_{CMC} (recall the critical value for which the micelle free zone forms is $4.25C_{CMC}$) and simulation results for these concentrations using the front trapping method. The computed dynamic tensions agree well with the data, affirming the treatment of the micelle breakup as fast with respect to diffusion and kinetic adsorption.

4.4 Discussion and Conclusion

In this section, we develop a theoretical framework to describe the surfactant transport and dynamic surface tension reduction due to surfactant adsorption to an initially clean interface from a bulk solution above the critical micelle concentration (C_{CMC}). Here we examine the case in which the rate of micelle breakdown is much faster than the rate of its bulk diffusion towards the surface. This will be the case as long as the actual micelle concentration is not too high. Our theoretical calculations show for $C_{14}E_6$ that above a critical micellar concentration i.e. $C_T \geq 4.25C_{CMC}$ diffusion of micelles from the bulk is fast enough to keep the monomer concentration in the sublayer at the C_{CMC} until equilibrium is achieved on the surface. Below a critical bulk micelle concentration i.e. $C_T < 4.25C_{CMC}$, micelle diffusion is not fast enough and the micelle concentration at the sublayer falls to zero at $t = a$, since then the micelle free zone occurs. The computed

dynamic tensions agree well with the experimental data, affirming the treatment of the micelle breakup as fast with respect to diffusion and kinetic adsorption.

The theory predicts that once the surfactant concentration is higher than the critical value, i.e. $C_T > 4.25C_{CMC}$, the dynamic surface tension relaxation is determined only by the kinetics. Since in this case, micelles exist everywhere in the solution and the monomer concentration is constant. The rate limiting step to adsorption is the kinetic one. The dynamic relaxation in concentration is given by integrating the Frumkin kinetic equation, with the relaxation in tension obtained from the equation of state. This is a limiting relaxation determined only by kinetics, and valid in principle for all bulk concentrations greater than the critical value. But the experimental data which is plotted in figure 4.13 shows that the dynamic surface tension relaxation becomes faster with increasing surfactant bulk concentration. This may indicate that micelle adsorption. The modeling of micelle adsorption is discussed in the future work.

Appendix

Equations (4.14)-(4.22) are most easily solved by using a front trapping method as we describe in the following. We define a variable $\Xi(z^*,\tau^*)$ defined on the domain $0 < z^* < \infty$ by the following relations:

$$\Xi(z^*,\tau^*) = C^*(z^*,\tau^*) \qquad (0 < z^* < \delta^*(\tau);\ \Xi(z^*,\tau^*) < 1.0)$$
$$\Xi(z^*,\tau^*) = C^*(z^*,\tau^*) + (n-1)\times C_M^*(z^*,\tau^*) \quad (\delta^*(\tau^*) < z^* < \infty;\Xi(z^*,\tau^*) \geq 1.0) \tag{4.26}$$

From the above boundary conditions on the monomer and micellar concentrations, it is clear that $\Xi(z^*,\tau^*)$ is a continuous function of z^*. We define a piecewise continuous diffusion coefficient B^* which is a function of $\Xi(z^*,\tau^*)$ as given by the relation:

$$B^*(\Xi(z^*,\tau^*)) = B \qquad (\Xi(z^*,\tau^*) < 1.0) \tag{4.27}$$
$$B^*(\Xi(z^*,\tau^*)) = B_M \qquad (\Xi(z^*,\tau^*) > 1.0).$$

Consider the following differential conservation equation for $\Xi(z^*,\tau^*)$:

$$\frac{d}{dz^*}\left\{B(\Xi(z^*,\tau^*))\frac{d}{dz^*}\Xi(z^*,\tau^*)\right\} = \frac{\partial\Xi(z^*,\tau^*)}{\partial\tau^*} \tag{4.28}$$

Subject to the boundary conditions:

$$\frac{\partial\Gamma^*}{\partial\tau^*} = C_s^*\left(1.0-\Gamma^*\left(\frac{k}{1+k}\right)\right) - \frac{1}{1+k}\Gamma^* \tag{4.29}$$

$$nB\frac{\partial\Xi(z^*,\tau^*)}{\partial z^*}\bigg|_{z^*=0} = \frac{\partial\Gamma^*}{\partial\tau^*} \tag{4.30}$$

$$\Xi(z^* \to \infty,\tau^*) = n \tag{4.31}$$

Subject to the initial condition:

$$\Xi(z^*,\tau^* = 0) = 1.0 + (n-1)\times C_M^*(z^*,t^* = a^*) \tag{4.32}$$

Where $C_M^*(z^*, t^* = a^*)$ is the micelle concentration distribution at the end of the induction period where the sublayer micelle concentration drops to zero. This concentration field was shown in Figure 4.9. The solution to the above equations (4.26)-(4.32) can be solved by a standard finite difference numerical technique, subdividing the z^* axis into partitions of thickness Δz^*, and discretizing $\Xi(z^*, \tau^*)$ by its values at the ends of each of the subdivisions. The numerical solution to these equations is equivalent to the equations prescribed earlier in which the mass transfer was described by two separate regions. The thickness $\delta^*(\tau^*)$ of the micelle free zone can be calculated from $\Xi(z^*, \tau^*)$ by finding the subdivision which brackets $\Xi(z^*, \tau^*) = 1.0$. Integrating (4.28) between these two subdivisions shows that the continuous system satisfies the discrete mass balance of eq. (4.18).

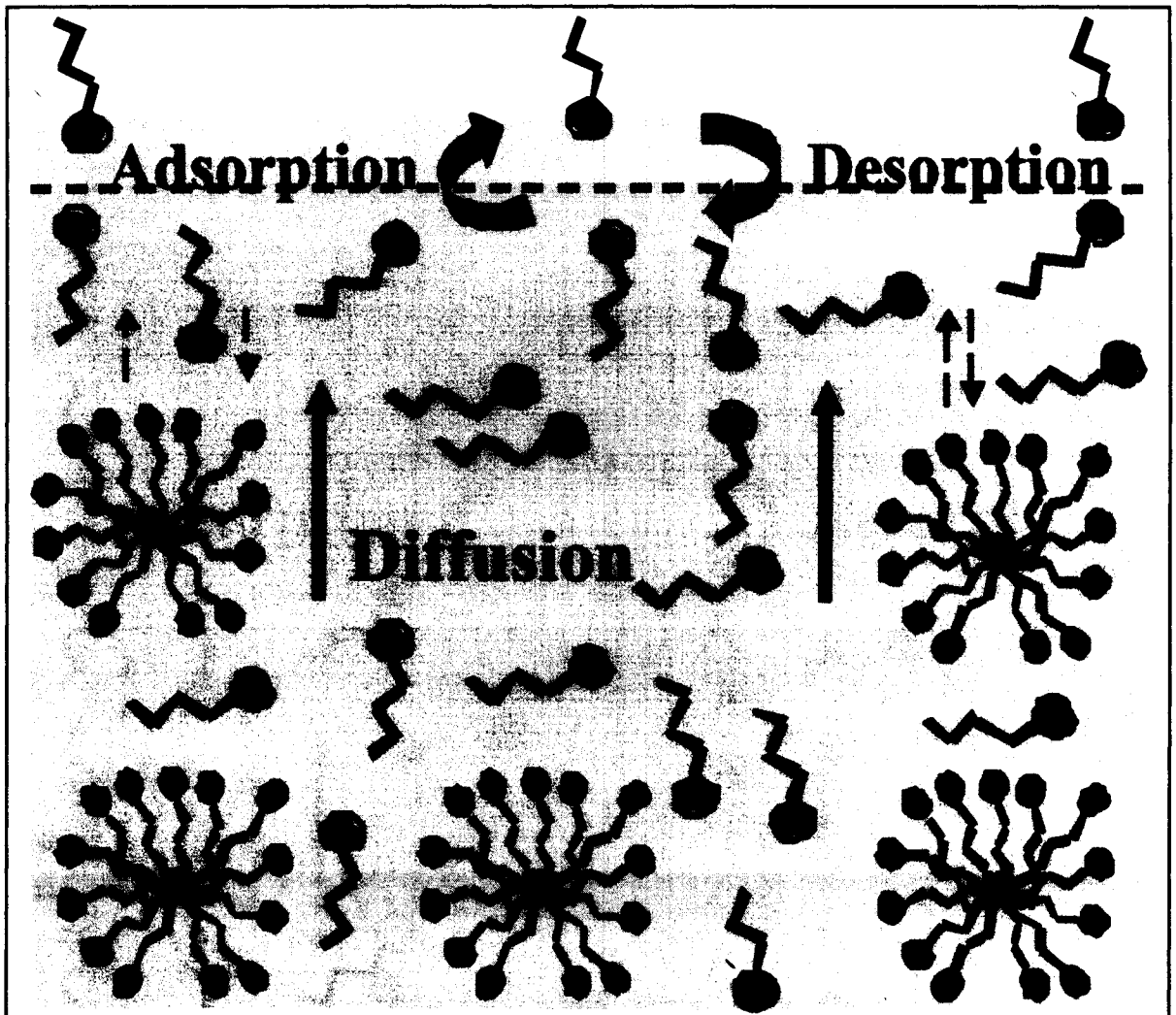

Figure 4.1 Schematic representation of surfactant transport from micellar solution

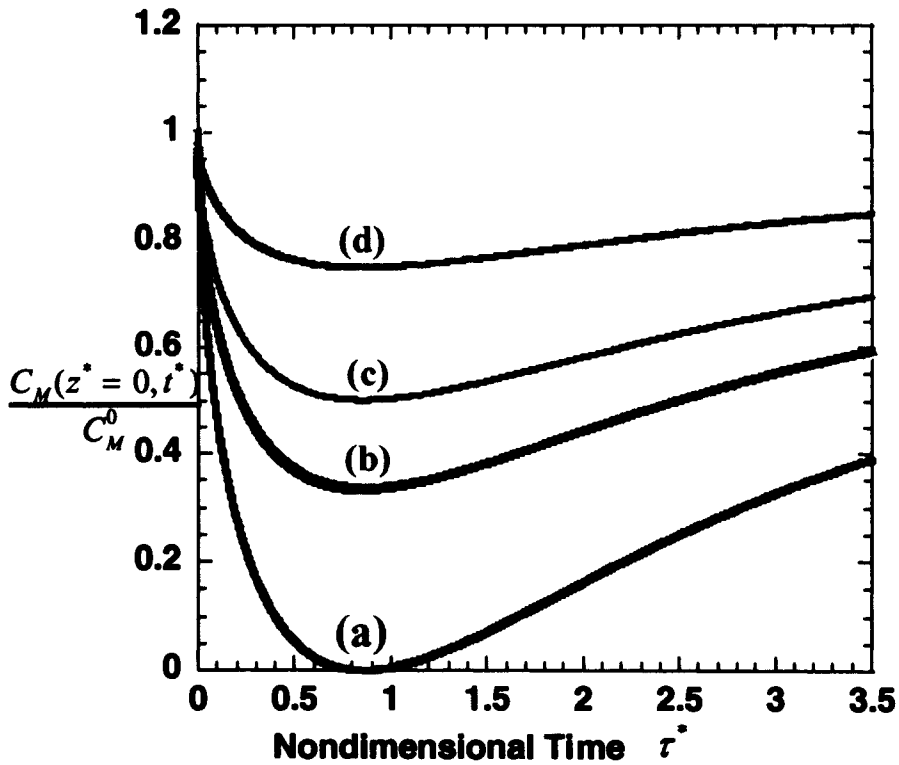

Figure 4.2 Non-dimensional Sublayer Micelle Concentration as function of non-dimensional time (a): $\Omega_M^0 = 0.609$ n=4.445, (b): $\Omega_M^0 = 1.5 \times 0.609$ n=6.179 (c); $\Omega_M^0 = 2.0 \times 0.609$ n=7.904 (d): $\Omega_M^0 = 3.0 \times 0.609$ n=11.357

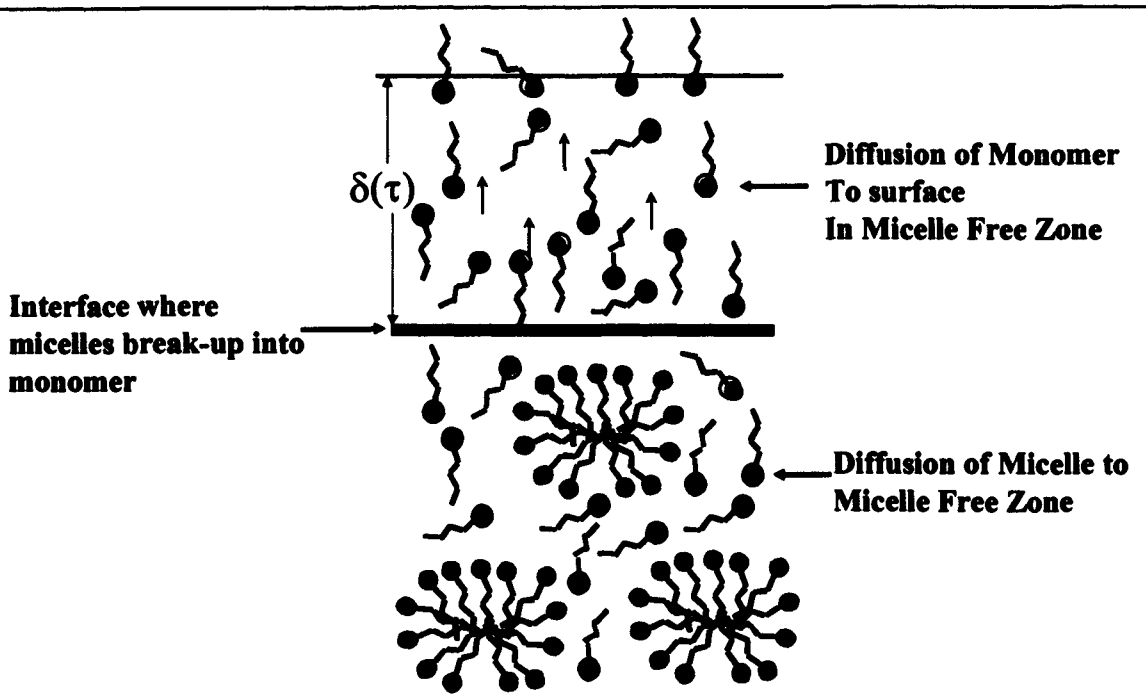

Figure 4.3 Micelle Free Zone

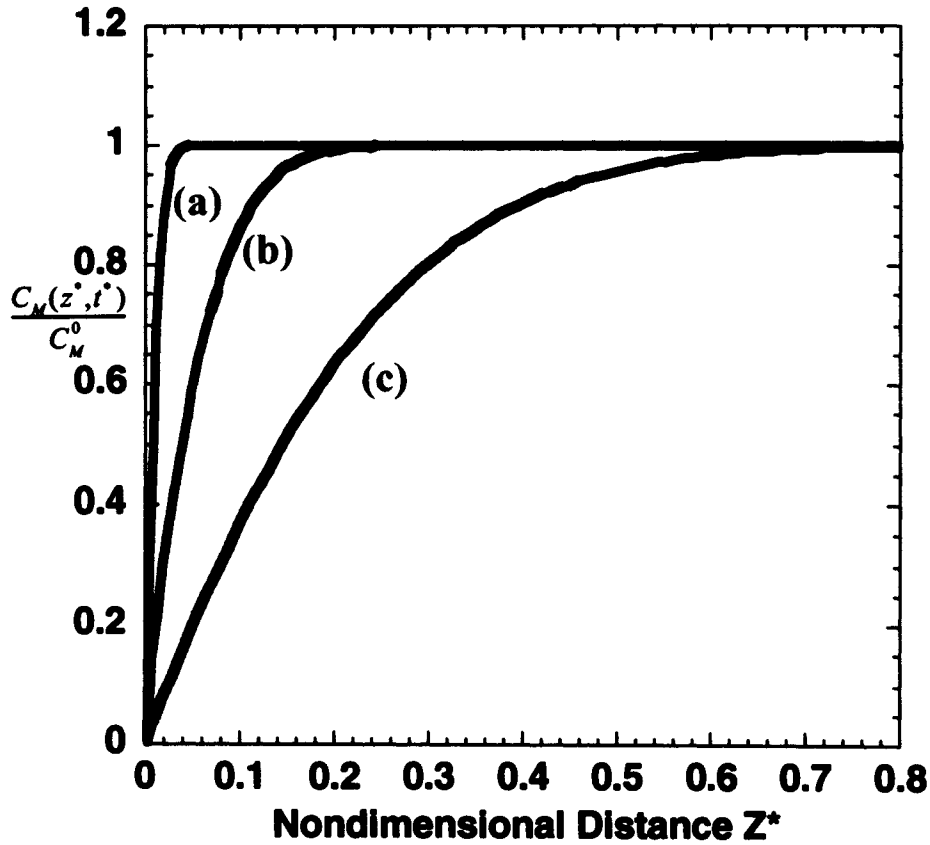

Figure 4.4 Non-dimensional micelle concentration at $t^* = a^*$:
(a)Ω_M^0 = 0.0477,n=1.27; (b)Ω_M^0 = 0.1768,n=2.0; (c):Ω_M^0 = 0.3537,n=3.0

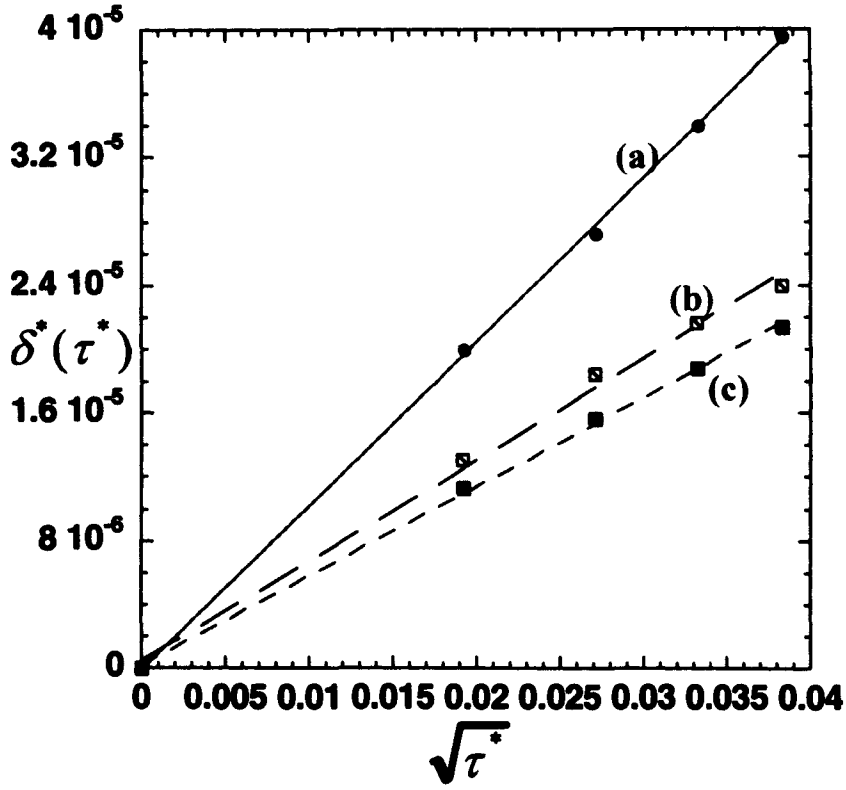

Figure 4.5 The non-dimensional moving boundary as function of square root of non-dimensional time (a);Ω_M^0 = 0.0477 n=1.27(b):Ω_M^0 = 0.1768 n=2.0 (c):Ω_M^0 = 0.3537 n=3.0

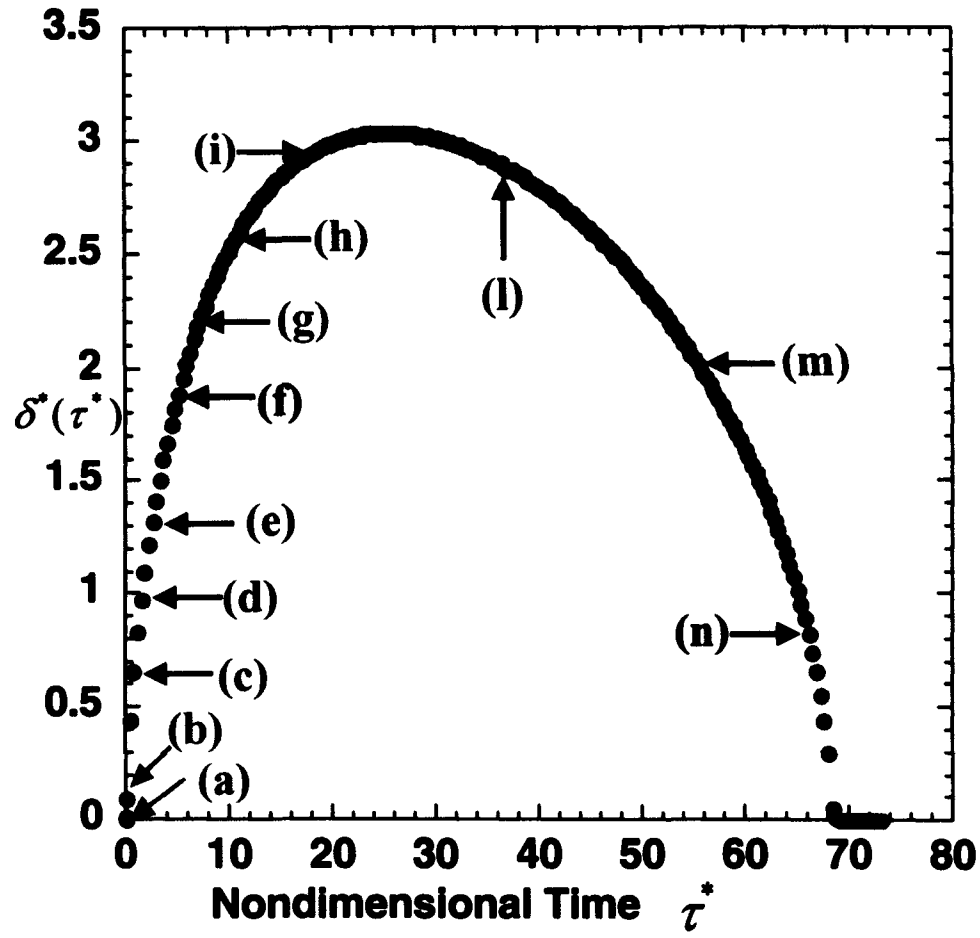

Figure 4.6a Non-dimensional moving boundary as a function of non-dimensional time at $\Omega_M^0 = 0.0477$ n=1.27 (a): $\tau^* = 0$ (b): $\tau^* = 0.3677$; (c): $\tau^* = 1.1031$ (d): $\tau^* = 1.8384$; (e) $\tau^* = 2.9414$ (f): $\tau^* = 5.5152$ (g): $\tau^* = 7.3537$ (h): $\tau^* = 11.0305$; (i): $\tau^* = 18.3841$ (l): $\tau^* = 36.7683$; (m) $\tau^* = 55.1524$; (n): $\tau^* = 66.1829$

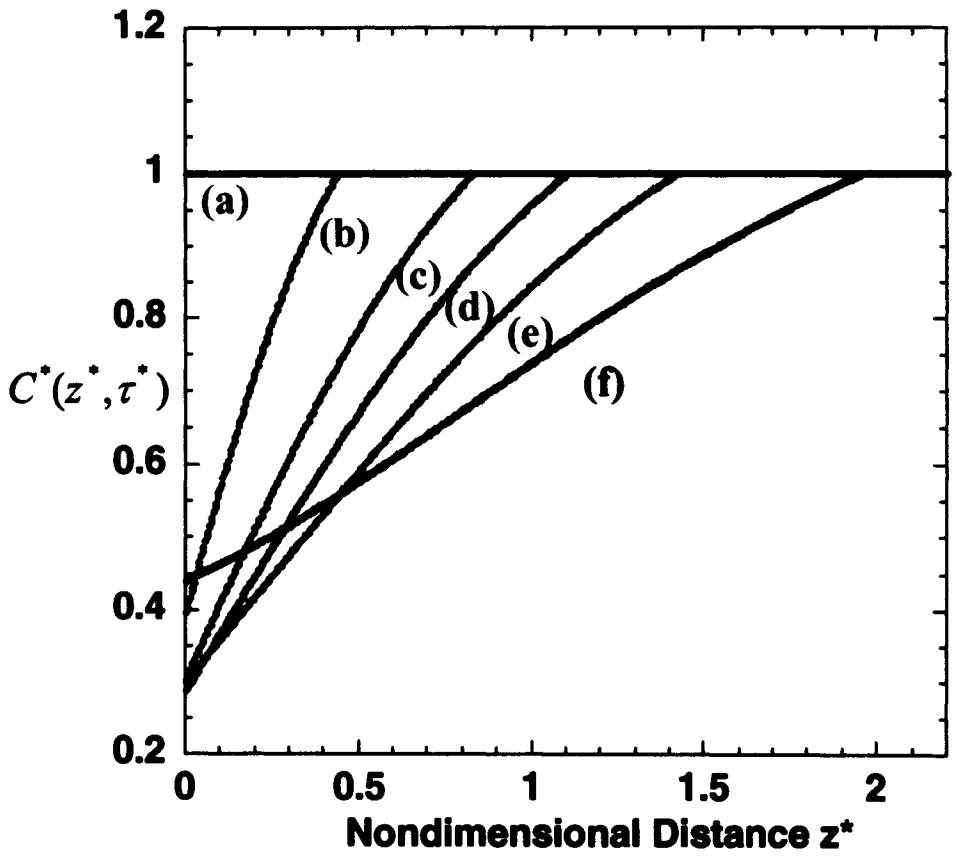

Figure 4.6b Non-dimensional monomer concentration distribution at different non-dimensional time at $\Omega_M^0 = 0.0477$ n=1.27 (a): $\tau^* = 0$ (b): $\tau^* = 0.3677$; (c): $\tau^* = 1.1031$ (d): $\tau^* = 1.8384$; (e) $\tau^* = 2.9414$;(f): $\tau^* = 5.5152$

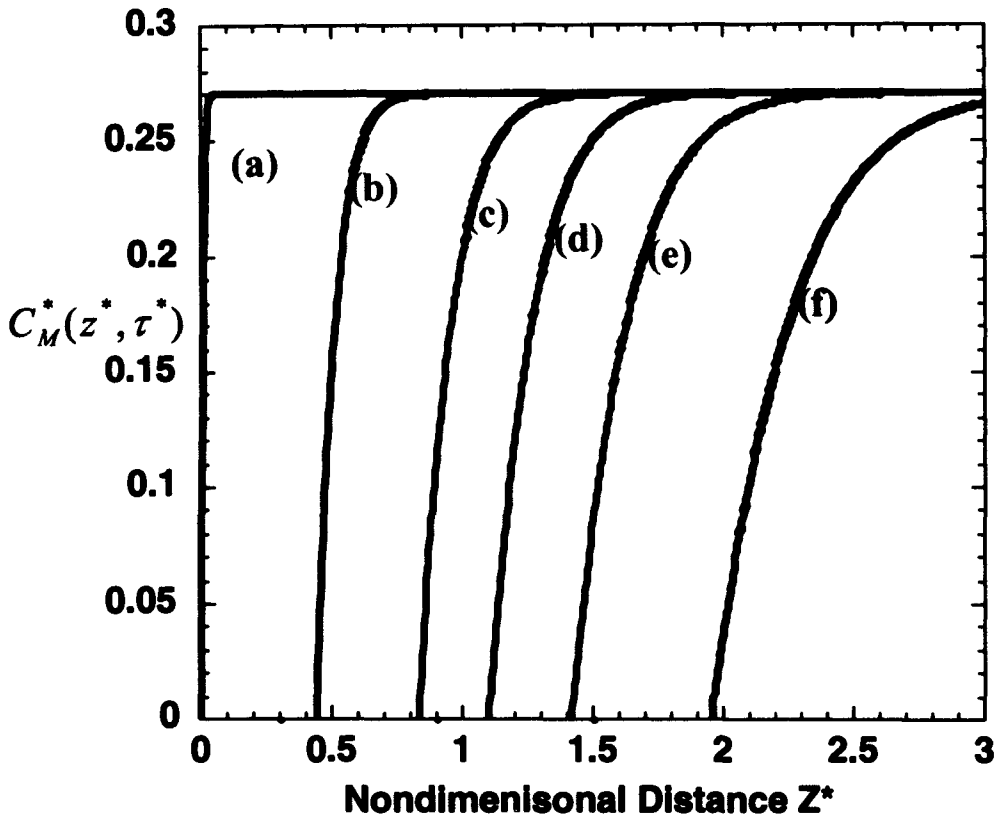

Figure 4.6c Non-dimensional micelle concentration distribution at different non-dimensional time at $\Omega_M^0 = 0.0477$ n=1.27 at (a): $\tau^* = 0$;(b): $\tau^* = 0.3677$; (c): $\tau^* = 1.1031$ (d): $\tau^* = 1.8384$; (e) $\tau^* = 2.9414$;(f): $\tau^* = 5.5152$

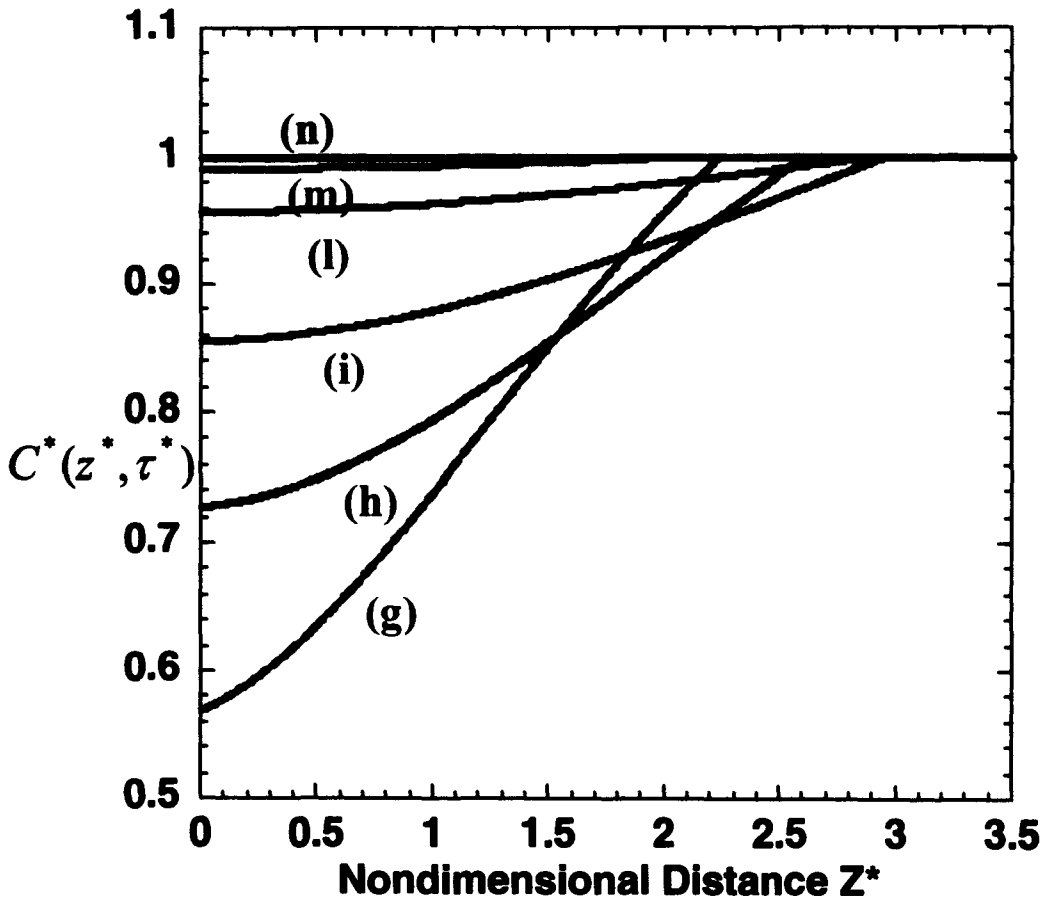

Figure 4.6d Non-dimensional monomer concentration distribution at different time at Ω_M^0 = 0.0477 n=1.27 (g): τ^* = 7.3537 (h): τ^* =11.0305 ; (i): τ^* =18.3841 (l): τ^* =36.7683; (m) τ^* =55.1524 ; (n): τ^* =66.1829

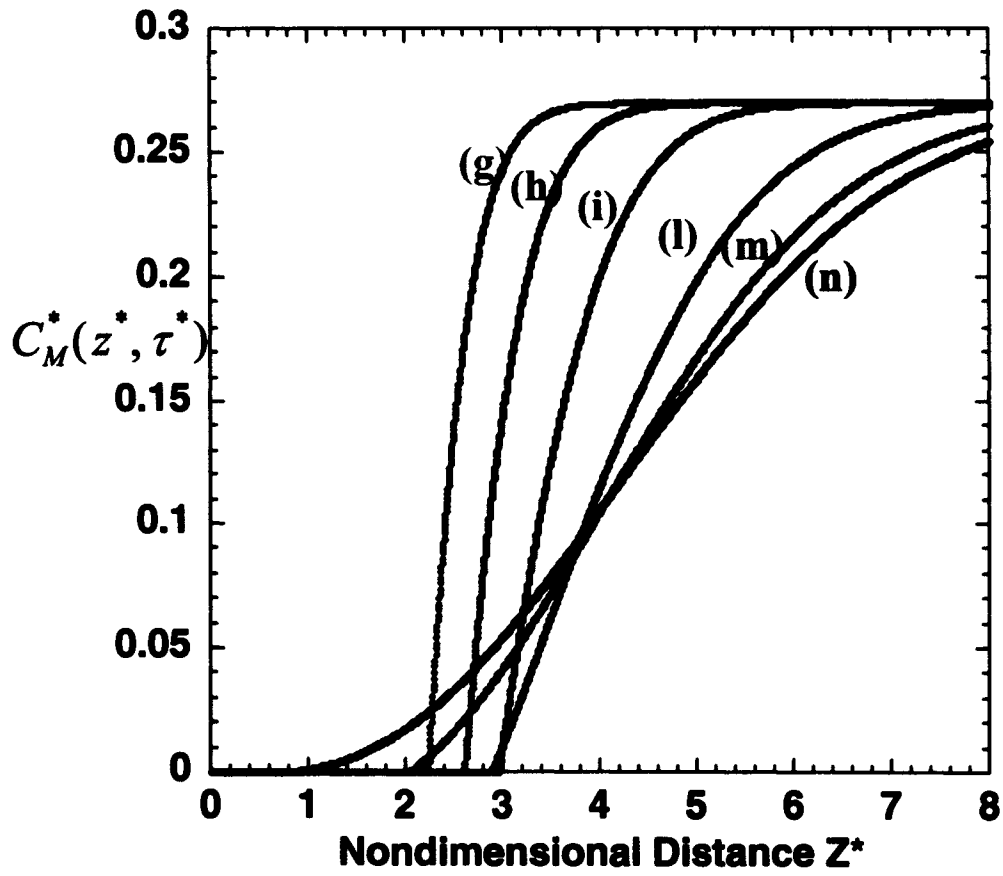

Figure 4.6e Non-dimensional micelle concentration distribution at $\Omega_M^0 = 0.0477$ n=1.27 (g): $\tau^* = 7.3537$ (h): $\tau^* = 11.0305$; (i): $\tau^* = 18.3841$ (l): $\tau^* = 36.7683$; (m) $\tau^* = 55.1524$; (n): $\tau^* = 66.1829$

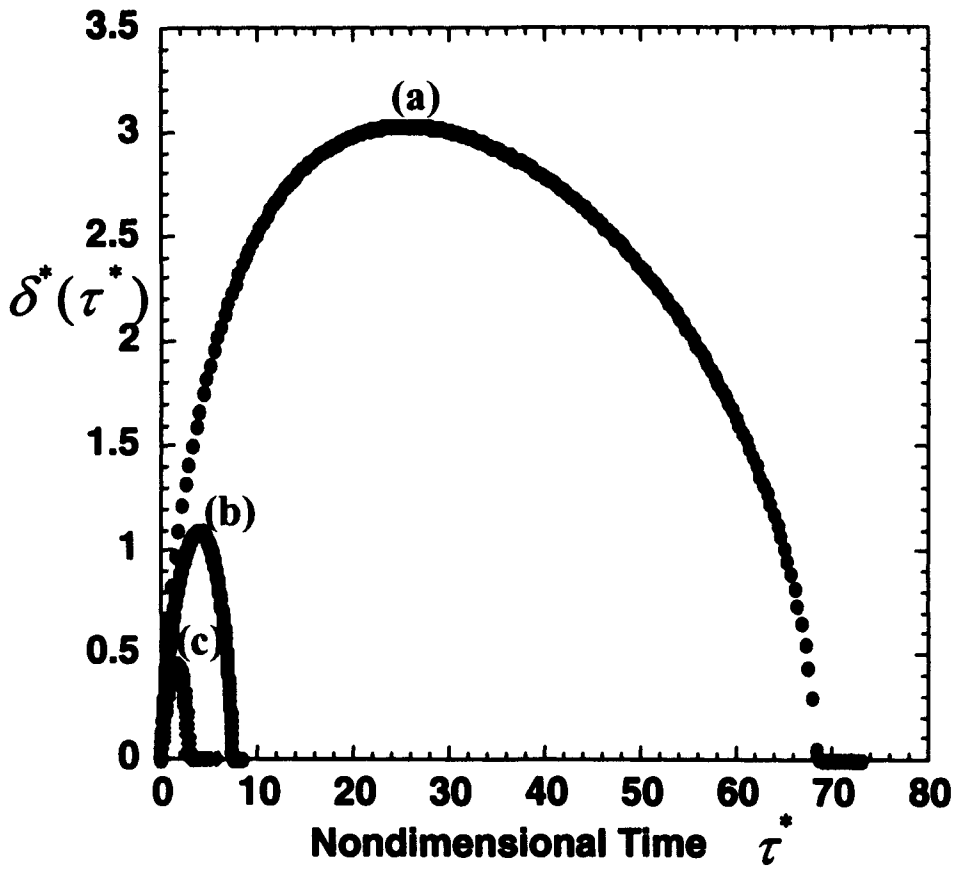

Figure 4.7 Non-dimensional moving boundary at different concentration (a):Ω_M^0 = 0.0477 n=1.27 (b):Ω_M^0 = 0.1768 n=2.0 (c):Ω_M^0 = 0.3537 n=3.0

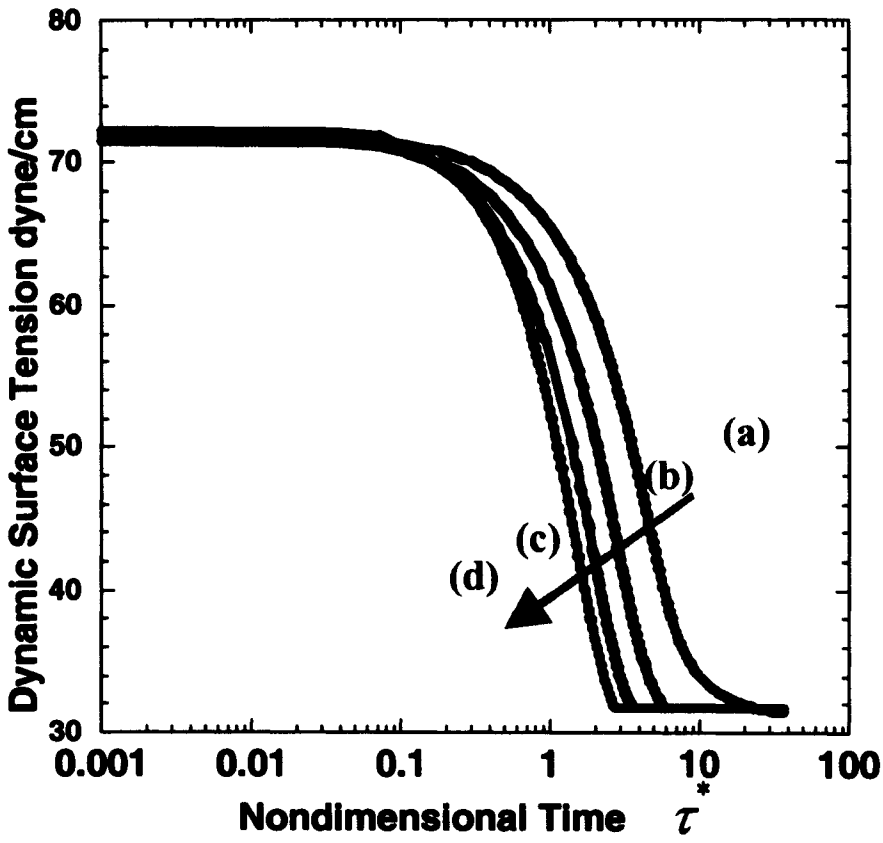

Figure 4.8 Simulation dynamic surface tension as function of non-dimensional time (a):Ω_M^0 = 0.0477 n=1.27 (b):Ω_M^0 = 0.1768 n=2.0 (c):Ω_M^0 = 0.3537 n=3.0 (d): kinetic limit

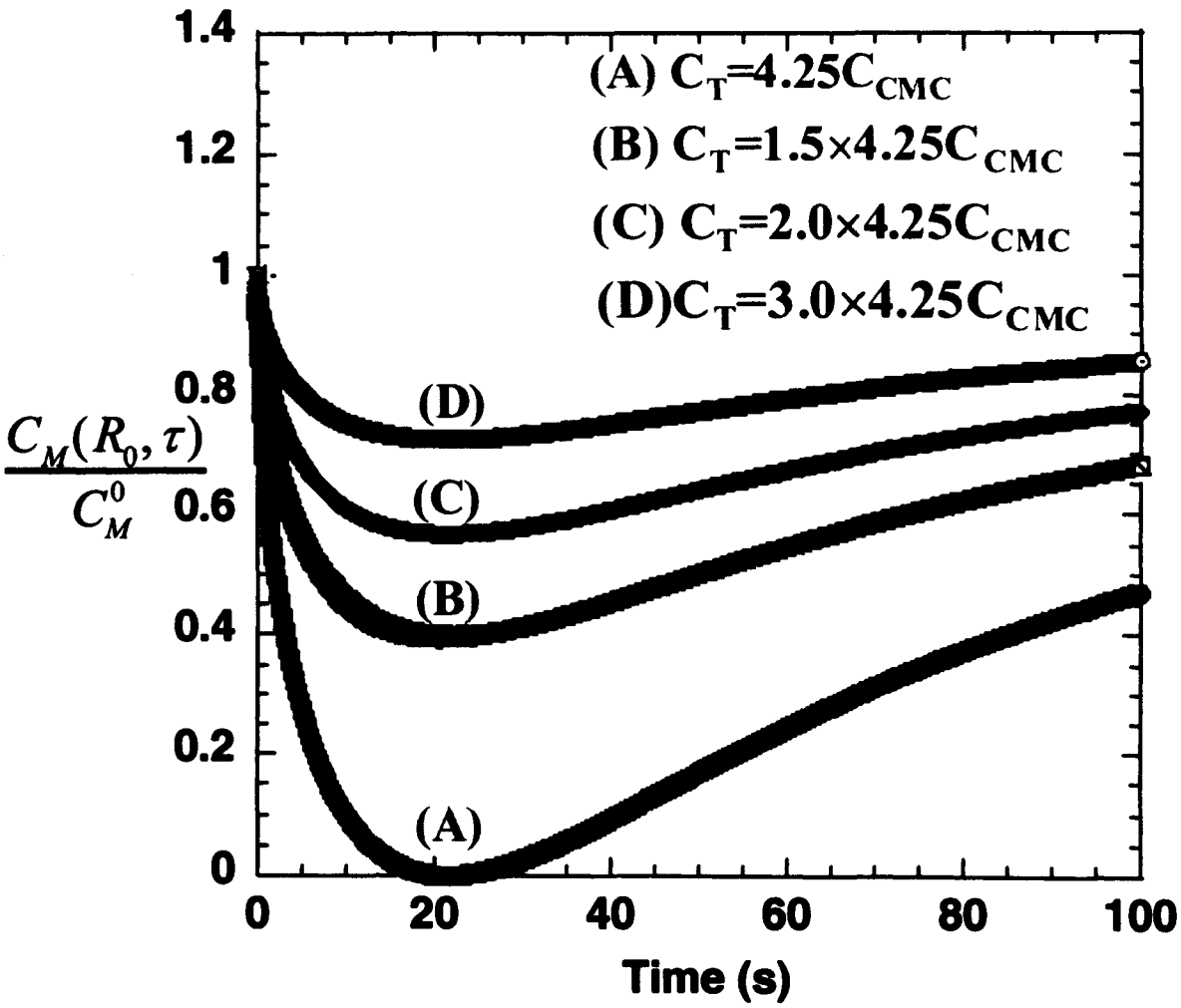

Figure 4.9 Non-dimensional micelle sublayer concentration $C_M(R_0,t) / C_M^0$ as function of time (A): C_T=4.25CMC (B): C_T=2×4.25CMC (C): C_T=3×4.25CMC (D): C_T=4×4.25CMC

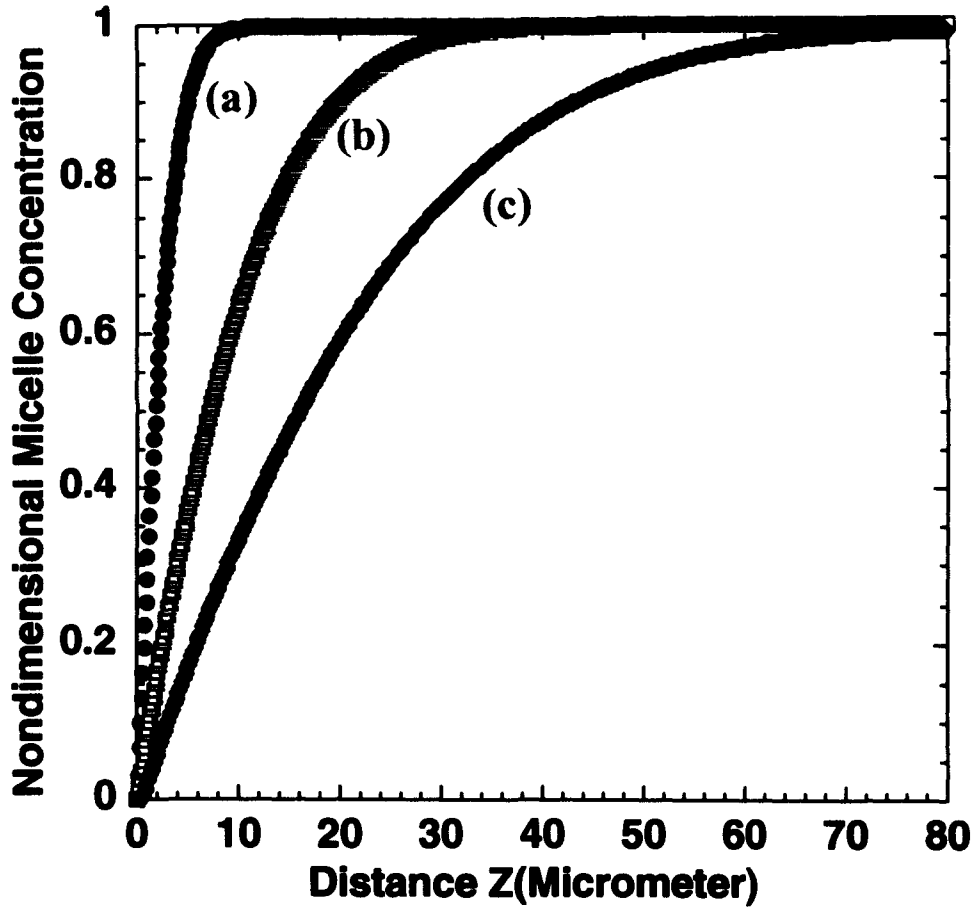

Figure 4.10 Micelle Concentration Distribution at t=a at Different Surfactant Concentration: (a) $C_T = 1.27C_{CMC}$ **(b)** $C_T = 2C_{CMC}$ **(c)** $C_T = 3C_{CMC}$

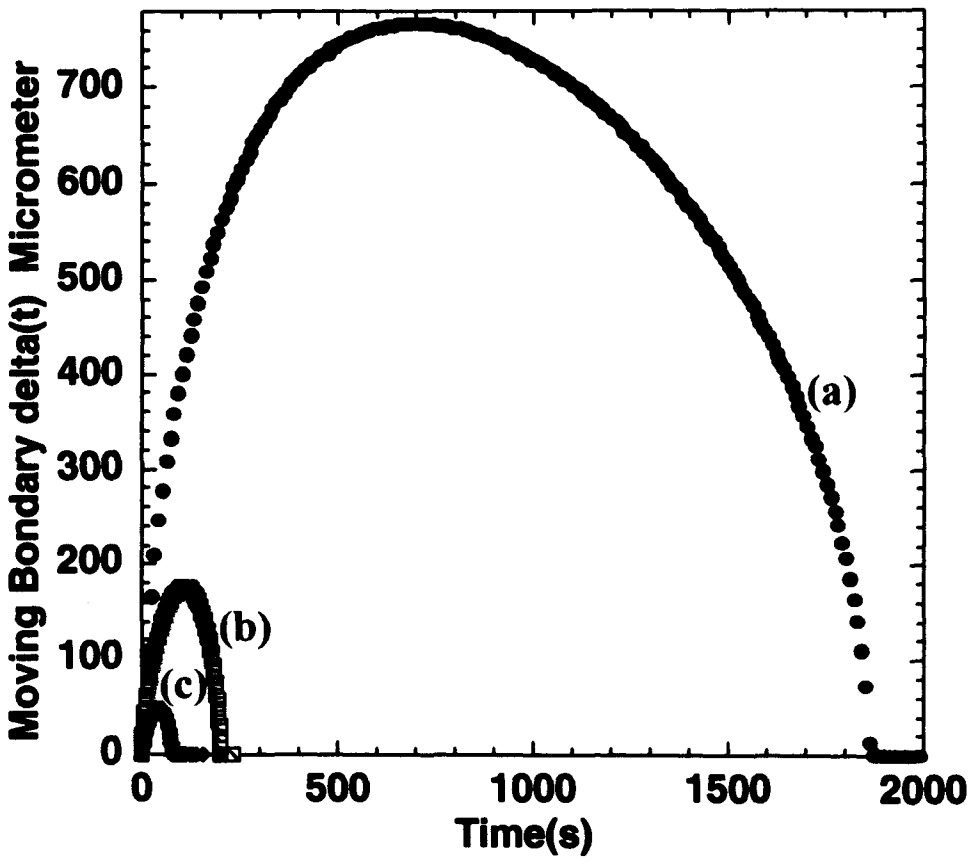

Figure 4.11 Moving boundary $\delta(\tau)$ at different surfactant concentration: (a) $C_T = 1.27C_{CMC}$ (b) $C_T = 2C_{CMC}$ (c) $C_T = 3C_{CMC}$

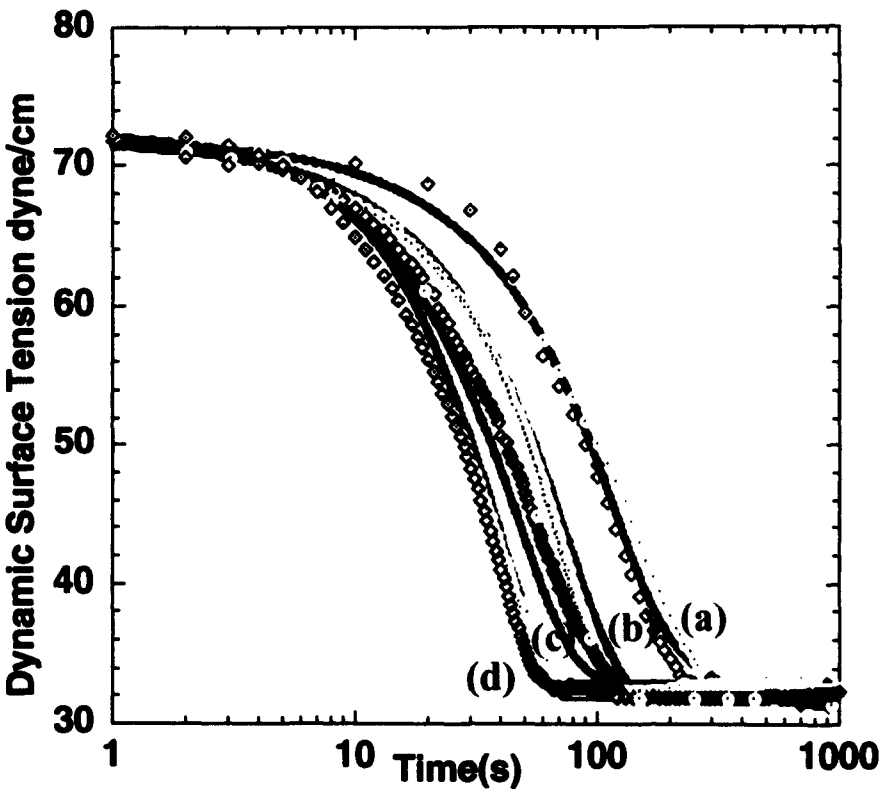

Figure 4.12 Dynamic surface tension measurement above the CMC but below the critical value micelle concentration (a) $C_T = 1.27C_{CMC}$ **(b)** $C_T = 2C_{CMC}$ **(c)** $C_T = 3C_{CMC}$ **(d)** $C_T = 4C_{CMC}$

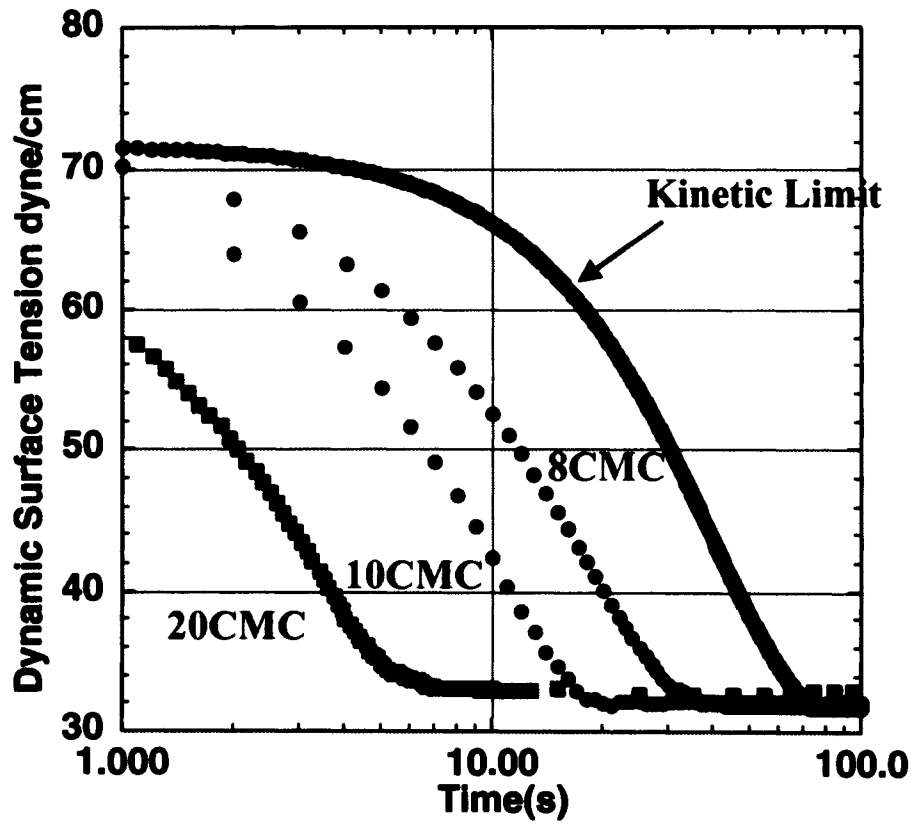

Figure 4.13 Dynamic surface tension at increasing bulk concentration

CHAPTER 5 EXPERIMENTAL VISUALIZATION WITH FLUORESCENCE MICROSCOPY METHOD

5.1 Introduction

The purpose of this work is to try to use solubilization of dyes to visualize our transport model[1], with the fluorescence microscopy technique. Fluorescence microscopy provides a number of possibilities, beside the adsorption methods[2]. Where fluorescence probes can be selectively excited, detected in a complex and observed in a very small number. Fluorescence microscopy has been widely used in biological process, such as, DNA sequences in the inter phase nucleus[3], living cells[4] et al. The ability to visualize the phase behavior of monolayers of amphiphilic molecules, produced by spreading or more importantly by adsorption from solution (Gibbs films), is a tremendous aid in understanding monolayer systems. Visual confirmation of two-phase coexistence states of myristic[5] pentadecanoic[6], and stearic acid[7] has been obtained with fluorescence microscopy. Direct evidence of the long-rang tilt ordering of the chains in the L_2 and more condensed monolayer phases has been obtained from polarized fluorescence microscopy (PFM) and polarization analysis of the reflecting in brewster angle microscopy (BAM)[8]. G-L_1-L_2 monolayer phase transitions for the least soluble polyethoxylates and these transitions lead to plateaus in dynamic tension reduction is demonstrated by fluorescence microscopy[9]. In fluorescence microscopy[10], a small amount (<1 mol%) of a water-insoluble amphiphilic dye with a fluorescing chromophore is spread onto the air-water surface along with the amphiphiles under study. The chromophore fluorescence is typically enhanced in a lipid environment while being

quenched by water. The monolayer is illuminated at the excitation frequency of the dye, and the interface fluorescence is optically filtered and observed.

Solubilization is a micellar phenomenon. It cannot occur below CMC, and also hydrocarbon chains of amphiphiles are not fluorescent at usable wavelength. By using right kind of fluorescent probes, which are molecules containing suitable chromophores that soluble in the micelles but not soluble in surfactant solutions, the surfactant micelles could be labeled with dyes under the mechanism of solubilization of micelles. Micelles could be illuminated at the excitation frequency of the dyes and monomers could not.

In fluorescence microscopy method, we use the insoluble fluorescence probe, NBD-HAD, to lable micelles. Fluorescence probes could dissolve into the micelles and stay on the surface but insoluble in the water. The dye fluoresces in the microenvironment of micelles but quenched in the aqueous solution at the excitation of the laser. The region with micelles is illuminated, but the region without micelles appears dark. The theoretical framework predicts that there are two regimes for surfactant transport from micellar solution to clean air/water interface. Regime I is the case when the concentration of surfactant solution is higher than the critical value (we recall that the critical value for $C_{14}E_6$ is 4.25CMC). Under such condition, the bulk micelle concentration is large enough that the bulk diffusion of micelles can match for all time the kinetic adsorption. Monomer concentration everywhere is CMC, and micelle free zone does not occur. Tension relaxation is determined only by adsorption kinetics. Since the micelles exist everywhere in the surfactant solutions, the surfactant solutions will appear to be bright everywhere at the excitation of the fluorescence laser. When the concentration of surfactant solution is higher than the CMC but lower than the critical

value, the system enters regime II. In this case, the bulk concentration of micelles is not high enough. Micellar diffusion cannot match kinetic adsorption, the sublayer concentration of micelles becomes zero at some time, and the edge of this micelle free zone forms and grows outward from the surface into the bulk. Outside this zone is micelle zone, monomer concentration is maintain at CMC, and micelles diffuse from the bulk to the front of the zone where they breakdown and supply monomers which then diffuses through the micelle free zone and absorbs onto the surface. In micelle free zone, there are no micelles exist. Upon illumination, the dye does not fluoresce in the micelle free zone because the dye is not soluble in water. In the micelle zone, the dye does fluoresce because of the solubilization of dye in the micelles. With the adsorption of monomers onto the surface, the surface becomes saturated and the front of micelle free zone returns to the surface. This dark region becomes smaller. Eventually when the equilibrium is achieved the front of micelle free zone will come back at the surface. This dark region will finally disappear.

5.2 Experimental Visualization with Fluorescence Microscopy Method

5.2.1 Materials

The poly(ethylene glycol) alkyl ether surfactant $C_{14}E_6(CH_3(CH_2)_{13}(OCH_2CH_2)_6OH)$ obtained from Nikko Chemical Company, Ltd.(Japan), is stored in the dark under nitrogen, and is used without further purification. Fresh aqueous solutions are prepared for each experiment using deionized water from a Milli-Q water purification system fitted with an Organex-Q column to remove trace

contaminants (Millipore, MA). The resistivity of the deionized water was at least 15MΩ cm.

For fluorescence observations, the surfactant solutions were doped with small amounts of the insoluble fluorophore NBD-HAD (4-(hexadecylamino)-7-nitrobenz-2-oxa-1,3-diazole) consisting of C16 tail and NBD-amine weakly polar headgroup, supplied by Molecular Probes, Eugene,OR.

In fluorescence method, insoluble fluorophore NBD-HDA is dissolved in HPLC-grade chloroform, stabilized with 0.5-1.0% ethanol, supplied by sigma, St. Louis, MO, or Fluka. All amphiphiles and solvents are used as received. The subpahse in all experiments is deionized water purified by a Mlli-Q filter system fitted with an Orgdnex-Q column to remove trace contaminants (Millipore,MA). The resistivity of the deionized water at least 15MΩcm).

5.2.2 Florescence Microscopy Observations

A schematic of our fluorescence setup is shown in Figure 5.1. As described in more detail by other authors, the main components are a light source for excitation of the fluorophore at the interface, an optical filter to isolate the fluorescence emission, and a high-sensitivity camera to view the fluorescence contrast in surfactant solution. The insoluble fluorophore used in this study, NBD-HDA, has its absorbance and emission bands with maxima at 468nm and 523 nm, respectively. To excite the NBD-HDA molecules, we used a 10 mW argon ion laser, $\lambda = 488nm$ (Ion Laser Technology, Salt Lake City, UT), impinging through the surfactant solution perpendicularly from the top using an adjustable mirror. The fluorescence emission passed through a microscope

objective and an emission filter with a lower cutoff wavelength of 515 nm (Omega Optical, Brattleboro,VT) to an ultrahigh sensitivity SIT vidicon camera (Hamamatsu model C2741-08, Hamamatsu-City, Japan). The fluorescence images were oberved on a monitor, video recorded, and /or captured on a 486 PC with a video frame grabber board (Data Translation DT2861, Marlboro, MA). Captured images were postprocessed to enhance contrast with NIH Image software, v.1.52.

We begin our experiments by obtaining the optimal concentration of dye solutions at which the good contrast could be observed between the fluorescence illumination of the micellar solution and of the surfactant solution below the CMC. We prepare insoluble NBD-HDA in HPLC grade chloroform at following concentrations: 6.4mg/L, 23mg/L, 80mg/L and 164mg/L. 4μL dye solution is spread from a microsyringe on the surface of surfactant solution at the concentration below and above CMC. (Recall the CMC for the $C_{14}E_6$ is about 4.4mg/L), several minutes is allowed for chloroform evaporation before observations were recorded; The gain for surfactant solutions at different concentration and different dye concentration is given in following table.

Table 5.1 Gain at different concentration of surfactant and dye solutions

Surfactant solution	Dye concentration (6.4mg/L)	Dye concentration (23.0mg/L)	Dye concentration (80.0mg/L)	Dye concentration (164mg/L)
2.6mg/L	0.1	0.1	0.1	0.1
3.95mg/L	0.1	0.1	0.1	0.1
4.76mg/L	0.1	0.1	0.1	1.0
8.78mg/L	0.1	0.1	0.2	1.5
20.86mg/L	0.2	0.2	0.2	4.5

At dye concentration of 164mg/L, we could observe the good contrast of fluorescence image between surfactant concentration above the CMC and below the CMC. When the dye solution concentration is below this value, there is not enough dyes solubilized in the

micelles to illumination the micelles upon the excitation of laser, we could not observe good image contrast between those surfactant solutions. In the fluorescence visualization experiment, a small amount (about 4μL) of dye solution in chloroform at concentration of 164mg/L is spread onto surface of the surfactant solution at concentration of 4.76mg/L, and 20.86mg/L (4.74CMC). Several hours are waited to allow the dyes to be solubilized into the micelles and fluorescence image is tested to make sure the solubilization of dyes in the micelles. By pulling out above surfactant solution into another clean cuvette or by aspirating small amount of water from surface, the clean air/water surface is created. The fluorescence image of surfactant solution appears bright throughout the surfactant solution from the top, which is shown in figure 5.2a. Upon the creation of the fresh air/water interface, surfactant monomers are adsorbed onto the surface, the adsorption of monomers disturbs the local equilibrium between the monomer and micelles, and cause the micelles to dissociate to supply monomers, the dyes solubilized in the micelles are also released onto the surface. When the concentration of surfactant solution is below the critical value (in case like 4.76mg/L), the diffusive transport of micelles is not fast enough to match kinetic adsorption, the kinetic adsorption of monomer is so fast, the micelle concentration at sublayer will drops to zero at t=a, since then the micelle free zone will occur. In the micelle free zone, there are no micelles present, only monomers exist. Because the dyes cannot be solubilized in the surfactant monomers, the region of micelle free zone will appears dark upon the excitation of laser, which is illuminated by figure 5.2b. Since the occurrence of the micelle free zone, the micelle free zone will migrate into the surfactant solution. With the adsorption, the surface becomes saturated, the kinetic adsorption rate decreases, the monomer flux across the micelle free zone

reduces, this also relaxes the micelle flux there which matches the monomer flux. The front of the micelle free zone starts to come back to the surface, the dark region of the fluorescence illumination become smaller, which is shown by figure 5.2c. Eventually the front of micelle free zone will come back to the surface, the dark region of the fluorescence image will finally disappear, which is indicated by figure 5.2d. When the surfactant concentration increases but still below the critical value, the micelle free zone also occurs. The micellar concentration gradient at the t=a is smaller than that at lower concentration, the driving force for the micelle free zone decreases. So the maximum distance between the surface and the front of micelle free zone $\delta(t)$ is less than that at lower concentration. When the concentration of surfactant solution is higher than the critical value, the micelle diffusion is fast enough to match the kinetic adsorption, in this case, the micelle free zone will not occur, the fluorescence image of surfactant solution will appears bright uniformly during the adsorption process, which is indicated by figure 5.3a-5.3d.

5.3 Conclusion

Fluorescence microscopy technique confirms our transport model[1], which describe the surfactant transport from micellar solution to the clean air/water interface. When the concentration of surfactant solution is higher that the CMC but blow the critical value, the micellar diffusion is not fast enough to match kinetic adsorption. The sublayer micellar concentration will decreases to zero at time t=a, a micelle free zone then occurs. The dark image between the bright images of surface and micelle region confirms the existence of micelle free zone. With adsorption of surfactant monomers, the surface becomes saturated. The kinetic adsorption rate decreases. This causes the matching

monomer flux reduced, micellar flux relaxation, and drives the micelle free zone back to surface. We observed this dark region become smaller and finally disappear when uniform micellar solution returns at equilibrium. When the concentration of surfactant solution is higher than the critical value, the micellar diffusive transport is fast enough to match kinetic adsorption. Micelles are present everywhere in the surfactant solution, monomer concentration is maintained at CMC and the micelle free zone will not occur. We observed the bright image through micellar surfactant solutions through the whole experimental process. This proves that there is no micelle free zone.

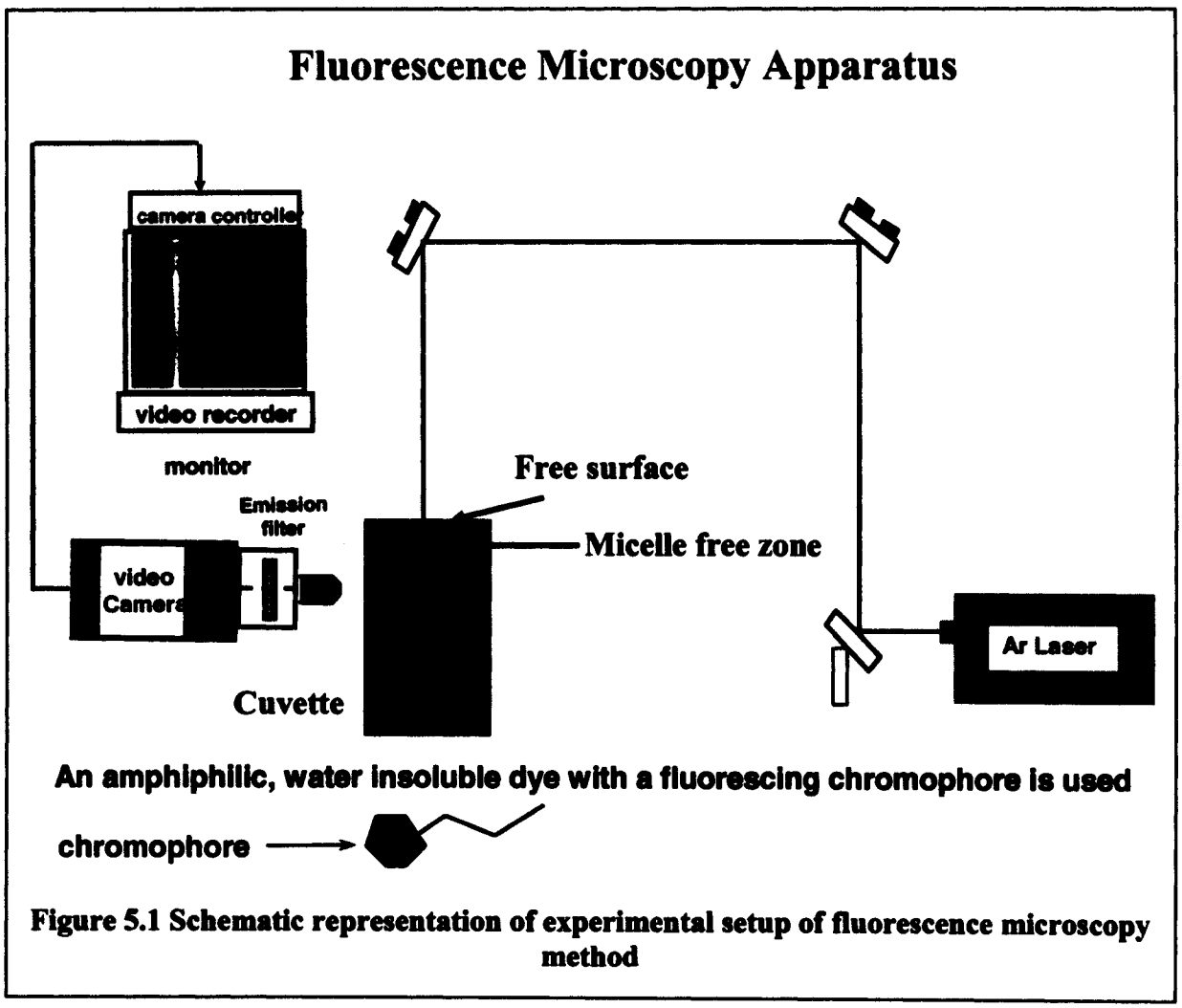

Figure 5.1 Schematic representation of experimental setup of fluorescence microscopy method

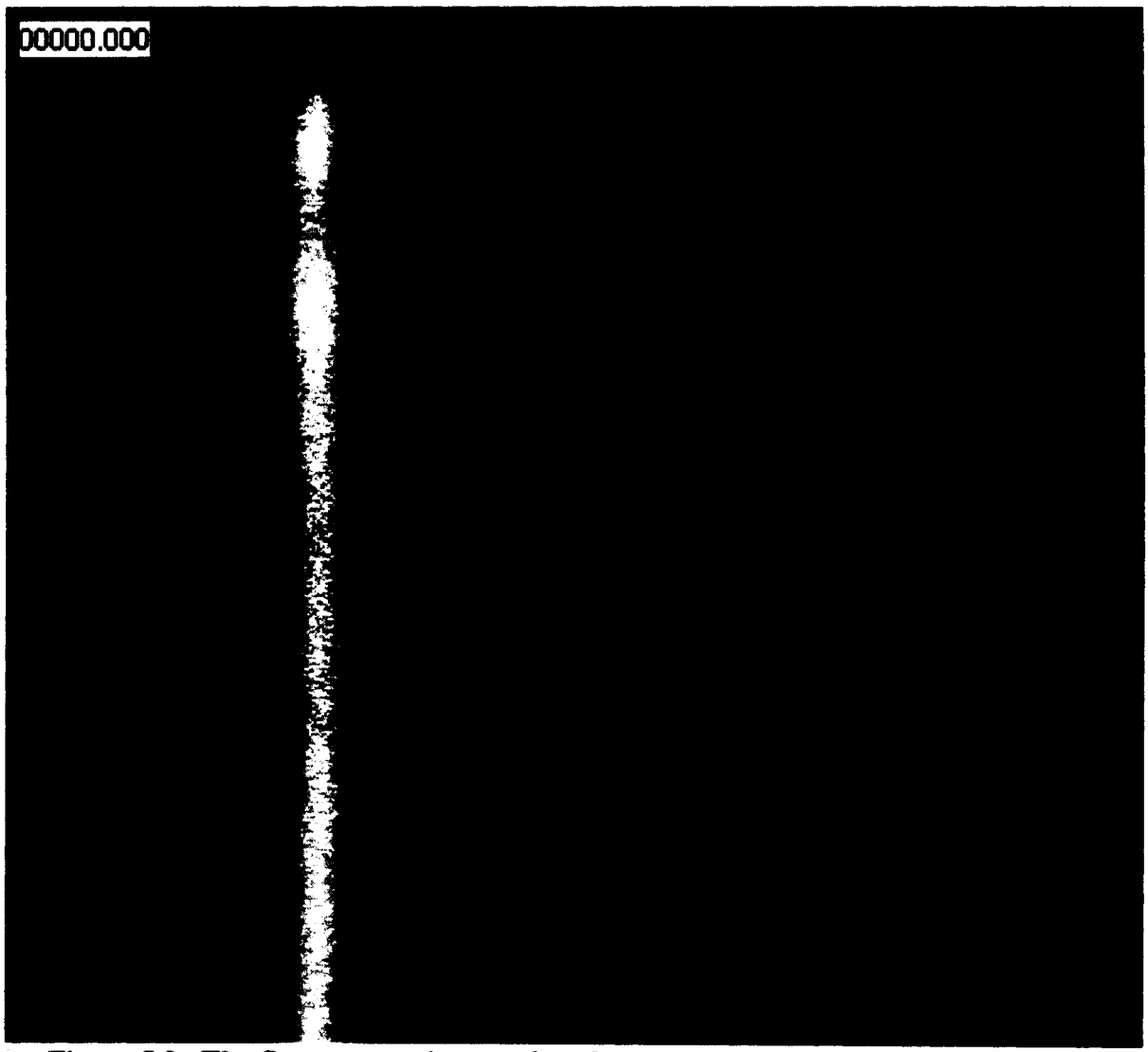

Figure 5.2a The fluorescence image of surfactant transport from micellar solution (4.76mg/L) at t=0

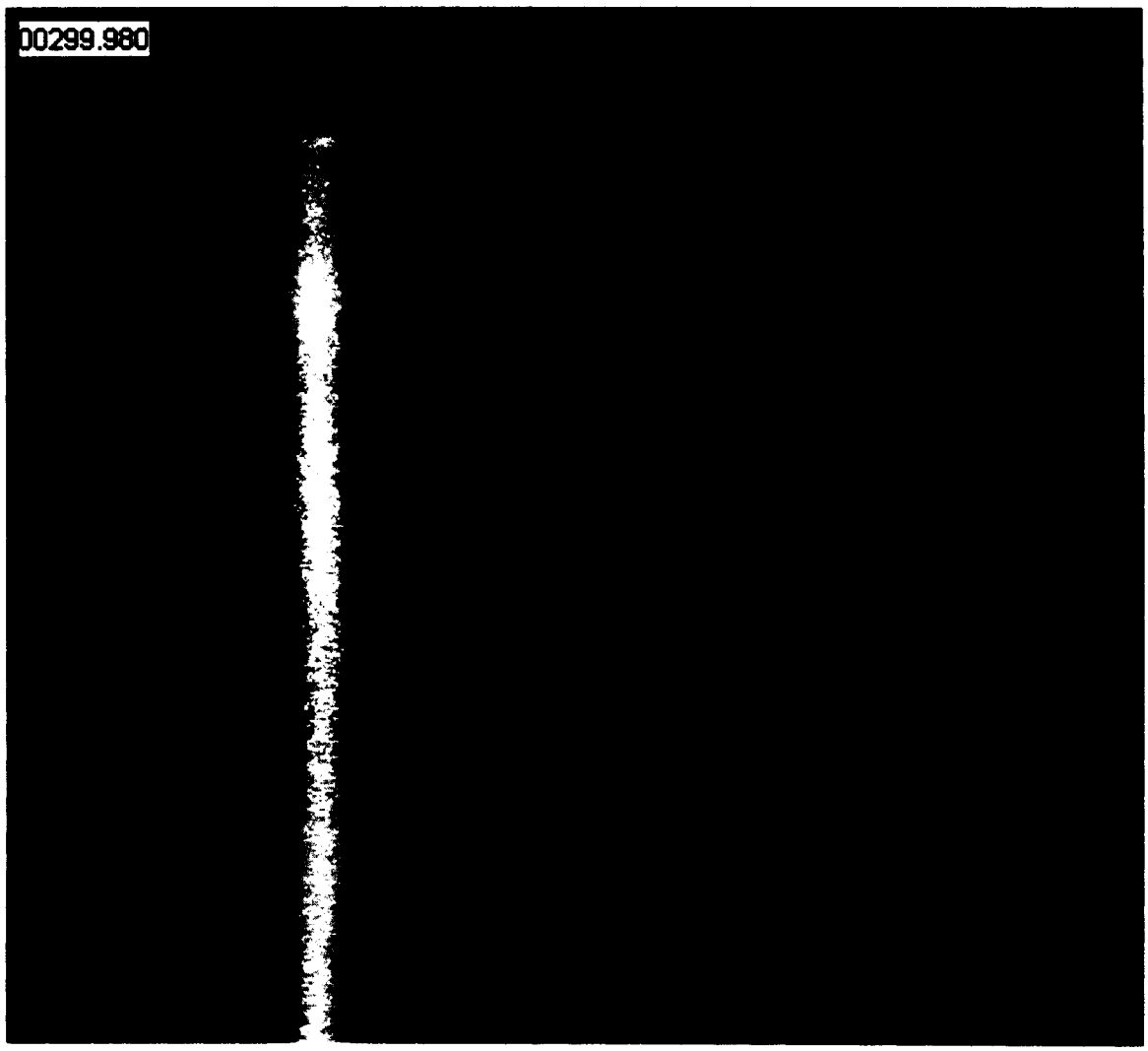

Fig. 5.2b The fluorescence image of surfactant transport from micellar solution (4.76mg/L) at t=300s

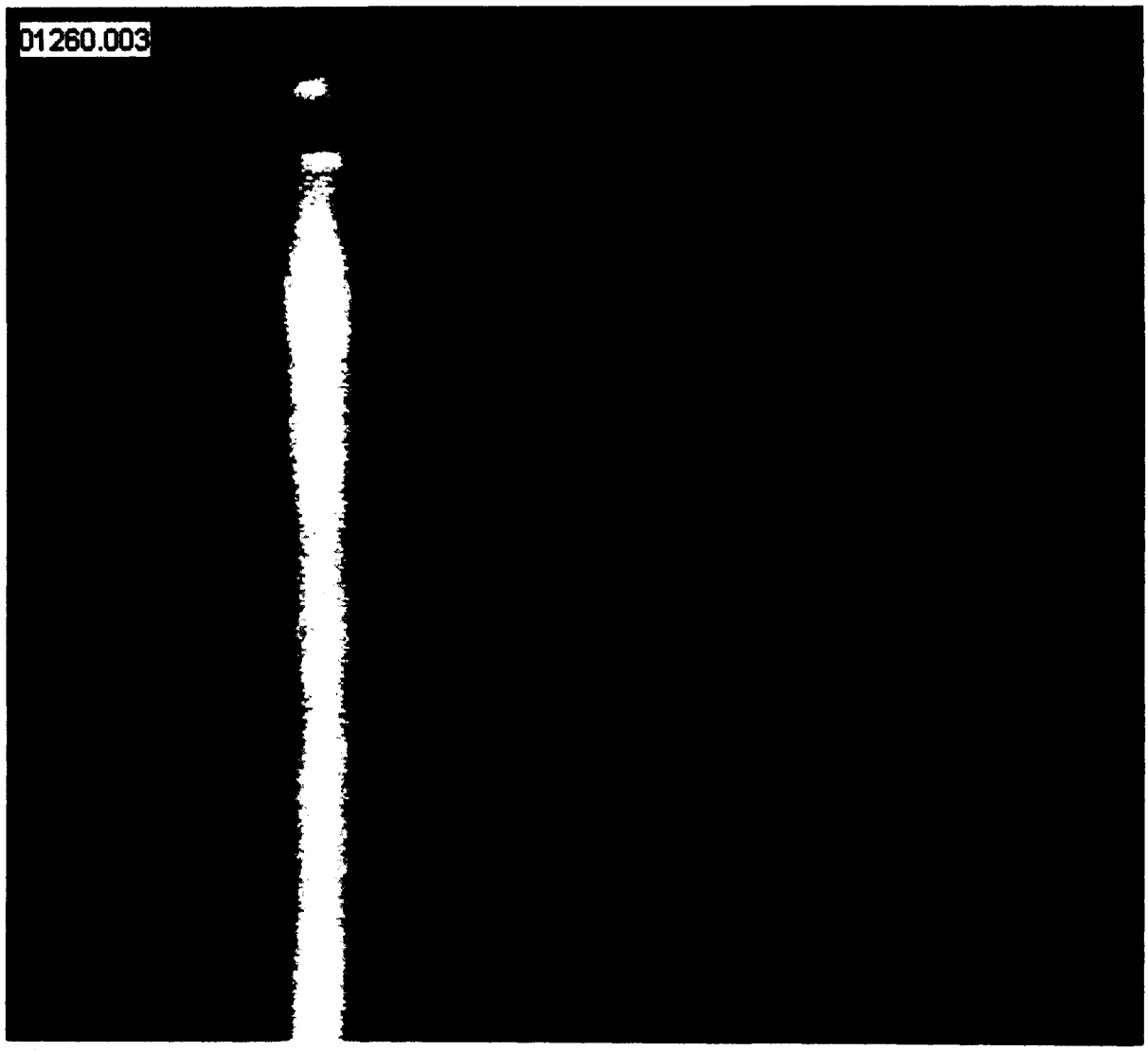

Fig. 5.2c The fluorescence image of surfactant transport from micellar solution (4.76mg/L) at t=1200s

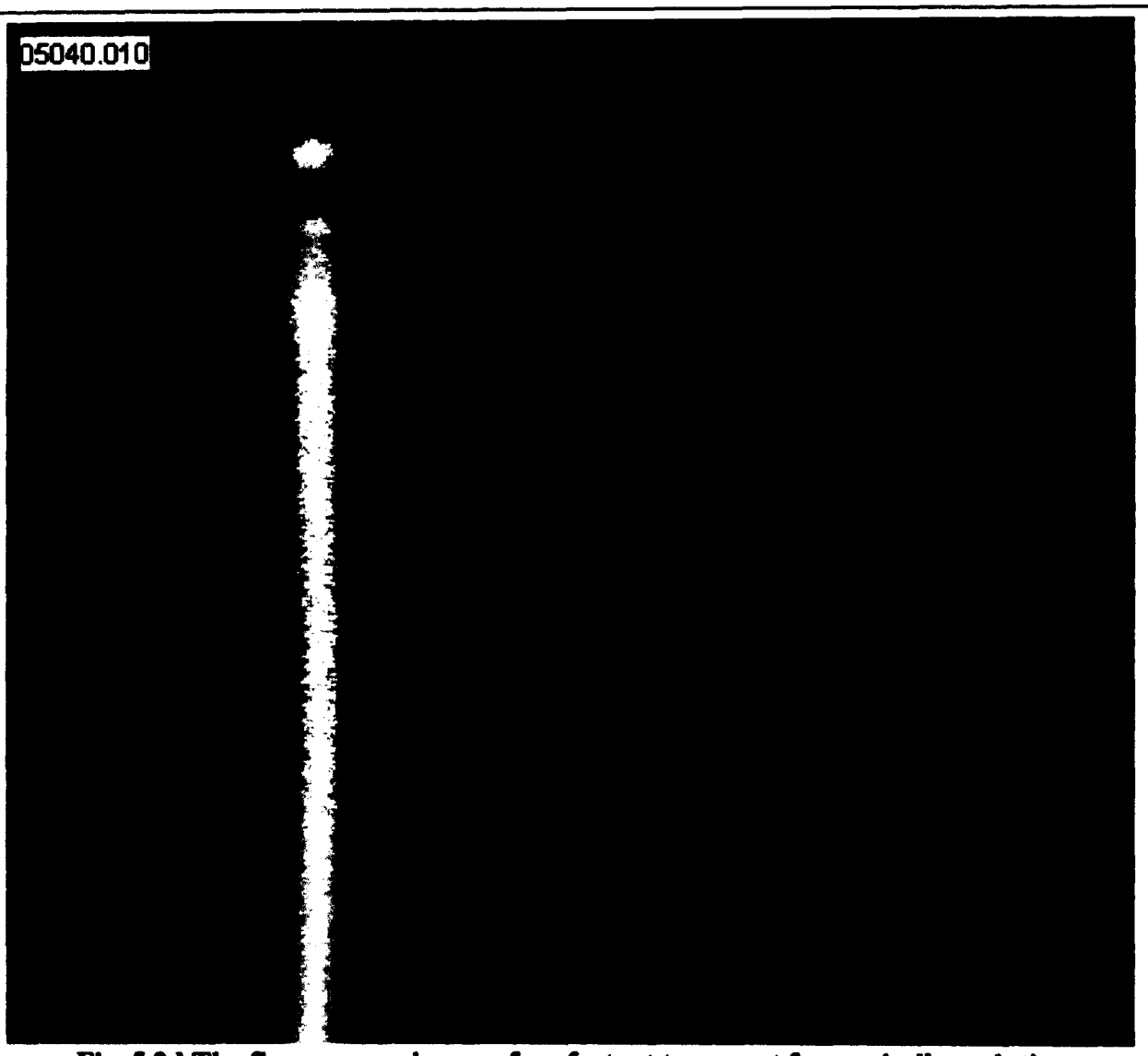

Fig. 5.2d The fluorescence image of surfactant transport from micellar solution (4.76mg/L) at t=5040s

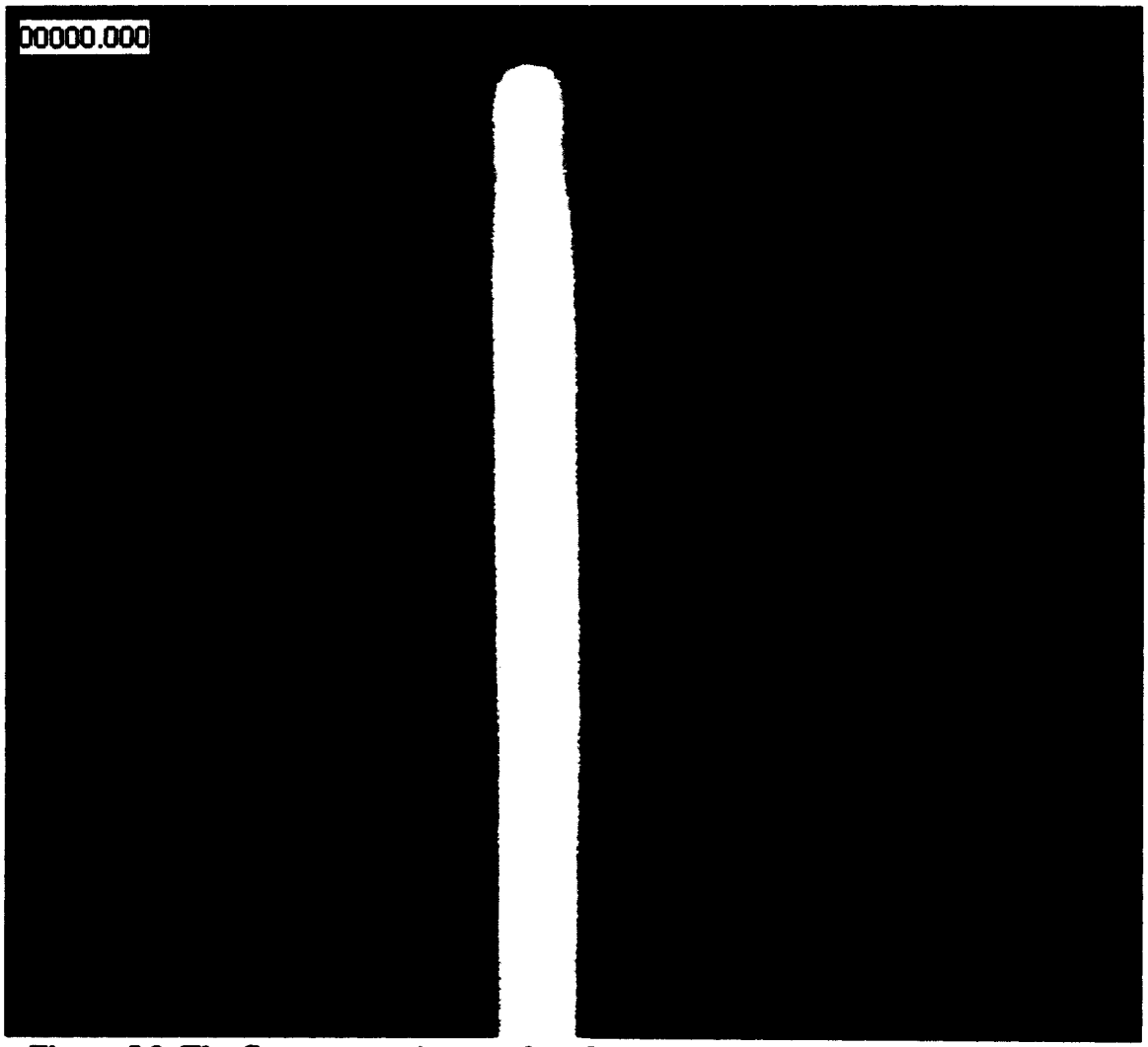

Figure 5.3aThe fluorescence image of surfactant transport from micellar solution (4.74CMC)at t=0s

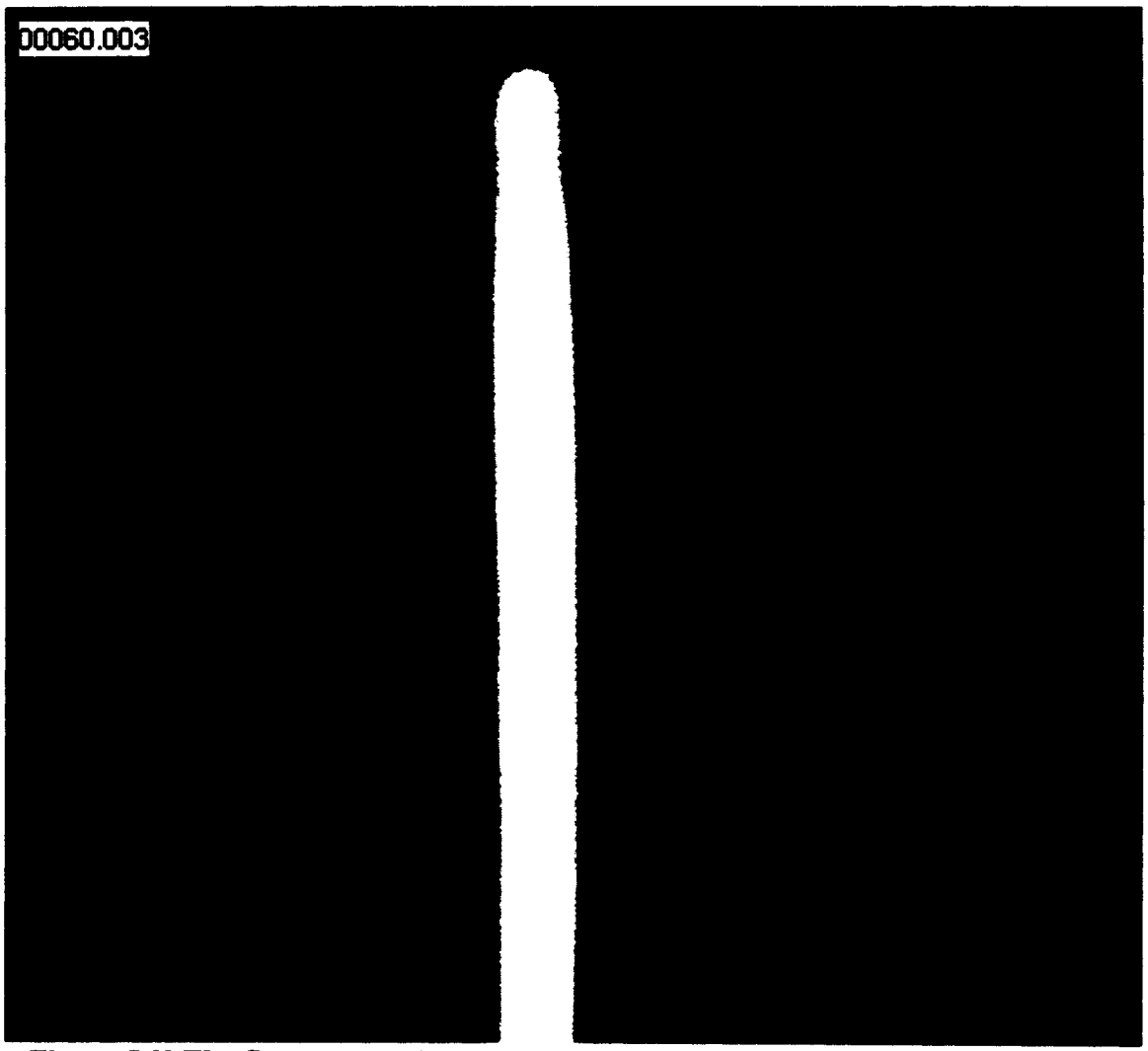

Figure 5.3bThe fluorescence image of surfactant transport from micellar solution (4.74CMC)at t=60s

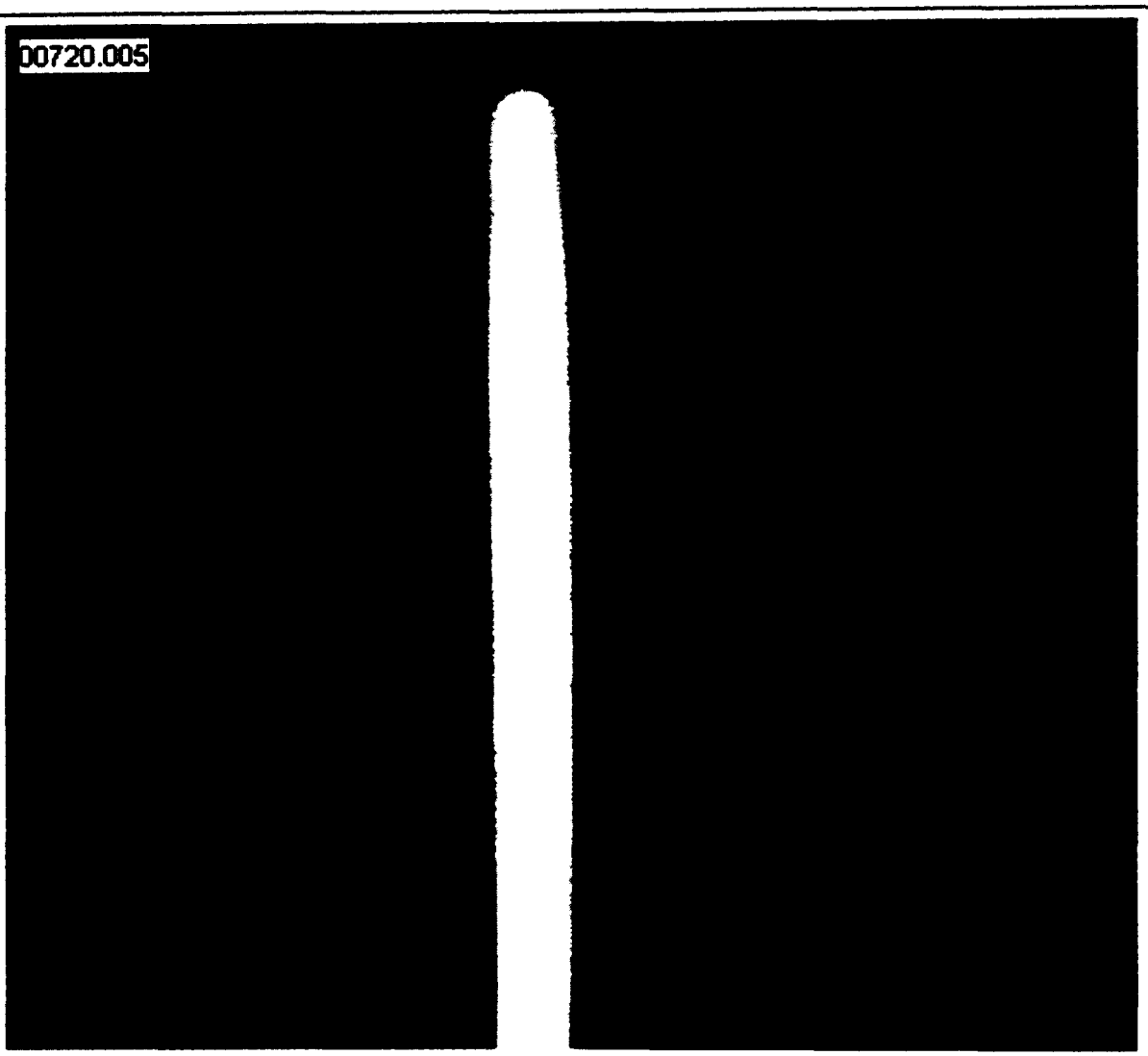

Figure 5.3cThe fluorescence image of surfactant transport from micellar solution (4.74CMC) at t=720s

Fig. 5.3dThe fluorescence image of surfactant transport from micellar solution(4.74CMC) at t=2880s

CHAPTER 6 FUTURE WORK

6.1 Model of micelle adsorption

The theory predicts that once the surfactant concentration is higher than the critical value, i.e. $C_T > C^*$, the dynamic surface tension relaxation is determined only by the kinetics. Since in this case, micelles exist everywhere in the solution and the monomer concentration is constant. The rate limiting step to adsorption is the kinetic one. The dynamic relaxation in concentration is given by integrating the Frumkin kinetic equation, with the relaxation in tension obtained from the equation of state. This is a limiting relaxation determined only by kinetics, and valid in principle for all bulk concentrations greater than the critical value. But the experimental data which is plotted in figure 4.13 shows that the dynamic surface tension relaxation becomes faster with increasing surfactant bulk concentration. This may indicate that micelles in the vicinity of the surface may be directly adsorbing onto relatively clean interface. Whether this adsorption involves the stable micelles at the center of the Gaussian distribution, or, as is more likely, the adsorption and unfolding of the less populous but more unstable rare aggregates and oligomers is unclear. In the future work, the adsorption of micelles will be accounted in the Frumkin kinetic framework. To account for micelle adsorption we consider follows: First the kinetic adsorption rate should be proportional to the aggregate population at the interface (oligomers and rare aggregate in particular); as these scale with the total concentration of surfactant in the aggregate phase ($\sigma C_M(r = R_0, t)$), we allow for the adsorption to be proportional to $\sigma C_M(r = R_0, t)$. Second, the adsorption should also be proportional to the available area on the surface and so the adsorption rate

is multiplied by the available area factor ($\Gamma_\infty - \Gamma$). Finally we assume that the adsorption of aggregates is not reversible; only monomer desorbs off of the surface. Thus we exclude processes which occur at collapse of insoluble monolayers in which the interface buckles and aggregates can be released into the sublayer. Therefore the Frumkin equation for kinetic exchange when micelles are present in the sublayer is augmented as follows:

$$\frac{d\Gamma}{dt} = \left[\beta C_{CMC} + \nu C_M(r = R_0, t)\right]\left\{\Gamma_\infty - \Gamma\right\} - \alpha\Gamma e^{K\Gamma/\Gamma_\infty} \tag{6.1}$$

Where ν represents the collision frequency of the aggregates with the surface multiplied by a factor which accounts for the number of overall monomers released per collision. The above expression has the property that the rate of adsorption of micelles decreases as the surface concentration increases; thus the adsorption of aggregated is favored onto relatively clean surfaces. We also note that since the augmented flux only contributes when micelles are present in the sublayer, the equilibrium between the bulk and the surface for concentrations below the CMC remains unaltered. The transport model is described by the micelle diffusion equation,

$$\frac{\partial C_M}{\partial t} = \frac{D_M}{r}\frac{\partial}{\partial r}\left\{r^2\frac{\partial C_M}{\partial r}\right\}, r > R_0 \tag{6.2}$$

subject to the boundary conditions that the micellar diffusive flux is equal to the rate of kinetic adsorption of surfactant to the surface,

$$\sigma D_M \left.\frac{\partial C_M}{\partial r}\right|_{r=R_0} = \left[\beta C_{CMC} + \nu C_M(r = R_0, t)\right]\left\{\Gamma_\infty - \Gamma\right\} - \alpha\Gamma e^{K\Gamma/\Gamma_\infty} \tag{6.3}$$

the surface mass balance

$$\sigma D_M \left.\frac{\partial C_M}{\partial r}\right|_{r=R_0} = \frac{\partial\Gamma}{\partial t} \tag{6.4}$$

and the initial and far field boundary conditions.

$$\sigma C_M(r \to \infty, t) = (n-1)C_{CMC}$$
$$\sigma C_M(r, t=0) = (n-1)C_{CMC} \tag{6.5}$$

The adsorption coefficient of micelles will be evaluated by comparison with experiments.

6.2 Fluorescence visualization by confocal microscopy

Confocal microscopy is an optical sectioning technique that produces high resolution images of samples free of out-of-focus light. In confocal microscopy, out-of-focus light is removed by allowing light from the focal plane of the lens to reach the detector. This is achieved by positioning a pinhole, which excludes out-of-focus light, in front of the detector. Consequently, only in-focus light passes through, producing a clear, well-resolved image. 'Confocal' refers to the fact that at the pinhole illumination light is co-incident with emitted light entering the detector. Confocal microscopy brings a lot of advantages such as: Much greater spatial resolution over non-confocal light microscopy; The ability to generate completely in-focus 3-D images. By changing the distance between the objective and the sample, optical sections through the sample can be imaged. These 'slices' are digitally stored on a computer and can be re-assembled to generate a three-dimensional image of the whole sample; Localization of multiple fluorescent signals in three dimensions within the same sample; Measurement between features in two and three dimensions; The potential to monitor changes in living samples over time, in two and three dimensions in multiple colors. In future work, the confocal microscopy technique will be applied to visualize the micelle free zone.

CHAPTER 7 CONCLUSIONS

This dissertation studies the transport dynamics of a water soluble nonionic surfactant $C_{14}E_6$ at the air/water interface from concentrations below the critical micelle concentration (CMC) to concentrations above the CMC. A method which involves using the pendant bubble as a monolayer film balance is used to directly measure the surface tension as a function of surface concentration. By fitting the directly measured equation of state and adsorption isotherm, equilibrium parameters are determined as follows: for the Langmuir model we find Γ_∞=2.40x10^{-6} mol/m^2 and α/β=8.3605×10^{-6} mol/m^3; for the Frumkin mechanism, Γ_∞=3.32x10^{-6} mol/m^2, α/β=2.068×10^{-6} mol/m^3 and K= 7.12. By numerically solving the transport equations for surfactant transport from aqueous solution at concentration below the critical micelles concentration, the kinetic constants are obtained as adsorption rate β=4.0 m^3/(mol s) and monomer diffusion coefficient D=6.0x10^{-10} m^2/s. Based on the assumption that the micellar breakup is infinitely fast than the monomer and micelle diffusion and monomer kinetic adsorption, surfactant transport from micellar solution could have two regimes. Our theoretical calculation shows that above a critical micellar concentration (C*) i.e. $C_T > C^*$ diffusion of micelles from the bulk is fast enough to keep the monomer concentration in the sublayer at the C_{CMC} until equilibrium is achieved on the surface. Below a critical bulk micelle concentration i.e., $C_T < C^*$, micelle diffusion is not fast enough and the micelle concentration at the sublayer falls to zero at $t = a$, since then the micelle free zone occurs. For model polyethoxylated surfactant $C_{14}E_6$, the $C^* = 4.25C_{CMC}$. At

CHAPTER 7 CONCLUSIONS

This dissertation studies the transport dynamics of a water soluble nonionic surfactant $C_{14}E_6$ at the air/water interface from concentrations below the critical micelle concentration (CMC) to concentrations above the CMC. A method which involves using the pendant bubble as a monolayer film balance is used to directly measure the surface tension as a function of surface concentration. By fitting the directly measured equation of state and adsorption isotherm, equilibrium parameters are determined as follows: for the Langmuir model we find Γ_∞=2.40x10^{-6} mol/m^2 and α/β=8.3605×10^{-6} mol/m^3; for the Frumkin mechanism, Γ_∞=3.32x10^{-6} mol/m^2, α/β=2.068×10^{-6} mol/m^3 and K= 7.12. By numerically solving the transport equations for surfactant transport from aqueous solution at concentration below the critical micelles concentration, the kinetic constants are obtained as adsorption rate β=4.0 m^3/(mol s) and monomer diffusion coefficient D=6.0x10^{-10} m^2/s. Based on the assumption that the micellar breakup is infinitely fast than the monomer and micelle diffusion and monomer kinetic adsorption, surfactant transport from micellar solution could have two regimes. Our theoretical calculation shows that above a critical micellar concentration (C*) i.e. $C_T > C^*$ diffusion of micelles from the bulk is fast enough to keep the monomer concentration in the sublayer at the C_{CMC} until equilibrium is achieved on the surface. Below a critical bulk micelle concentration i.e., $C_T < C^*$, micelle diffusion is not fast enough and the micelle concentration at the sublayer falls to zero at $t = a$, since then the micelle free zone occurs. For model polyethoxylated surfactant $C_{14}E_6$, the $C^* = 4.25C_{CMC}$. At

concentration between CMC and 4CMC, the micelle free zone could as large as several hundred micrometers. Fluorescence microscopy technique visualized the existence of micelle free zone and illuminated the micelle region. The computed dynamic tensions agree well with the experimental data, affirming the treatment of the micelle breakup as fast with respect to diffusion and kinetic adsorption.

Bibliography

References for Chapter 1:

1.Rosen, M.C.; Cohen, A.; Dahanayake, M.; Hua, X. Y., Journal of Physical Chemistry, **86**, 541(1982).

2.Evans, D.F.; and Wennerstrom, H., The Colloid Domain Where Physics, Chemistry, Biology, and Technology Meet, 2 ed; Wiley-VCH: New York, 1999.

3.Chang, C.-H.; Franses, E. I., Colloids and Surfaces A: Physicochemical and Engineering Aspects, **100**, 1(1995).

4.Oh, S. G.; Shah, D. O., Langmuir, **8**(4), 1232(1992).

5.Hua, X. Y.; Rosen, M. J., Journal of Colloid and Interface Science, **124**, 652(1988).

6.Rosen, M. J.; Zhu, Z., Journal of the American Oil Chemists Society, **70**, 65(1993).

7.Tadros, T., Role of Surfactants in the Transfer and Performance of Agrochemicals. In Surfactants in Agrochemicals; Tadros, T. Ed.; Marcel Dekker: New York, 1994; Vol. 54; pp 207-259

8.Furmidge, C., Journal of Sci. Food Agric., **13**, 127(1962).

9.Furmidge, C., Journal of Colloid Science, **17**, 309(1962).

10.Ford, R. E.; Furmidege, C.G.L., Impact and Spreading of Spray Drops on Foliar Surfaces. In Wetting; Society of Chemical Industry: London, 1967; Vol. 25; p417-432.

11.Spillman, J., Pesticide Science, **15**, 97(1984).

12.Wirth, W.; Storp, S.; Jacobson, W., Pesticide Science, **33**, 411(1991).

13.Reichard, D.; Cooper, J.; Bukovac,M.; Fox, R., Pesticide Science, **53**, 291(1998).

14.Bikeman, J., Foams, Springer Verlag: New York,1973.

15.Oh, S.; Klein, S.; Shah, D., AICHE Journal, **38**, 149(1992).

16.Oh, S.; Shah, D., Langmuir, **7**(7), 1316(1991).

17.Shiao, S.; Patist, A.; Free, M. L.; Chhabra, V.; Hibers, P.D.T.; Gregory, A.; Patel, S.; Shah, D. O., Colloids and Surfaces A: Physicochemical and Engineering Aspects, **128**, 197(1997).

References for Chapter 2:

1.Adamson, A.; Gast, A., Physical Chemistry of Surfaces, 6ed , New York: John Wiley, 1997.

2.Aveyard, R.; Haydon, D., An Introduction of the Principles of Surface Chemistry, Cambridge University Press: London, 1973.

3.Pan, R.; Green, J.; Maldarelli, C., Journal of Colloid and Interface Science, **205**, 213(1998).

4.Chang, C.-H.; Frances, E. I., Colloids and Surfaces A: Physicochemical and Engineering Aspects, **100**, 1(1995).

5.Miller, R.; Joos, P.; Fainerman,V. B., Advances in Colloid and Interface Science, **49**, 249(1994).

6.Miller, R.; Kretzschmar, G., Advances in Colloid and Interface Science, **37**, 97(1991).

7.Kretzschmar, G.; Miller, R., Advances in Colloid and Interface Science, **36**, 65(1991).

8.Ward, A. H.; Tordai, L., The Journal of Chemical Physics, **14**(7), 453(1946).

9.Borwankar, R. P.; Wasan, D. T., Chemical Engineering Science, **38**(10), 1637(1983).

10.Fainerman, V. B., Colloid Journal USSR, **39**, 91(1977).

11.Fainerman, V. B., Colloid Journal USSR, **40**, 437(1978).

12.Sutherland, K. L., Australia Journal of Scientific Research, **A5**, 683(1952).

13.Hansen, R. S., Journal of Colloid Science, **16**, 549(1961).

14.Nagarajan, R.; Ruckenstein, E., Equation of State for Fluids and Fluid Mixtures, Chapter 15, Elsevier: Amsterdam,2000.

15.Israelachvili, J., Intermolecular and surface force,Academic Press, 1991.

16.Tanfor, C., The Hydrophobic Effect, Wiley: New York, 1980.

17.Isrealachvili, J. N.; Mitchell, D.J.; Ninham, B.W., Journal of Chemical Society Faraday Transaction I, **72**, 1525(1976).

18.Attwood, D., Journal of Physical Chemisty, **72**, 339(1968).

19.Elworthy, P. H.; McDonald, C., Koll. Z., **195**, 16(1964).

20.Hoffmann, H.; Kielman, H.S.; Pavlovic, D.; Platz,G.; Ulbricht, W., Journal of Colloid and Interface Science, **80**, 237(1981).

21.Ottewill, R. H.; Storer, C.C.; Walker, T., Transaction of Faraday Society, **63**, 2796(1967).

22.Lang, J.; Djavankht, A.; Zana, R., Journal of Physical Chemistry, **84**, 1541(1980).

23.Lianos, P.; Zana, R., ibid, **84**, 3339(1980).

24.Evans, D. F.; Wennerstrom, H., The Colloid Domain Where Physics, Chemistry, Biology, and Technology Meet, ed. 2nd., New York: Wiley-VCH: New York, 1999.

25.Aniansson, E. A. G.; Wall, S. N., The Journal of Physical Chemistry, **78**(10), 1024(1974).

26.Aniansson, E. A. G.; Wall, S. N., The Journal of Physical Chemistry, **79**(8), 857(1975).

27.Aniansson, E. A. G.; Wall, S. N.; Almgren, M.; Hoffmann, H.; Kielmann, I.; Ulbricht,W.; Zana, R.; Lang, J.; and Tondre, C., The Journal of Physical Chemistry, **80**(9), 905(1976).

28.Inoue, T.; Tashiro, R.; Shibuya, Y.; Shimozawa, R., Journal of Colloid and Interface Science, **73**, 105(1980).

29.Kresheck, G. C.; Hamori, E.; Davenport, G.; Scherage, H. A., Journal of the American Chemical Society, **88**(2), 246(1966).

References for Chapter 3:

1.Lin, S.-Y.; McKeigue, K.; and Maldarelli,C., AIChE Journal, **36**(12), 1785(1990).

2.Pan, R.; Green, J.; and Maldarelli, C., Journal of Colloid and Interface Science, **205**, 213(1998).

3.Kwok, D. Y.; Volhardt, D.; Miller, R.; Li, D.; and Neuman, A. W., Colloids Surf. A: Physicochemical Engineering Aspects, **88**, 51(1994).

4.Li, J.; Miller, R.; Wustneck, R.; Mohwald, H.; and Neumann, A. W., Colloids Surf. A: Physicochemical Engineering Aspects, **96**, 295(1995).

5.Huibers, P. D. T.; Lobanov, V. S.; Katritzky, A. R.; Shah, D. O.; and Karelson, M., Langmuir, **12**, 1462(1996).

References for Chapter 4:

1.Aniansson, E. A. G.; Wall, S. N., The Journal of Physical Chemistry, **78**(10), 1024(1974).

2.Aniansson, E. A. G.; Wall, S. N., The Journal of Physical Chemistry, **79**(8), 857(1975).

3.Aniansson, E. A. G.; Wall, S. N.; Almgren, M.; Hoffmann, H.; Kielmann, I.; Ulbricht, W.; Zana, R.; Lang, J.; and Tondre, C., The Journal of Physical Chemistry, **80**(9), 905(1976).

4.Lucassen, J., Faraday Discuss. Chem. Soc., **59**(76), (1975).

5.Kresheck, G. C.; Hamori, E.; Davenport, G.; and Scherage H. A., Journal of the American Chemical Society, **88**(2), 246(1966).

6.Miller, R., Colloid & Polymer Science, **259**, 1124(1981).

7.Joos, P.; and Hunsel, J. V., Colloids and Surfaces, **33**, 99(1988).

8.Joos, P.; and Rillaerts, E., Journal of Physical Chemistry, **86**, 3471(1982).

9.Li, B.-Q.; Joos, P.; and Uffelen, M.V., Journal of Colloid and Interface Science, **171**, 270(1995).

10.Petrov, P.; and Joos, P., Journal of Colloid and Interface Science, **181**, 530(1996).

11.Geeraerts, G.; and Joos,P., Colloids and Surfaces, **90**, 149(1994).

12.Makievski, A.V.; Fainerman, V. B.; and Joos, P., Journal of Colloid and Interface Science, **166**, 6(1994).

13.Fang, J. P.; and Joos, P., Colloids and Surface, **65**, 113(1992).

14.Fang, J. P.; and Joos, P., Colloids and Surfaces, **65**, 121(1992).

15.Fainerman, V. B., Kolloid. Zh., **43**, 94(1981).

16.Dushkin, C. D.; Ivanov, I. B.; and Kralchevsky, P. A., Colloids and Surfaces, **60**, 235(1991).

17.Dushkin, C.D.; and Ivanov, I. B., Colloids and Surfaces, **60**, 213(1991).

18.Noskov, B. A., Advances in Colloid and Interface Science, **95**, 237(2002).

19.Dushkin, C. D.; Iliev, T. H.; and Radkov, Y. S., Colloids & Polymer Science, **273**(4), 370(1995).

20.Danov, K.D.; Valkovska, D. S.; and Kralchevsky, P.A., Journal of Colloid and Interface Science, **251**, 18(2002).

21.Fainerman, V.B.; Lylyk, S.V.; and Prikladnoj, Zh., Chimii. (in Russian), **56**, 2217(1983).

22.Fainerman, V. B.; Rakita, Yu. M., Kolloid. Zh., **52**, 106(1990).

23.Fainerman, V. B., Colloids Surface, **62**, 333(1992).

24.Fainerman, V. B.; Makievski, A.V.; and Joos, P., Colloids and Surfaces, **69**, 249(1993).

25.Evans, D. F.; and Wennerstrom, H., The Colloid Domain Where Physics, Chemistry, Biology, and Technology Meet,ed. 2nd. 1999, New York: John Wiley & Sons, Inc.

26.Patist, A.; Kanichy, J. R.; Shukla, P. K.; and Shah, D. O., Journal of Colloid and Interface Science, **245**, 1(2002).

27.Tiberg, F.; Jonsson, B.; and Lindman, B., Lagmuir, **10**, 3714(1994).

28.Brinck, J.; Jonsson, B.; Tiberg, F., Langmuir, **14**(5), 1058(1998).

References for Chapter 5

(1) Song,Q.; Couzis, A.; Maldarelli, C.; Somasundaran, P.; Strikwerda, J. C., submitted.

(2) Nederlof, P. M.; Flier S. van der; Wiegant, J.; Raap A. K.; Tanke, H.J.; Ploem, J.S.; Ploeg, M. van der, (1990) Cytometry 11,126-131.

(3) Kohen, E.; Kohen, C.; Hirschberg, J.G.; Santus, R.; Morlière P.; Kasten, F. H.; Ghadially, F.N., In Encclopedia of Human Biology, Vol. 5 R. Dulbecco (ed.). Academic Press, San Diege,1991, pp. 561-585.

(4) Suresh, K. A.; Nittmann, J.; Rondelez, F., Europhys. Lett, 1988, 6

(5) Moore, B.G.; Knobler, C. M.; Akamatsu, S.; Rondelez, F., J. Phys. Chem. 1990,94,4588

(6) Moore, B.; Knobler, C. M., J. Chem. Soc., Faraday Trans. 2 1986,82,1753

(7) Moy, V. T.; Keller, D. J.; Gaub, H. E.; McConnell, H.M., J. Phys. Chem. 1986, 90, 3198

(8) Qiu, X.; Ruiz-Garcia, J.; Stine, K. J.; Knobler, C. M., Phys. Rev. Lett. 1991, 67,703

(9) Lösche, M.; Möhwald, H., Rev. Sci. Instrum., 1984,55,1968

(10) Meller, P. ,Rev. Sci. Instrum., 1988, 59, 2225